WADC TR 58-343
ASTIA Document No.

METHODS OF FLIGHT VEHICLE NOISE PREDICTION

Peter A. Franken, Edward M. Kerwin, Jr.
and
the Staff of Bolt Beranek and Newman Inc.
Cambridge, Massachusetts

Contract No. AF 33(616)-5274

Project No. 1370
Task No. 13786

Aircraft Laboratory
WRIGHT AIR DEVELOPMENT CENTER
AIR RESEARCH AND DEVELOPMENT COMMAND
UNITED STATES AIR FORCE
Wright-Patterson Air Force Base, Ohio

FOREWORD

This report was prepared for the Aircraft Laboratory, Wright Air Development Center, Wright-Patterson Air Force Base, Ohio. The research and development work was accomplished by Bolt Beranek and Newman Inc., Cambridge, Massachusetts, under Air Force Contract No. AF 33(616)-5274, Project No. 1370, "Aeroelasticity, Vibration and Noise", and Task No. 13786, "Methods of Noise Prediction and Measurements". Mr. Joseph R. Bengoechea of the Dynamics Branch, Aircraft Laboratory is task engineer. Research was started 15 May 1957 and is continuing. This report covers methods of predicting noise levels and spectra inside and on the surface of flight vehicles. WADC -TN-58-189 will be issued describing a sonic facility capable of testing flight vehicle structures in extremely high intensity noise field. Two other reports will be published under this contract: (a) a report describing a sonic facility for testing airborne electronic components, (b) a report covering evaluation of the airborne electronic components testing facility and siren after final construction.

ABSTRACT

Detailed engineering procedures are presented for estimating sound pressure levels on or within a flight vehicle. The report is oriented for use by the aircraft engineer in making preliminary estimates of noise levels on or in a vehicle, when the vehicle is still in the design stage. Therefore, the procedures are expressed in terms of general parameters (such as mechanical power, typical dimensions, forward speed) which may be obtained to a satisfactory degree of accuracy long before flight testing.

The first step in the procedure is the estimation of noise levels exterior to the vehicle. Contributions from the various sources of noise that may be encountered are estimated. The effects of forward speed and altitude on exterior noise levels are considered in some detail.

Next, the basic noise-transmitting properties of panel structures are studied. The effects of coincidences, resonances, damping, etc., are included.

Finally, the particular vehicle geometry of interest is considered. The source and transmission properties already determined can then be combined, with appropriate geometrical corrections for the character of the receiving space, to yield the desired estimates of interior noise levels.

Several examples are worked out in detail to illustrate the application of the report procedures to typical vehicle configurations.

PUBLICATION REVIEW

This report has been reviewed and is approved.

FOR THE COMMANDER:

RANDALL D. KEATOR
Colonel, USAF
Chief, Aircraft Laboratory

TABLE OF CONTENTS

LIST OF ILLUSTRATIONS

SECTION I
INTRODUCTION

Scope

This report contains procedures for estimating acoustic noise in flight vehicles. It presents methods for estimating sound pressure levels on the outside surfaces of a vehicle and within vehicle apartments. Attention is concentrated on the vehicle proper, and the estimation of sound pressure levels at a distance is not considered.

This report is not intended to be a text on physical acoustics. In general, formalism and mathematical details are minimized in an effort to present a workable set of engineering charts and procedures. The material in this report is directed to the engineer concerned with the effects of acoustical noise on structures, electronic components or other equipment, and personnel. The report is to be used primarily to obtain preliminary estimates of noise levels in the early design stages of future vehicles.

However, in some sections of the report, additional mathematical details and background information have been included. Thus, users of the report may extend the range of applicability of the estimation procedures, and may adapt the procedures to cases that are not specifically covered.

The sources of noise considered in Section II of this report are described usually in octave bands of frequency in the frequency range of 20 to 10,000 cps. The procedures for estimating source levels are expected to be accurate to $\pm$ 3 db. The estimation of a noise reduction for a structure necessarily

introduces additional uncertainty. Nevertheless, we expect that the total tolerance on average noise levels within a receiving space (based on source levels and noise reduction) will be $\pm$ 5 db or less. Where an appreciable range of levels is expected in a receiving space, this fact is included in the estimating procedures.

The availability of acoustical data specific to a given problem will, of course, improve the accuracy of the procedures set forth in this report. In addition where judgment of an acoustical situation is required, the reader can expect improved facility and accuracy as his experience grows.

Section III is devoted to procedures and charts for estimating the acoustic transmission loss (TL) of various panel structures. The frequency range of interest is divided into regions according to the different types of panel behavior expected at various frequencies. Theoretical information on the transmission loss of flat plates and cylindrical shells is also presented in this section.

The transmission loss as determined in Section III is a more-or-less basic property of a panel. However, a determination of the net noise reduction (NR) afforded by the panel must take account of the interaction between transmitted noise field and the receiving space. In addition, an adjustment to TL must be made if the air density and temperature in the receiving space are different from sea-level density and room temperature. Section IV contains charts of corrections to TL for small, medium, and large receiving spaces for various amounts of acoustic absorption. Corrections for ambient conditions in the receiving space are also given.

Section V of this report contains a number of examples which illustrate the use of the charts and procedures for the reader. Appendix A is a reprint of an article containing charts for estimating the natural frequencies of vibration of different types of structures.

The material contained in this report is based on the most reliable and newest data available to the authors at the time of preparation. It should be emphasized that in some cases these data are incomplete and tentative. Data obtained subsequent to the publication of this report will undoubtedly resolve some of the problems, and may be included in later revisions of the report.

A number of government agencies and private organizations have been contacted during the preparation of this report. We wish to express our appreciation to those groups and individuals who made information available for use here.

General Terminology

The basic acoustic quantities used in this report are sound pressure level (SPL) and sound power level (PWL). These are logarithmic quantities related to the sound pressure p (measured in microbars) and the sound power W (measured in watts), respectively. The units of both SPL and PWL are decibels (db). The quantities are defined in the following table:

	Definition	Reference Quantity
SPL	$20 \log \left(\frac{p}{p_{ref}}\right)$	$p_{ref} = 0.0002$ microbar
PWL	$10 \log \left(\frac{W}{W_{ref}}\right)$	$W_{ref} = 10^{-13}$ watt

PWL is a computed quantity which expresses the noise-radiating properties of a source in a fundamental and useful way. Under standard conditions of temperature and pressure, PWL is related to the "space average" sound pressure level (SPL_{avg}) approximately by:

$$PWL \doteq SPL_{avg} + 10 \log S \qquad (1)$$

where

$$SPL_{avg} = 10 \log \left(\overline{p^2} / p_{ref}^2\right) \qquad (2)$$

where $\overline{p^2}$ is the average of the squared acoustic pressure over a surface S (in square feet) enclosing the sound source. For the case of a non-directional source, SPL_{avg} is the SPL at any point on a spherical surface S with the source at its center. Corrections for conditions other than standard temperature and pressure are discussed at the appropriate part of the report.

Other acoustic quantities of interest (such as transmission loss and noise reduction) will be defined as required in the report.

SECTION II
NOISE SOURCES

In this section of the report we will describe the various sources of noise occurring in flight vehicles. Three different general types of noise sources will be considered:

A. Noise sources associated with the vehicle power plant;
B. Noise sources associated with aerodynamic disturbances other than those generated by the power plants directly (noise caused by atmospheric turbulence or boundary layer fluctuations);
C. Noise sources associated with internal equipment, such as air-conditioning.

When a plane wave of sound is incident on a plane rigid surface, the sound pressure at the surface is twice the sound pressure in the incident wave. This situation is commonly called "pressure doubling". The actual situation encountered in measuring sound pressures at the surface of vehicle structures is not as simple as might be indicated by this example of pressure doubling. The estimation procedures given in this section give sound pressure levels associated with <u>free space</u>, that is, in the absence of any surface. As an engineering approximation we will say that when the surface on which the sound pressure level is desired is plane, 3-6 db should be added to the numbers given by the procedures in this section, and when the surface is curved, 0-3 db should be added to the free space sound pressure levels given in this section.

A. Power Plant Noise

1. Propeller Noise

Symbols Used in Propeller Noise Discussion

c	ambient velocity of sound
D	propeller diameter
f_1	blade passage frequency
f_{max}	peak of vortex noise spectrum
L_1, L_2	"partial levels" obtained from Figs 2, 3 respectively
$L_{0.7}$	projected width of propeller, defined in Fig 8
m	number of propeller blades
M_t	propeller tip Mach number
r	distance from far field measurement point to center of propeller disc
W	mechanical power to propeller
x, y, z,	cartesian coordinates with origin at center of propeller disc (see Fig 1)
ρ	ambient air density

The noise radiated by aircraft propellers has been the subject of considerable study.* The data used in the present study includes measurements made by Bolt Beranek and Newman Inc. (BBN), NACA (Langley Field), and Harvard University's wartime Electro-Acoustic Laboratory.

It is convenient to divide the observation region into two parts, which we designate "near field" and "far field". The near field consists of those observation points which are located one propeller diameter or less from the propeller plane. The far field consists of those points which are more than one

*A list of some of the important references on the subject of propeller noise is given at the end of this report.

propeller diameter from the propeller plane.

a. Near Field of Propeller Noise

The geometry of the region of interest in the near field is shown in Fig 1. x is the distance, measured from the propeller plane, along an axis parallel to the axis of rotation of the propeller. y is the distance along a line in the propeller plane, perpendicular to the blade at its point of closest passage to the measurement point P. z is the distance from the propeller tip at its point of closest passage to the measurement point P in the propeller plane. The propeller cylinder is the circular cylindrical surface whose axis is the propeller axis and whose diameter is the propeller diameter.

The near field prediction procedure given here applies only in the region outside of the propeller cylinder. (This is the region in which a fuselage would be located.) The analysis is not valid for predicting propeller noise levels directly in front of or directly behind the propeller disc, i.e., inside the propeller cylinder. The work of Ref 4 has shown that the propeller noise levels and spectrum vary markedly with radial position near the propeller disc.

The near field estimation procedure is as follows:

(1) Find the overall sound pressure level at the point of interest by adding algebraically the partial levels given in Figs 2 and 3. The partial level L_1 is determined as a function of W, the power to the propeller in horsepower, and D, the propeller diameter in feet, from Fig 2. Similarly, partial level L_2 is given by Fig 3 as a function of z/D, the dimensionless tip distance, and M_t, the propeller tip Mach number.

The free space overall SPL is given by:

$$SPL_{overall} = L_1 + L_2 + 20 \log \frac{3}{m} - 10 \log \left(\frac{^{\circ}F + 460}{528} \right) \qquad (3)$$

where m is the number of propeller blades. The analytical expression represented by Figs 2 and 3 and Eq (3) is:

$$SPL_{overall} = 20 \log W - 40 \log D - (33.4 - 24.4\ M_t) \log \left(\frac{z}{D} \right) + 36.6\ M_t + 75.8 + 20 \log \left(\frac{3}{m} \right) - 10 \log \left(\frac{^{\circ}F + 460}{528} \right) \qquad (4)$$

(2) Adjust the value found in item 1 above by using the appropriate distance x/D from the propeller plane and Fig 4. (The only data available on the variation of SPL with x/D are for a propeller tip Mach number of 0.6.)

(3) Determine the relative contributions of the vortex noise sources and rotational noise sources from Fig 5.

(4) Add on a decibel scale the rotational noise spectrum and the vortex noise spectrum. The rotational and vortex noise spectra are given in Figs 6 and 7, respectively. The blade passage frequency f_1 is:

$$f_1 = m \frac{(RPM)}{60} \qquad (5)$$

The length $L_{0.7}$ is defined geometrically in Fig 8. The resultant near field spectrum is obtained by adding Figs 6 and 7 as prescribed in Fig 5.

As examples of the use of Fig 3, Figs 9, 10, and 11 show contours of constant sound pressure in the propeller plane, for tip Mach numbers of 0.4, 0.6, and 0.8. The SPL contours are circles of constant z/D, centered at the propeller axis. The contours are drawn for 3 db increments in sound pressure level, with a reference level of zero taken arbitrarily at z/D equal to 0.1. The spacing between contours is seen to decrease rapidly as the propeller disc is approached, i.e., for small z/D. Also, the SPL decreases less rapidly with the tip distance at larger M_t than at smaller M_t.

b. Far Field of Propeller Noise

For observation points located more than about one propeller diameter from the propeller plane, a different procedure must be used for estimating the propeller noise:

(1) Calculate the overall power level (PWL) of the propeller noise from Fig 12.

(2) Obtain the "space average" sound pressure level (SPL_{avg}) by assuming spherical spreading of sound from the center of the propeller disc. Thus:

$$SPL_{avg} = PWL - 10 \log (4\pi r^2) + 10 \log \frac{\rho c}{(\rho c)_r} \qquad (6)$$

where r is the distance from the center of the propeller disc to the observation point. The last term in Eq (6) corrects for changes in ambient ρc with altitude and temperature. The quantity:

$$- 10 \log \frac{\rho c}{(\rho c)_o} \equiv \Delta B \qquad (7)$$

is plotted as a function of ambient pressure and temperature ratios in Fig 32.

(3) For the angular region from 145° to 180° measured from the forward propeller axis, apply a directivity correction of -6 to -10 db, to SPL_{avg}. This angular region corresponds to the rear of the fuselage.

(4) Use the octave band spectrum of propeller noise for the rear of the fuselage given in Fig 13. f_1 is the blade passage frequency defined in Eq (5).

2. Exhaust Noise of Internal Combustion Engines

Under certain conditions, the exhaust noise of internal combustion engines may be a significant contributor in determining the noise levels on or within an aircraft. We present an estimation procedure for obtaining the noise levels associated with this exhaust noise:

(1) Obtain the overall power level of the engine exhaust noise source from Fig 14. Fig 14 is a plot of the relation:

$$PWL = 125 + 10 \log HP \text{ db} \qquad (8)$$

where HP is the total horsepower delivered by the engine shaft to the propeller, auxiliary pumps, generators, and other equipment. The line in Fig 14 shows an experimental spread of $\pm$ 5 db.

(2) Use the spectrum shape given in Fig 15 to obtain the PWL exhaust noise spectrum. The frequency f_a is the average cylinder firing frequency of the engine.

(3) The SPL at a point a distance x from the engine exhaust can then be found from the relation:

$$SPL = PWL - 10 \log (4\pi x^2) \qquad (9)$$

where spherical divergence of sound has been assumed.

3. Turbojet Noise

Symbols Used in Turbojet Noise Discussion

D	exhaust nozzle diameter
f_{max}	peak of far field power level spectrum
ΔF	overall contour correction factor
ΔG	additional correction factor for afterburning engine
v	relative expanded jet velocity
x	axial distance from exhaust nozzle
$\Delta\phi$	angular correction factor

The field about a turbojet may be divided into two major regions -- near field and far field. The behavior of acoustical quantities such as sound pressure and particle velocity is much more complicated and consequently less well understood in the near field than in the far field. However, it is generally the near field that is of interest in the study of noise in and on aircraft. In general, points less than 75 to 100 ft distance from the jet exit nozzle lie in this near field.

We present here an estimation procedure for obtaining the overall sound pressure level and relative spectrum shape at a point in the near field of a turbojet engine. The reference contour of overall sound pressure level is given in Fig 16. The operating conditions for this reference contour are those of a contemporary turbojet engine operating at 100% rpm. The exit velocity is 1850 ft per second and the exit diameter 22 in. The near field estimation procedure may be itemized as follows:

(1) A correction factor ΔF is derived from the exit velocity of the source whose near field is to be determined by:

$$\Delta F = 80 \log \frac{v}{1850} \text{ db} \qquad (10)$$

where v is the relative jet velocity in feet per second. Figure 17 is a plot of this correction factor. v is defined as:

$$v = \frac{\text{net thrust}}{\text{mass flow}} \qquad (11)$$

(2) An angular shift $\Delta\phi$ in the contour pattern of overall SPL is obtained from Fig 18.

(3) ΔF is applied to the reference contour values of Fig 16, and the contour pattern is rotated about the exhaust nozzle as prescribed by $\Delta\phi$. Positive values of $\Delta\phi$ represent rotations away from the jet axis. The adjusted contours then form the predicted near field.

(4) The shape of the spectrum is given by Fig 19 as a function of the quantity x/D, the axial distance downstream from the jet nozzle. The peak frequency f_{max} is defined as:

$$f_{max} = 0.2 \frac{v}{D} \qquad (12)$$

This prediction procedure is to be used for turbojets operating at or near 100% rpm. For turbojets with afterburner, the following modified prediction procedure has been found to be reasonable:

(1) A correction factor ΔF is obtained from Fig 17 using the exit velocity v of the turbojet at 100% rpm (without afterburner). Another correction factor ΔG is obtained from Fig 20 using the developed thrust of the turbojet at 100% rpm.

(2) An angular shift $\Delta\phi$ in the reference contour pattern of overall SPL is obtained from Fig 18 using the exit velocity of the turbojet at 100% rpm.

(3) $\Delta F + \Delta G$ is applied to the reference contour of Fig 16, and the reference contour pattern is shifted about the exhaust nozzle as prescribed by $\Delta\phi$. The adjusted contours then form the predicted near field, where the diameter D is the engine exhaust diameter at 100% rpm.

(4) The shape of the frequency spectrum is given by Fig 19 where the peak frequency is 1/2 octave lower than the peak frequency defined for the turbojet at 100% rpm. 3 to 5 db should be added for frequencies 3 octaves or more above f_{max}.

The effects of motion and of ambient condition changes on turbojet noise are considered in Part 5 of this section.

4. Missile Noise

Symbols Used in Missile Noise Discussion

subscript a	refers to ambient quantities
c	velocity of sound
D	missile exhaust nozzle diameter
G	near field function
k	wave number
m	mass flow through exhaust nozzle

M	Mach number
subscript r	refers to missile at rest
R	distance from source to receiver
T	rocket jet temperature
v	expanded relative jet velocity
x	distance from rocket exhaust nozzle plane to measurement point
x_o	distance from rocket exhaust nozzle plane to average location of noise source of frequency f
ρ	rocket jet density
η	efficiency of conversion of mechanical power to acoustical power

The source mechanism which produces noise from the exhaust of a missile is very similar to the source mechanism involved in conventional turbojets. However, since we are generally interested in the noise along the missile surface upstream of the jet nozzle, it is convenient to give here an estimation procedure which is specialized to this case. This procedure is based on the limited amount of information now available on missile noise.

The procedure may be summarized as follows:

(1) Find the efficiency of conversion of mechanical power to acoustic power, from Fig 21. The efficiency η is given in this figure as a function of the ratio of expanded jet velocity v to ambient sound velocity c_a. The parameter describing the various lines is a ratio of jet and ambient densities and temperatures $\frac{\rho}{\rho_a}\left(\frac{T}{T_a}\right)^2$. For very large rockets it is seen that the efficiency η is expected to approach a constant value.

(2) Compute the mechanical stream power of the rocket which is given by $1/2\ mv^2$ in watts, where m is the mass flow of the rocket and v is the expanded jet velocity. In MKS units m is in kilograms/sec, and v is in ft/sec. The overall PWL of the missile noise source is then given by:

$$PWL = 10 \log \eta + 10 \log \frac{\frac{1}{2} mv^2}{10^{-13}} \qquad (13)$$

(3) Find the average source distance x_o, which is the distance from the jet nozzle to the average location of the source of frequency f. The diameter of the rocket nozzle is D. The average source distance in terms of x_o/D is given as a function of Strouhal number fD/v in Fig 22.

(4) Compute the source-to-receiver distance R appropriate to the geometry. For cases in which the exhaust stream extends directly back of the missile along the longitudinal axis of the missile:

$$R = x + x_o \qquad (14)$$

where x is the distance from the rocket exhaust nozzle plane to the observation point, and x_o has been obtained in Item 3.

(5) Find the near field function $10 \log G^2 (kR)$ from Fig 23, where:

$$k = \frac{2\pi f}{c_a} \qquad (15)$$

(6) Obtain the sound pressure level at the desired point from the expression:

$$SPL = SPL_o - 20 \log R + 10 \log G^2 \qquad (16)$$

where the reference sound pressure level SPL_o is given relative to the overall power level in Fig 24.

(7) The effects of motion may be estimated by adding to the above equation the quantity $20 \log \rho / [\rho_r (1 - M)]$:

$$SPL_{flight} = SPL + 20 \log \frac{\rho_a}{\rho_{ar} (1 - M)} \qquad (17)$$

where ρ_{ar} is the ambient density with the missile at rest, and ρ_a is the ambient density with the missile in motion. It is assumed in this equation that the relative velocity of the exhaust gases is approximately constant. This assumption has been found reasonable for certain classes of missiles. A more detailed procedure for estimating the effects of motion and of ambient condition changes on rocket noise is given in Part 5 of this section.

The spectrum shown in Fig 24 is somewhat broader than the conventional turbojet spectrum because of the multiple nozzle configuration usually found in large missiles. The spectrum of Fig 24 is based on data from a rocket with two nozzles, each about 4 ft in diameter, with centers 10 ft apart. Smaller dimensions would lead to a somewhat narrower spectrum.

5. Effects of Forward Motion and Ambient Condition Changes on Turbojet and Missile Noise

subscript a	refers to ambient quantities
A	effective open area of exhaust nozzle
c	velocity of sound
F	gross thrust
F_{net}	net thrust
subscript j	refers to jet quantities
m	mass flow through exhaust nozzle
M	Mach number
subscript o	refers to reference quantities
p	sound pressure
P	static pressure
T	temperature
v	expanded relative jet velocity
v_1	forward velocity
w	sound power
ρ	density
ϕ	velocity potential

a. Effects of Forward Motion

(1) Simplified Procedure

We consider first the special case of constant altitude. Figure 25 shows the engine operation parameters needed to describe the situation. Net thrust and mass flow (relative to static values) are given as functions of forward speed. The data are from the G. E. Aircraft Propulsion Data Book, 1957 Edition, and apply to a contemporary turbojet engine that can generate about 9000 lbs gross thrust at sea level at 100% rpm. For the case being considered, the engine is at 92.7% rpm and at sea level.

The change in overall sound power level (ΔPWL) due to changes in operating conditions radiated by a subsonic jet aircraft is:

$$\Delta PWL = 70 \log \frac{v}{v_o} + 10 \log \frac{m}{m_o} + 10 \log \frac{T_j}{T_{jo}} + 35 \log \frac{T_{ao}}{T_a} \qquad (18)$$

where m is the total mass flow through the exhaust nozzle, T is temperature, and the subscripts o, a and j refer to reference, ambient, and jet conditions, respectively. The relative velocity v is related to gross thrust F and forward velocity v_1, or net thrust F_{net}, by:

$$v = \frac{F}{m} - v_1 = \frac{F_{net}}{m} \qquad (19)$$

Equation (18) will be derived later in this section.

The information contained in Fig 25 can be combined with Eq (18) to obtain an estimate of the effects of forward velocity. An additional factor, concerning the propagation of sound in a moving medium, must also be taken into account. (This factor is considered in detail later in this section.) The resulting ΔSPL is given in Fig 26 as a function of forward speed. The jet temperature T_j is assumed to vary less than 10% over the range of speeds considered. ΔSPL is given for several typical locations of the observation point.

It should be noted that, at high subsonic velocities and in certain frequency ranges, the turbojet noise we are considering here will be masked by boundary layer noise or, in some cases, equipment noise. The extent of this masking can be determined only by considering individual cases.

Derivation of ΔPWL

The jet fluid of a turbojet engine has essentially the same molecular weight as the ambient fluid. Then, sound power w has been found to be proportional to:

$$w \alpha \frac{\rho_a A v^8}{c_a^5} \tag{20}$$

where ρ is density, A is effective open area of the jet nozzle, c is the velocity of sound, and v is the velocity defined in Eq (19). It is now assumed that the ideal gas law is valid and that the static pressure in the jet stream equals the ambient pressure. The following proportionalities then hold:

$$m \alpha \rho_j A v \tag{21}$$

$$c_a \alpha T_a^{\frac{1}{2}} \tag{22}$$

$$\rho_a \alpha \frac{P_a}{T_a} \tag{23}$$

$$\rho_j \alpha \frac{P_a}{T_j} \tag{24}$$

where P is pressure. Equations (21) through (24) may be substituted into Eq (20) to obtain:

$$\Delta PWL = 10 \log \frac{w}{w_o} = 70 \log \frac{v}{v_o} + 10 \log \frac{m}{m_o} + 10 \log \frac{T_j}{T_{jo}} + 35 \log \frac{T_{ao}}{T_a} \tag{18}$$

ΔPWL is plotted as a function of $\frac{m\ T_j}{m_o T_{jo}}\ (\frac{v}{v_o})^7$, for various values of the ambient temperature, in Fig 27.

The case of very large rocket engines must be considered separately. For such noise sources the sound power radiated is proportional to:

$$w \alpha mv^2 \tag{25}$$

and ΔPWL becomes

$$\Delta PWL = 10 \log \frac{m}{m_o} + 20 \log \frac{v}{v_o} \tag{26}$$

ΔPWL is plotted for this case as a function of $\frac{v}{v_o}$ for various values of the mass flow ratio $\frac{m}{m_o}$ in Fig 28. In general, because of the lower power dependence on v for the case of large rockets, a larger reduction in noise with forward speed will be found for contemporary turbojets than for large rockets.

Sound Propagation in a Moving Medium

In order to estimate the effects of motion on the noise field, it is necessary to select a simple model for mathematical analysis. The model chosen consists of a simple monopole source and receiver moving together rigidly at a constant subsonic velocity along the x-axis of a Cartesian coordinate system. According to Blokhintsev[1], the velocity potential ϕ for a monopole is given by:

$$\phi = \frac{\mathcal{F}\left(t - \frac{R}{c}\right)}{R^* \sqrt{1 - M^2}} \tag{27}$$

---

(1) "Acoustic of a Nonhomogeneous Moving Medium", D. I. Blokhintsev (translated as NACA TM 1399, pp 80-85).

where $\mathcal{F}(t)$ is the time dependence of the source, M is the Mach number of the source-receiver system, c is the velocity of sound, and:

$$R = \frac{M\xi + \sqrt{\xi^2 + (1-M^2)\,(y^2 + z^2)}}{1 - M^2} \tag{28}$$

$$R^* = \frac{\sqrt{\xi^2 + (1-M^2)\,(y^2 + z^2)}}{\sqrt{1 - M^2}} \tag{29}$$

$$\xi = x - v_1\, t \tag{30}$$

$$v_1 = Mc \tag{31}$$

Sound pressure p is related to ϕ by:

$$p = \rho \left(\frac{\partial \phi}{\partial t} - v_1 \frac{\partial \phi}{\partial \xi} \right) \tag{32}$$

which yields:

$$p \simeq \rho \frac{\dot{\mathcal{F}}(t - \frac{R}{c})}{R^* (1-M^2)^{3/2}} \left\{ 1 + \frac{M\xi}{\left[\xi^2 + (1-M^2)\,(y^2 + z^2)\right]^{1/2}} \right\} \tag{33}$$

Figure 29 gives the partial correction factor to PWL for propagation in a moving medium, as a function of Mach number, for typical observation orientations. It is important to note that the ratio of sound power radiated to mechanical stream power should not exceed approximately 1%.

Oestreicher[2] has shown that a dipole source in a subsonic stream acts qualitatively similar to the monopole as indicated in Fig 29.

b. Effects of Ambient Condition Changes

(1) Simplified Procedure

When in flight, a jet aircraft encounters ambient conditions which may vary over a significant range. It is convenient to consider here the special case of constant forward speed. Figure 30 shows the engine operation parameters needed to describe the situation. This figure gives the net thrust or mass flow (relative to sea level values) as a function of altitude. The information applies to a contemporary turbojet engine that can generate about 9,000 lbs gross thrust at 100% rpm at sea level. The data are based on a constant 92.7% rpm and 550 knots. The curve is adapted from the G. E. Aircraft Propulsion Data Book, 1957 Edition.

Equation (18) for the change in PWL radiated by a subsonic jet aircraft was derived earlier, in considering the effects of forward motion. It is also useful in the present study of ambient conditions:

$$\Delta PWL = 70 \log \frac{v}{v_o} + 10 \log \frac{m}{m_o} + 10 \log \frac{T_j}{T_{jo}} + 35 \log \frac{T_{ao}}{T_a} \qquad (18)$$

(2) H. L. Oestreicher, J. Acoust. Soc. Am. 29, 1223 (1957)

where m is the mass flow through the engine, T is temperature, and the relative velocity v is related to gross thrust F and forward velocity v_1, or net thrust F_{net}, by:

$$v = \frac{F}{m} - v_1 = \frac{F_{net}}{m} \tag{19}$$

The information contained in Fig 30 can be combined with Eq (18) and the description of the ICAO Standard Atmosphere (NACA TN 3182) to obtain an estimate of the effects of ambient conditions. Figure 31 gives the resulting ΔSPL as a function of altitude, for several values of the jet temperature ratio. The information contained in Fig 31 is for constant rpm and speed, as noted earlier. The combination of Fig 26 (ΔSPL as a function of speed, at constant altitude) and Fig 31 (ΔSPL as a function of altitude, at constant speed) forms an estimation procedure for changes in noise radiated by contemporary turbojet engines.

(2) Generalized Procedure

It is useful to consider changes in noise radiated by a jet in a general form. Figure 27 gives ΔPWL for contemporary turbojets (Eq 18), and Fig 28 gives ΔPWL for large rocket engines (Eq 26).

The relation between PWL and SPL must now be considered in general. It may be written:

$$\Delta SPL = \Delta PWL - \Delta B \tag{34}$$

where

$$\Delta B = 10 \log \frac{\rho_{ao}\, c_{ao}}{\rho_a\, c_a} = 10 \log \frac{P_{ao}}{P_a} + 5 \log \frac{T_a}{T_{ao}} \tag{35}$$

In obtaining Eq (35) we have assumed the validity of the ideal gas law. Equation (35) is plotted in Fig 32. This factor must be taken into account when the quantity $\rho_a c_a$ changes, for example, for a change of altitude.

We can summarize the generalized estimation procedure for changes in jet noise by listing the charts required for each type of change:

For effects of	Use Figs
Change of ambient conditions on	
1) contemporary turbojet	27, 32
2) large rocket	28, 32
Change of forward speed on	
1) contemporary turbojet	27, 29
2) large rocket	28, 29

B. Aerodynamic Noise

1. Boundary Layer Noise

Symbols Used in Boundary Layer Noise Discussion

d	distance from leading edge of skin to observation point
f	frequency
f_{max}	peak of boundary layer noise spectrum
p	sound pressure
Re	Reynolds number
Q	free stream dynamic pressure
S	Strouhal number
V	free stream velocity
δ	boundary layer thickness
ν	kinematic viscosity

The high speed flow occurring over an aircraft surface generates a turbulent boundary layer in a region near the surface. The fluctuating pressures exerted on the surface by this layer are convected along with the flow and set up motion of the aircraft skin.

Recent studies of boundary layer pressure fluctuations include subsonic measurements on wind tunnel surfaces, on airplane wings, and inside airplane cabins. In addition, theoretical studies have been made recently on pressure fluctuations in subsonic boundary layers.[1/] To date, however, completed studies on supersonic boundary layers have not been made available.

---

1. R. H. Kraichnan, J. Acoust. Soc. Am. 29, 65 (1957).

The results of the measurements inside cabins of subsonic aircraft are shown in Fig 33. The ordinate of Fig 33 is 20 log p/Q, where p is the root mean square boundary layer pressure and Q is the free stream dynamic pressure. The boundary pressure has been approximated by correcting the cabin measurements for the pressure transmission properties of the aircraft skin (see section III). The abscissa of Fig 33 is the Strouhal number, defined as:

$$S = f \frac{\delta}{V} \tag{36}$$

where f is the frequency, δ is the boundary layer thickness, and V is the free stream velocity. Fig 33 shows that the boundary layer pressure fluctuations exhibit a broad spectrum which reaches a maximum at S approximately equal to 0.4 for octave band data. We use this figure as the basis for our procedure for estimating boundary layer surface pressures.

Measurements of boundary layer pressure fluctuations on wind tunnel and airplane wing surfaces are generally made with flush mounted microphones. These measurements usually give 20 log p/Q values about 5 to 10 db lower than those shown in Fig 33. These differences are generally believed to be caused by cancellation of some of the fluctuations over the microphone sensing area. Consequently, the information given in Fig 33 is believed to be more directly applicable for use in our estimation procedure. The estimation procedure is as follows:

(1) Calculate the free stream dynamic pressure Q for the conditions of interest. Figure 34 gives Q as a function of Mach number and altitude.

(2) Obtain the overall sound pressure level from the expression:

$$SPL = 20 \log Q + 86 \text{ db} \quad (37)$$

where SPL is the level of the overall pressure fluctuations at the surface (relative to 0.0002 microbar), and Q is the free stream dynamic pressure in lbs/sq ft obtained in Item I.

(3) Estimate the boundary layer thickness δ from the expression:

$$\frac{\delta}{d} = 0.129(Re_d)^{-1/7} \quad (38)$$

where d is the distance in feet from the leading edge of the skin to the observation point. Eq (38) is plotted in Fig 35. Reynolds number Re is defined as:

$$Re = \frac{Vd}{\nu} \quad (39)$$

where ν is the local kinematic viscosity in ft^2/sec. For a typical present-day commercial transport a typical value of δ might be 0.2 ft.

(4) Determine the maximum of the boundary layer noise spectrum f_{max} from:

$$f_{max} = 0.4 \frac{V}{\delta} \text{ cps} \quad (40)$$

where f_{max} is the maximum of the octave band spectrum, V is the stream velocity outside the boundary layer in ft/sec, and δ is obtained in

Item 3. Use the spectrum shape given in Fig 33. The overall SPL calculated from Eq 37 is approximately 5 db greater than the octave band SPL at f_{max}.

Of course, the value of the boundary layer surface pressure in any particular situation will be affected by the aircraft geometry, the position of the measurement location along the aircraft, the aircraft altitude, protuberances near the measurement position, and similar items. The estimation procedure given here is intended to represent an average over the known information.

In the absence of any organized data for supersonic boundary layers, we propose that the estimation procedure given here be used for both subsonic and supersonic conditions. It should always be noted, however, that this procedure is based on data taken under subsonic conditions only.

2. Pressure Fluctuations Caused by Atmospheric Turbulence

Another possible noise source of aerodynamic origin is the variations in ambient velocity (and temperature) that occur in the atmosphere. In passing through these fluctuations, a rapidly moving vehicle will encounter pressure fluctuations. Under operating conditions of present-day vehicles, noise from these fluctuations has not yet been identified. However, these fluctuations may become important in higher performance vehicles of the future, and therefore a brief discussion of these fluctuations is given here. Attention is restricted to variations in ambient velocity, but the arguments may be extended to include variations in temperature.

The primary purpose of this discussion is to point out the existence of this potential noise source and to make some rough estimates of the magnitude of the noise.

Significance of the Problem

Fluctuations in dynamic pressure due to atmospheric turbulence may contribute significantly to the acoustic environment on and in high-speed flight vehicles. The dynamic pressure q of the flow past a vehicle is

$$q = \frac{1}{2} \rho U^2 \qquad (41)$$

where U = flight velocity
ρ = density of ambient air

The dynamic pressure q acts at forward flow stagnation points on an aircraft. In addition, a fraction of this pressure, either positive or negative, can be observed at almost all points on the aircraft surface. Thus, it seems reasonable to expect that fluctuations in q will be felt, at least partially, almost everywhere on the aircraft. (See R. I. Cole, "Pressure Distributions on Bodies of Revolution at Subsonic and Transonic Speeds" NACA RM L52D30 (1952); this report contains a good bibliography. See also texts on fluid dynamics concerning pressure distributions on bodies in a flow.)

Lift and drag forces are directly related to q through lift and drag coefficients. Thus, we expect these forces to vary with fluctuations in q. Time varying forces on the aircraft will result, and certain modes of vibration may be excited.

The flow into ram-air intakes and engine inlets is dependent on the dynamic pressure. Fluctuations in q will thus modulate the inlet flow. We do not know whether or not this mechanism can trigger or excite an instability in the aircraft powerplant and its supply ducts. However, the possibility exists.

An obvious effect of fluctuations in dynamic pressure is the local excitation of the aircraft skin. This excitation is of interest just as airborne noise or boundary-layer noise is. We now estimate the pressure magnitudes and frequencies involved.

Noise Spectrum

In regions of turbulence the local turbulent velocity component, v, acts as a perturbation of the velocity U. A fluctuation p in dynamic pressure is thereby generated (neglecting density variations):

$$p = \delta q = \rho U \delta U = \rho U v \tag{42}$$

Actually the turbulent velocity is a function of turbulence scale, ℓ. Thus, $v = v(\ell)$, and $p = p(\ell)$. The turbulence scale and the frequency of the disturbance felt by the aircraft are related as follows:

$$f = \frac{U}{\ell} \tag{43}$$

An idea of the frequencies involved at several flight Mach numbers can be had from the following table:

Turbulence Scale, ℓ (ft)	Approximate Frequency of Pressure Fluctuations, cps		
	M = 1	M = 3	M = 10
1000	1	3	10
100	10	30	100
10	100	300	1000

In this "acoustic" study we cannot be concerned with disturbances of arbitrarily low frequency. Even if we limit our interest to frequencies above 3 cps, or perhaps 10 cps, we may find that significant pressures are associated with very high flight speeds.

The fluctuating pressure, Eq (1), may be related to the dynamic pressure:

$$\frac{p}{q} = \frac{\rho U v}{\frac{1}{2}\rho U^2} = 2\,\frac{v}{U} \qquad (44)$$

For high subsonic flight current estimates of the magnitude of boundary-layer pressure fluctuations are of the order of 10^{-3} q to 3 x 10^{-3} q.

In order that the fluctuating pressures generated by atmospheric turbulence be comparable to these boundary layer pressure fluctuations, we would require

$$v \triangleq 10^{-3}\,U$$

or, for near-sonic flight,

$$v \doteq 1 \text{ ft/sec}$$

This value appears to be in line with the experimental findings of NACA.*

An alternate expression of the magnitude of the pressure fluctuations is

$$\frac{p}{P_a} = \frac{\rho U v}{\rho c^2/\gamma} = \gamma \frac{U}{c} \frac{v}{c} = \gamma M \frac{v}{c} \tag{45}$$

Here

P_a = ambient pressure at altitude
$= \rho c^2/\gamma$
c = speed of sound (ambient)
γ = ratio of specific heats
$= 1.4$ for air
$M = U/c$ = flight Mach number

For high subsonic flight ($M = 0.7$)

$$\frac{p}{P_a} \doteq \frac{v}{c} \tag{46}$$

and we have, approximately, for $c \doteq 10^3$ ft/sec,

v (ft/sec)	p
1	$10^{-3}\ P_a$
10	$10^{-2}\ P_a$

*H. L. Crane and R. G. Chilton, NACA TN 3702 (1956)

The following table indicates the order of magnitude of the sound pressure levels expected at various altitudes for $v \doteq 10$ ft/sec and $M \doteq 1$ ($p_{ref} = 0.0002$ microbar):

Altitude (ft)	P_a (μ bar)	20 log $\frac{P_a}{p_{ref}}$ (db)	20 log $\frac{10^{-2}P}{p_{ref}}$ (db)
0	10^6	194	154
20,000	4.6×10^5	187	147
50,000	1.1×10^5	175	135
100,000	1.1×10^4	155	115

The pressures estimated above represent the maximum values expected. On some parts of the vehicle surface the pressure fluctuations will probably be 15-20 db lower. As mentioned earlier, experience with future vehicles will indicate the actual importance of this potential noise source and will provide data for improving these preliminary estimates.

C. Noise of Internal Equipment

Under certain conditions, the mechanical equipment located within aircraft, such as air conditioning, pressurization equipment, fans, etc., may make significant contributions to the noise levels within the aircraft. The many different types of such mechanical equipment, and the many possible uses of acoustical absorbing material within the aircraft, make an analytical study of this problem extremely difficult. Therefore, the approach in this part of the report will be to present measurements of noise within aircraft. These data are grouped by the type of aircraft.

Figure 36 is the range of typical sound pressure levels measured in the passenger compartment of twin reciprocating engine business aircraft under cruise conditions. Figures 37 through 42 give similar information measured in commercial aircraft. Data taken on the Convair 440, Viscount, Super-G Constellation, Stratocruiser, and Caravelle are included in these figures.

In the case of military aircraft measurements are not as readily available as the case of commercial aircraft. In particular, measurements in supersonic aircraft have not been released, although they are in existence. We must therefore confine our interest in military aircraft to subsonic planes.

Figure 43 gives the range of typical sound pressure levels measured in the cockpits of subsonic jet bombers. Figure 44 gives similar information for the cockpits of subsonic jet fighters. It should be pointed out that these levels were measured in smooth level flight. Under other operating conditions, for example, with gear, flaps, or speed brakes extended, the levels will in general be higher than those given in Figs 43 and 44. Noise from the extension of speed brakes, etc. will, in general, affect the higher frequencies more than the lower frequencies.

Preliminary observations indicate that mechanical equipment noise is the predominant noise source at all frequencies in contemporary high performance jet aircraft. In contemporary propeller-driven aircraft, mechanical equipment noise contributes primarily to the high frequencies.

In the absence of further data we propose that, in the frequency ranges in which mechanical equipment noise is significant,

the information in Figs 36 through 44 be used to estimate the noise from internal mechanical equipment in aircraft similar to those described in these figures. We propose also that, for newer aircraft than described in these figures, the noise levels be scaled by the mechanical power supplied to the principal mechanical equipment within the aircraft. Thus, for an aircraft utilizing mechanical equipment twice as large as the corresponding aircraft described here, the estimated internal noise levels would be 3 db higher than those given here for the corresponding aircraft.

It must be borne in mind that the noise levels due to the internal equipment must always be added to those from the power plant and from boundary layer surface fluctuations, in order to find the total noise levels expected within an aircraft. In certain cases it may be convenient to use the information in Figs 36 through 44 to scale the power plant or boundary layer noise contributions, according to the procedures given in Parts A and B of this section. Such a scaling avoids estimating the noise reduction properties of the aircraft structure, but requires that we know the frequency ranges in which power plant noise and boundary layer noise are significant. The relative contributions of power plant noise and boundary layer noise can be determined, for the particular operating conditions of interest, from the procedures of Parts A and B of this section.

The noise of certain types of internal equipment may be associated with a jet of air in a reverberant space, such as a cockpit or an equipment bay. The following procedure permits estimates of this noise:

1. Calculate the mechanical power in the air jet stream, W, in watts.

2. Using an efficiency of conversion of mechanical power to acoustic power of 6×10^{-5} (see Fig 21), obtain the overall PWL of the jet from:

$$PWL = 10 \log \frac{W}{10^{-13}} - 42 = 10 \log W + 88 \qquad (47)$$

3. Use Fig 45 for the shape of the PWL spectrum. The maximum of the jet noise spectrum f_{max} is defined by:

$$f_{max} = 0.2 \frac{V}{D} \qquad (48)$$

where V is the jet exit velocity and D is the nozzle diameter or the smaller dimension of the exhaust nozzle. The conversion from PWL to SPL appropriate to reverberant spaces are discussed in detail in section IV.

SECTION III
ESTIMATION OF PANEL TRANSMISSION LOSS

In this report we make use of the quantity called acoustic transmission loss (TL) in describing the noise-transmitting properties of a given panel or structure. The transmission loss of a structure is customarily defined as follows*:

$$TL = 10 \log \frac{1}{\tau} = 10 \log \frac{I_1}{I_2} \qquad (49)$$

where $\tau = \frac{I_2}{I_1}$ is the transmission coefficient, that is, the ratio of the transmitted intensity I_2 to the incident intensity I_1. The transmitted intensity I_2 is determined as though no reflections take place on the receiving side of the panel. The effects of the receiving space on the sound field must be considered separately. (See Section IV).

Transmission loss is defined as above for plane waves. In a plane wave $I = \frac{P^2}{\rho c}$ and therefore Eq (49) may be written:

$$TL = 10 \log \frac{P_1^2/\rho_1 c_1}{P_2^2/\rho_2 c_2} \qquad (50)$$

where P is the root-mean-square acoustic pressure in the incident or transmitted wave, and

ρc is the characteristic impedance of the air adjacent to the panel on the receiving side or on the side of incidence.

---

*Logarithms to the base 10 are used throughout this report.

For the particular, but very frequently encountered, case in which the ambient conditions are the same on both sides of the panel, we have $\rho_1 c_1 = \rho_2 c_2$, and therefore:

$$TL = 10 \log \frac{p_1^2}{p_2^2} \qquad (51)$$

It is useful for our purposes to interpret TL in terms of the pressures in the acoustic waves, principally because our concern with noise is in terms of its pressure rather than its intensity. That is, questions of structural fatigue, equipment malfunction, hearing loss to personnel, and annoyance are related more nearly to acoustic pressure than to acoustic intensity.

Note that when we speak of "an incident acoustic wave", we mean the acoustic wave from the source as this wave would exist in free space before the panel is introduced. That is, the pressure in the incident wave does not include a pressure increase at the surface of the panel due to wave reflection. Thus, we may expect to use our values of transmission loss directly with the free-field source acoustic pressures as estimated according to the procedures in Section II. The cases of boundary-layer pressures and other fluctuating pressures of aerodynamic origin are somewhat special in that these pressures exist at the surface of a flight vehicle. These special cases are discussed later in this section.

Transmission loss is a semi-basic property of a given panel, that is, in many instances the TL of a panel may be specified independent of the situation in which the panel is to be used. We do, however, allow the TL to be a function of the angle of incidence of the forcing sound wave. Moreover, the TL is

actually a function of the characteristic impedance of the air, on both the transmitting and receiving sides of the panel. In addition, for incident sound fields other than plane-wave fields, we find in some cases that the TL, when defined in terms of transmitted intensity relative to incident intensity, no longer has the form that it has for plane waves.

A more basic property of a panel is its transmission impedance, which relates the acoustic pressure difference across the panel to the local panel velocity. While the transmission impedance is more basic than TL, it is also considerably more complicated to use in the cases where it would add accuracy to the solution of a problem. Therefore, as a compromise between complexity and usefulness, we use TL in this report.

The introductory discussion in Section IV indicates how we develop a value of noise reduction (NR) for a panel whose TL we have estimated. The noise reduction is then the quantity that we use directly in determining the sound pressure level in a receiving space behind a panel.

The values of TL that we estimate using the procedures presented in Section III are assumed to be for reference ambient conditions on both sides of the panel. These ambient conditions are room temperature and sea level pressure. In Part C of Section IV we will consider the corrections due to changes in ambient condition. We assume that the panels are surrounded by air. Other corrections would be required for a panel in contact with other gases. These corrections can be derived from the material in Part C of Section IV.

A. General Approach and Summary of Procedures

In estimating the acoustic transmission loss of a given aircraft structure, we divide the frequency range of interest into a number of regions. We estimate the transmission loss in each region by appropriate procedures, and then join the estimates.

A general structure or panel can have the following types of behavior in frequency regions listed in order, running from low frequencies to high frequencies:

Region a. Panel motion controlled by stiffness of panel and supporting structure

Region b. Panel motion subject to major panel or structure resonances

Region c. Panel motion controlled principally by panel surface weight (mass-law region)

Region d. Panel motion affected by coincidence effect (transmission loss drops below mass law)

Region e. Panel motion governed by panel damping in recovery from coincidence "dip"

Region f. Panel motion at highest frequencies governed by damping and panel-size effects.

Not every panel or structure will exhibit all of the types of behavior listed above. The various regions can overlap or can fall outside the frequency range of interest.

Summary of Procedures for Estimating TL

The following steps are involved in estimating the TL of a panel (These procedures are illustrated in Figure 49):

1. Preparatory to estimating the transmission loss, calculate the following quantities for the panel under consideration:

   a) Frequencies at which major panel or structural resonances are expected. The resonances of interest are those for which the panel has a large average displacement. See Section III-B.

   b) Mass-law transmission loss for 45° angle of incidence at 400 cps, as given by Fig 46 or by the following equation:

$$TL_{400} = 21 + 20 \log g \text{ (db)} \qquad (52)$$

   where g = average panel surface weight, lbs/sq ft^2. Eq (52) is valid for g > 0.25 lbs/ft^2. A curve showing mass-law TL for the panel should be drawn based on the information in Fig 46. This 45° mass-law curve is the reference curve used in several of our procedures for estimating TL.

   c) Coincidence frequency f_c, the frequency at which the velocity of bending waves in the panel equals the velocity of sound in the space on the receiving side of the panel. See Section III-H. In certain cases, for example, with plates stiffened by longitudinal members, it is possible to have two coincidence frequencies: a lower coincidence corresponding to the velocity of bending waves in the total structure, including stiffeners, and an upper coincidence frequency determined by the velocity of bending waves in the plate (skin) alone.

d) An estimate of the damping of the panel in the frequency range just above coincidence. The degree of damping of a panel is described in terms of a damping factor, η. This damping factor is directly associated with the sharpness or "Q" of the panel resonances, with the decay rate of a given disturbance in the panel, with the attenuation of bending waves in the panel, etc. We specify three degrees of damping as follows:

Damping Category	Approximate Damping Factor, η
Low	0.007
Medium	0.03
High	0.1

Panels to which no damping materials have been applied are expected to fall into the category "low damping". In order that a panel have "high damping", it must either be of rather special construction, or must be heavily treated with damping material. The category "high damping" represents a probable practical upper limit of damping in aircraft structures. Panels having only a moderate amount of damping material applied are expected to fall into the category "medium damping". Untreated panels with rather "lossy" edge conditions will probably also fall into the medium damping category.

2. Low Frequency Region Below Major Resonance

Estimate the TL at a frequency $\frac{f_1}{4}$ in the stiffness-controlled region below the first major panel resonance from the following relation:

$$TL\left(\frac{f_1}{4}\text{ , stiffness}\right) = 20 \log (gf_1) - 29 \qquad (53)$$

where

g = panel surface weight (lbs/ft^2)

f_1 = fundamental resonance frequency (cps)

Estimate the TL in the region below resonance by passing a line with slope -6 db per octave through the TL value estimated at $\frac{f_1}{4}$.

An equivalent alternate procedure for determining the TL at $\frac{f_1}{4}$ is the following:

a) Mark the frequency f_1, the fundamental resonance frequency of the panel, on the reference, 45° mass law chart mentioned in Item 1b above.

b) Choose the TL at $\frac{f_1}{4}$ to be 2 db higher than the 45° mass law attenuation at f_1.

c) Pass a line with slope -6 db per octave through the point at $\frac{f_1}{4}$.

3. Medium and High Frequency Regions Above Major Resonances.

Estimate the transmission loss at medium and high frequencies above the major panel and structural resonances as follows:

a) In the region near and above f_c, the sound coincidence frequency, use the curves in Fig 47 to estimate TL; refer to the damping estimate of Item 1d above.

b) At frequencies above about 5 f_c adjust the estimated TL curve to pass through an appropriate part of the shaded region in Fig 47. The larger the panel (with respect to the wavelength of bending waves in the panel) the higher the curve should lie in the shaded region. Likewise, the effect of high panel damping would shift our estimate upward in the shaded region.

c) In the frequency range starting about two octaves above the major panel resonance and extending up to about 0.5 f_c, estimate the TL to be the reference mass-law TL for 45° incidence. Join this part of the estimated TL curve smoothly to the segment of the curve described in a) above.

4. Region of Major Structural Resonances

Estimate a TL curve that will join the low-frequency TL estimated in 2 above to the medium-frequency TL estimated in 3 above choosing a range of values as follows:

a) Use the reference TL line as an upper limit, except where the TL rises to join the low-frequency estimates.

b) As a lower limit, use the minimum value given in Fig 48 according to the amount of damping estimated for the major resonances. The abscissa parameter, TL_m, is the value of the reference, 45° mass-law TL curve at f_1, the fundamental resonance frequency. See Section III-B for further discussion of minimum TL at resonance.

B. Panel Motion as a Function of Frequency

1. Panel Transmission Loss in the Stiffness-Controlled Region Below Major Resonance

To the best of our knowledge, the problem of stiffness-controlled transmission loss of panels below the first major panel resonance has been a practically unexplored field. Nevertheless, the problem can be an important one for certain types of aircraft structures at very low frequencies. It is possible to calculate the approximate stiffness-controlled TL of certain very simple flat panels. The estimating scheme that we present here for discrete-frequency excitation of flat panels is based on the results of such calculations. The scheme is, however, untested in detail, and therefore must be regarded as tentative.

When panel curvature is introduced, the determination of transmission loss becomes exceedingly complex. We may make a rough grouping of curved panels into:

a) Curved panels forming an integral part of a large curved structure, e.g., a cylindrical fuselage; and

b) Curved panels that are sufficiently constrained or otherwise isolated from adjacent structures, so that these panels may be said to behave practically as independent panels.

In the former case it is obvious that the panel motion must be strongly dependent on the overall motion of the structure of which the panel is a part. It is becoming increasingly evident that at the lower frequencies (say below about 300 cps

for a 10-ft-diameter aircraft fuselage) stresses in directions parallel (or tangential) to the panel surfaces become extremely important. The state of our understanding of the behavior of complex structures with curved surfaces is not sufficiently advanced for us to present a general scheme for estimating transmission loss for such structures at low frequencies.

However, in the case of curved panels that are more or less independent of adjacent panels, we propose as a first approximation the tentative scheme for flat panels as an estimating scheme. As the scheme for flat panels is tentative, its extension to curved panels is even more so. It may, however, serve as a starting point in discussing the behavior of such panels.

We have calculated the effective stiffness for uniaxial bending of a flat plate clamped at its ends and unconstrained at its two sides. This stiffness is the ratio of a uniform pressure to the average panel displacement. As such, this stiffness can be used directly to determine the acoustic transmission loss of such a panel where the TL is completely controlled by stiffness.

For this same flat-panel structure we have calculated the fundamental resonance frequency. This resonance frequency depends on the surface mass of the panel and on the same grouping of parameters that appears in the expression for average stiffness. The resulting situation is somewhat parallel to that for a simple mass-on-a-spring configuration, where the mass and the spring stiffness determine the resonance frequency uniquely.

We may say that only a fraction, s, of the total surface mass of the panel participates fully in the motion at resonance, that is:

$$m_{effective} = s\ m \qquad (54)$$

For the panel configuration that we have chosen to study, we have expressed the average panel stiffness in terms of the resonance frequency and the effective surface mass. We expect that at a frequency two octaves below the fundamental frequency, f_1, the panel motion will be stiffness-limited. The resonance frequency and the effective surface mass combine in such a way as to give us the following relation at a frequency $\frac{f_1}{4}$:

$$TL\ \frac{f_1}{4},\ \text{stiffness} = TL\ (f_1, .45^\circ\ \text{mass law}) + 10 \log s^2 + 15 \qquad (55)$$

where:

$TL\ (f_1, 45^\circ\ \text{mass law})$ is the mass-law transmission loss for 45° incidence that would be calculated at a frequency equal to the resonance frequency, considering the total surface mass.

Our calculations indicate that for the panel that was analyzed, a value of s a little greater than 0.2 seems appropriate. Using this value of s we obtain the following tentative relation for the stiffness-limited transmission loss of a panel at a frequency two octaves below its fundamental resonance:

$$TL\left(\frac{f_1}{4},\ \text{stiffness}\right) = TL\ (f_1, 45^\circ\ \text{mass law}) + 2$$

$$= 20 \log (gf_1) - 29 \qquad (56)$$

where:

g is the total surface weight of the panel (lbs/sq ft)

f_1 is the fundamental resonance frequency.

Information for use in estimating the fundamental resonance frequency for flat panels of various shapes is presented in Appendix A, "Vibration Frequency Charts".

In extending our scheme for flat plates to "independent" curved plates ("type b" discussed earlier), we reason as follows: Curvature of the plate increases the plate stiffness. Curvature also raises the fundamental resonance frequency, thus a panel stiffness estimated on the basis of the fundamental resonance frequency will increase as curvature is introduced into the panel. The assumption that we make is that the relation between stiffness and resonance frequency for curved plates is about the same as that for flat plates. The appropriateness of this assumption remains to be tested. It is, however, a step in the right direction.

The estimation of the fundamental resonance frequency for a curved panel is not a simple matter. Fig 50 shows data presented by Regier on one particular panel, indicating the upward shift in resonance frequencies due to curvature. The data in the figure are for an aluminum alloy panel 11 x 13 inches in size, 0.032 in. thick. The curved panels were cylindrically curved with a radius of curvature of 4 feet. Although not directly comparable, the two modes in Fig 50 that should most likely indicate the upward shift in "fundamental" panel resonance are the 100 cps resonance for the flat panel and the 350 cps resonance for the curved panel. The 280 cps mode for the curved panel actually would have zero average displacement, and would not be the most significant from the noise transmission point of view.

We expect that the stiffening effects of internal pressurization may be lumped with other stiffening effects. Thus, when estimates of the fundamental resonance frequency are available

for panels subject to pressurization, these estimates should be used in determining the stiffness controlled transmission loss.

2. Effective TL for Broad-band Noise at Panel Resonance.

The procedure given above for panel TL at resonance has been based on the assumption that the noise source has a well-defined frequency. This assumption is satisfactory for certain noises encountered in flight vehicles, e.g., propeller noise. However, many noises are "broad-band" in character, and this assumption requires re-examination for such noises. In particular, the effective TL measured near panel resonance may be significantly higher for broad-band noise than has been estimated above. This measured increase in TL is due to the finite bandwidth of the measurement filter. Thus, if the bandwidth of the panel resonance is significantly narrower than the filter bandwidth, as is often the case, the measured TL will appear greater than the predicted TL. This increase in TL can be expressed in simple form if the spectrum of the noise incident on the panel is essentially flat over the bandwidth of the filter. This requirement is met by many broad-band noises. Then, for octave and for third-octave filters:

$$\Delta TL_{eff} = 10 \log \frac{1}{2\,\eta} \text{ for octave filters} \qquad (57)$$

$$\Delta TL_{eff} = 10 \log \frac{1}{\eta \cdot 4 \cdot (2)^{1/6}} \text{ for third-octave filters} \qquad (58)$$

This quantity is given in the following table for three typical ranges of damping. The "Q" of the panel resonance, also given in the table, is the reciprocal of the relative bandwidth of the resonance, or:

$$Q = \frac{f_o}{\Delta f} = \frac{1}{\eta} \qquad (59)$$

where Δf is the resonance bandwidth between "half-power" points.

APPARENT INCREASE IN TL AT A RESONANCE, WHEN TL IS DETERMINED FOR A BAND OF NOISE RATHER THAN FOR A PURE TONE

Panel Damping Factor η	Q	TL_{eff}, Octave Band	TL_{eff}, 1/3-Octave Band
Low (0.007)	140	20 db	15 db
Medium (0.03)	33	13.5 db	8.5 db
High (0.1)	10	8.5 db	3.5 db

3. Acoustic Flanking Paths

In a manner analogous to the way in which the transmission of noise through a low-transmission-loss section of a panel can by-pass a high-transmission-loss section of the panel (see Section III-D), noise transmission by "stray" acoustic paths can limit the effectiveness of a given panel or structure. Such stray paths are referred to as flanking transmission paths. In aircraft structures it is practically impossible to eliminate all flanking paths. As a result the transmission loss of most aircraft structures, including many double-wall structures, is limited to a maximum value of from 50 to 60 db. Only in very special cases it is possible to achieve higher values of transmission loss.

Some flanking transmission paths are easily found. These include small holes in the structure, thin spots in a panel, gaps in the acoustic blanket, direct vibration ties between the leaves

of a double wall, and the like. More subtle, however, is the transmission of vibration from the panel to its supporting structure and thence to the inside of the receiving space. Flanking sound can be radiated directly from the inside surfaces of structural members (e.g., belt frames, hat sections, etc.), or can actually travel through several structural members, even around corners, to be radiated from interior surfaces of the receiving space. Structural limitations often prevent the use of adequate vibration breaks in these flanking paths. A useful method of reducing the radiation from surfaces of the receiving space is to apply blanket layers with an impervious outer septum, or in the case of a floor, to use a carpet on a resilient pad.

C. The Effect of Acoustical Blankets on TL

Acoustical blankets are useful in increasing the transmission loss of a given aircraft structure. The blankets, which are usually required to serve also as thermal insulation, are placed near the inside surface of the structure, sometimes with an air space separating the two.

In the thickness customarily used in aircraft (i.e., 1 to 4 inches) acoustical blankets have relatively little effect on the transmission loss of single panels up to frequencies of about 400 cps. Above this point, however, the increase in transmission loss due to the presence of the blanket becomes significant. The improvement at very high frequencies usually exceeds the mass law transmission loss of the blanket alone.

Figure 51 presents approximate transmission loss increases for several thicknesses of blanket. The curves are based on measurements and calculations made for typical aircraft-type

glass-fiber blanket (very fine fibers) but should hold approximately for any high-flow-resistance material of about the same density and thickness.

D. Composite Panels

When the panel with which we are dealing is made up of several parts, each of which may have a different transmission loss, we must estimate an effective transmission loss for the composite panel. With such a panel, varying amounts of acoustic power are transmitted through the several sub-areas of the panel. The contributions of these "parallel" paths combine to determine the resultant sound pressure level in the receiving space behind the panel. Fig 52 presents a chart that can be used to determine an effective (i.e., based on average transmitted intensity) transmission loss for two panel-sub-areas when taken together.

As an example, consider a panel 90% of which has a TL of 35 db, the remaining 10% of the panel surface having a TL of 20 db. Refer to Fig 52.

$TL_1 = 35$ db

$TL_2 = 20$ db

$TL_1 - TL_2 = 15$ db

% occupied by $S_2 = 10\%$

$\Delta TL = 6$ db

$TL_{composite} = 35 - 6 = 29$ db

When more than two sub-areas go to make up a panel, we may simply take them two at a time, using Fig 52. Thus, if our panel

has areas, S_1, S_2, and S_3, compromising 50%, 30%, and 20%, of the total area, respectively, we may combine the sub-areas as follows: Treat sub-areas S_1 and S_2 as making up 5/8ths and 3/8ths of a two-area panel; determine the average TL. Now combine the area $S_1 + S_2$, with its average TL, with S_3, assigning area ratios of 8/10ths and 2/10ths, respectively; determine the average TL for the complete panel.

When sub-areas of different types (e.g., skin panels and windows) go to make up a given panel, the transmission loss curves for these sub-areas will in general be different. Thus, the average TL of the composite must be determined at a sufficient number of frequencies so that the average curve may be estimated.

E. Double-Wall Structures

Where double-wall structures are present in aircraft, we expect that one wall will be moderately heavy, being a structural wall, while the second wall will be somewhat lighter, presumably having been introduced for noise-control purposes. In considering such a double-wall structure, we first estimate the resonance frequency at which the two leaves of the wall resonate with each other through the stiffness of the air gap between them. Fig 53 can be used to estimate this resonance frequency f_o, for an angle of sound incidence θ (For normal incidence $\theta = 0.$). Fig 53 does not include the stiffening effects of boundaries or support.

At frequencies more than one octave below the double-wall resonance, we may treat the double wall as a single wall with average properties governed by the total surface weight of the double-wall or by the stiffness and resonance considerations outlined for single walls above.

Above the double-wall resonance we expect the TL to vary between upper and lower limits as resonances and anti-resonances occur in the air space. These limiting values are:

a) Upper limit = $TL_1 + TL_2$

where TL_1 refers to the heavy (structural) wall, and TL_2 to the inner wall. Where blankets are placed in the air space; their TL should be included in TL_2 at high frequencies.

b) Lower limit = TL_{1+2}

TL_{1+2} is the TL of a single wall having a total mass equal to that of both walls taken together.

The presence of acoustical blankets in the space between the two leaves of the double wall serves to reduce the severity of the air space resonances. The tendency is then for the TL curve to lie closer to its upper limit, with less variation from point to point. An additional effect of the blankets is to maintain more nearly isothermal conditions (acoustically) making the spacing between the walls appear to be larger.

Figure 54 illustrates the double-wall behavior discussed above. Obviously a more detailed estimation procedure would be desirable for double-wall structures. We hope that present and future studies will make such a procedure possible. It is of interest to note that experiments to date indicate that double-wall structures in buildings seldom, if ever, show the theoretical maximum TL. The same is probably true of double-wall aircraft structures.

F. Transmission Loss for Boundary-Layer Noise

Only rather limited data are available on the subject of the transmission loss of structures for boundary-layer noise. These data indicate that for present-day aircraft structures (principally passenger-aircraft structures) the transmission loss for boundary-layer noise does not differ appreciably from that for airborne noise.

Theoretical studies of the problem have indicated, however, that the phenomena involved in the transmission of boundary-layer noise are sensitive to the amount of damping inherent in the transmitting structure. Thus, we expect that structures having significantly more damping (for bending waves) than is found in contemporary passenger aircraft, will have higher noise reduction for boundary-layer noise. The increase in noise reduction is expected particularly in the frequency range above the "hydrodynamic coincidence frequency frequency", f_h. This coincidence frequency is defined as that frequency at which the velocity of bending waves in the transmitting panel just equals the average convection velocity of turbulent vortices in the boundary layer. Recent work by Willmarth* has shown that this convection velocity is about 0.8 of the free-stream velocity. We may estimate a value of f_h using the following relation:

$$\frac{f_h}{f_c} = 0.64\ M^2 \tag{60}$$

where f_c = critical frequency for sound coincidence

M = Flight-vehicle Mach number

*W. W. Willmarth, NACA Technical Note - to be published.

Our present estimate is that the noise reduction for boundary-layer noise above f_h should increase as 10 log η as the damping of a given structure is increased.

We will use the notation TL_h to describe the transmission loss for boundary-layer noise. TL_h is in reality a sound pressure level difference between the boundary-layer noise levels at the outside surface of the panel and the free-space noise levels on the inside of the panel.

Although the boundary-layer noise-generation mechanism is different from the usual ~~incident~~-sound case, once the sound energy is transmitted through the panel we treat it as though it were the same as the incident-sound case. Thus, we will follow the procedures of Section IV to convert TL to NR, for both boundary-layer noise and airborne sound.

G. Example: Estimation of TL_o of the Fuselage Sidewall of a Passenger Aircraft.

To illustrate the application of the procedures set forth in this section, let us work out an example in detail. We wish to estimate TL_o for the fuselage sidewall of a passenger aircraft, in the frequency range of 50-10,000 cps.

The sidewall is constructed as follows:

a) Fuselage diameter: 10 ft

b) Skin: 0.040 in. Aluminum alloy

c) Belt frame (hoop) spacing: 19 in.

d) Stringer (longeron) spacing: 19 in.

e) Stringer section: Z section, 0.75 in. web, 0.75 in. flanges.

f) Sidewall cross section:

Item		Surface Weight lb/ft^2
skin	0.040 in.	0.56
stringers		0.28 (avg)
Medium damping on skin		0.2
	Total skin panel weight	1.04
Air space	1 in.	
Blanket	3 in.	0.15
Trim layer (impervious)		0.05

1. Estimate f_1, the Fundamental Resonance Frequency.

Combined surface weight of skin and stringers is about 1.5 x the times the skin surface weight or about 0.84 lb/ft^2.

Bending stiffness of skin and stringer combination can be calculated (as a composite beam) to be about 720 times the bending stiffness of the skin alone.

Then the ratio of $\frac{B}{m}$ (bending stiffness-to-surface mass) for the skin-stringer combination is about $\frac{720}{1.5} = 480$ times that for the skin alone. A resonance frequency of a bar or plate usually varies with $\sqrt{\frac{B}{m}}$, and thus should be about a factor of $\sqrt{480} = 22$ times higher for the composite than for the skin alone.

From Appendix A, for a plate 19 in. long, 0.040 in. thick, supported at its ends and free at its edges, f_1 is about 10 cps. This would be the fundamental frequency of the skin plate supported on two belt frames, neglecting curvature.

From Appendix A, f_1 for a clamped-clamped plate with the same dimensions as above would be about $\frac{72}{31} = 2.3$ times that for the simply supported plate, or about 23 cps. The actual boundary conditions at belt frames are probably somewhere between clamped and supported, giving us a skin plate resonance at about 15 cps.

Thus, we might estimate the composite skin-stringer resonance at 22 x 15 = 330 cps, again neglecting curvature. We can show that, for not too wide a section of the skin, (say a width of 2 ft), the stiffening effect of the stringers is greater than that of the curvature (5 ft radius). Realizing its approximate nature, let us accept our estimate of $f_1 = 330$ cps. There will be other resonances in the structure in this general frequency range. We shall take account of this in sketching an estimate of TL_o.

2. Estimate f_c, the Sound-Coincidence Frequency

From Fig 56, for $c_2 = 1130$ ft/sec., plate thickness = 0.040 in.

$$f_c = 12{,}000 \text{ cps}$$

We can show that the coincidence frequency will vary with the reciprocal of the quantity $\sqrt{B/m}$. Thus for the skin-stringer composite we would estimate

$$f_c' = \frac{12{,}000}{22} \doteq 550 \text{ cps}$$

Actually we do not expect a strong coincidence effect to appear in TL_o for our structure at this lower frequency for two reasons:

a) The wavelength of sound at 550 cps is approximately 2 ft. Thus, the span of the fuselage skin between belt frames is less than 1 wavelength, and there is no appreciable unimpeded space for strong bending waves to build up.

b) There may be some tendency of the skin to move relative to the stringers, thus weakening the coupling between the two. If the skin and stringers do not move in unison a strong coincidence is less likely.

Therefore let us plan to include only a small correction to TL at the lower coincidence, 550 cps. The upper coincidence at 12,000 cps falls above the frequency range of interest.

3. Estimate TL_o

As we build up our estimate of TL_o, we plot the various portions of the curve in Fig 55.

From Eq (53) $TL_{400} \doteq 21$ db for 1.04 lb/ft^2 total skin panel surface weight.

From Fig 47 allow for 1/3 of the TL decrease due to a coincidence effect (medium damping) for the lower coincidence $f_c' = 550$ cps.

From Fig 47 allow for the beginning of the coincidence dip (medium damping) at $f_c = 12{,}000$ cps.

At $\frac{f_1}{4} \doteq 82$ cps, estimate the stiffness-controlled TL to be 21 db, i.e., 2 db higher than the reference mass law TL at f_1.

(See Section III-A-2). As an estimate of TL for the stiffness-controlled region, pass a straight line through this point at -6 db/octave.

From Fig 48 note that the minimum discrete-frequency TL in the resonance region is about 2 db. Sketch the range of values of TL expected around f_1. Allow a somewhat broad resonance dip to account for other possible resonances near f_1.

From Fig 51 add to the estimated panel TL the attenuation increase due to the acoustical blanket. Note that the values of TL rise very rapidly above about 600 cps.

Limit the maximum values of TL_o to 55 to 60 db because of probable flanking transmission (See Fig 55).

In Fig 55 draw in a smooth TL_o curve joining the various partial curves. Pass the TL_o curve through the upper part of the TL spread around resonance, because the presence of a thick blanket should help reduce the effects of panel resonances.

H. Transmission Loss - Theoretical Discussion

In order to study analytically the sound-transmitting properties of an aircraft structure, it is necessary to assume a simplified geometry for the structure. In this section we will outline the known information on the transmission loss of thin plates and cylindrical shells. Both of these geometries are of interest, since flat portions of a wing surface may behave approximately like thin plates, and an aircraft fuselage or missile skin is usually similar to a cylindrical shell in some frequency ranges.

1. Thin Plates

When a sound wave is incident on one side of a plate, bending waves are set up in the plate. These bending waves in turn radiate sound on the other side of the plate.

The velocity of propagation, c_B, for bending waves in a thin, plane, elastic plate is a function of the frequency, f, of the waves, the total plate thickness, h, and the elastic constants and density of the plate material. For aluminum or steel plates:

$$c_B = 51\sqrt{hf} \tag{61}$$

where c_B is in ft/sec, f is in cps, and h is in inches. This relationship is plotted as the family of lines labelled "Curves of c_B" in Fig 56.

At certain frequencies the plate motion will become relatively large, and the sound transmission loss of the plate will therefore be low. One group of these frequencies is called resonances. For a plate of length ℓ, simply supported at its ends, the fundamental resonance occurs when ℓ is half a wavelength, or:

$$c_{B_{res}} = 2\,\ell f_1 \tag{62}$$

where ℓ is in ft and f_1 is the fundamental resonance frequency in cps. Curves of $2\,\ell f$ are plotted in Fig 56.

Equations (61) and (62) may be solved simultaneously for f_1 by a graphical method in Fig 56. Thus, f_1 is determined by the intersection of the appropriate curve of c_B and the appropriate curve of $2\,\ell f$. For example, we choose ℓ equal to 1.5 ft and h

equal to 0.080 inches. These are realistic dimensions for the skin of a jet transport. The appropriate curves intersect at a fundamental resonance frequency of 24 cps. In an actual fuselage the skin curvature and the coupling to adjacent panels will affect the resonance frequency. Below a resonance frequency the plate motion is dependent primarily on the plate stiffness, above a resonance frequency the motion is dependent primarily on the plate mass, and near the resonance frequency the motion is dependent primarily on the plate damping.

There exists another frequency, f_c, at which the plate motion becomes large. This occurs when the "trace velocity" $c_s/\sin\theta$ of the incident sound equals c_B. c_s is the local velocity of sound in air, and θ is the angle between the normal to the plate and the direction of sound propagation. The value of the sound coincidence frequency may be found from Fig 56. For example, for grazing incidence ($\theta = 90^o$) and near sea level (c_s = 1100 ft/sec), Fig 56 shows that f_c for a steel or aluminum plate 0.080 inches thick is 6200 cps. The amplitude of plate motion near coincidence may be larger than it is near resonance.

In describing the acoustic radiation from bending waves on a plate, it is useful to consider as a reference the radiation from the uniform transverse vibration of the plate. Thus, we introduce the concept of radiation factor, s, in Fig 57. A traveling wave with amplitude x_o on a plate radiates an intensity I. If the plate were vibrating uniformly with the same amplitude, it would radiate an intensity I_o. Then

$$s = \frac{I}{I_o} \qquad (63)$$

The radiation factor s is a function of the plate length as well as of the frequency of the wave. Fig 58 shows the effect of the plate length on the radiation factor. These curves were derived by Gösele[1] for a finite portion of an infinitely long plate; aside from low frequency resonance effects, however, the curves exhibit the behavior of finite plates.

The transmission coefficient of a wall, τ, is defined as the ratio of the power incident on the wall to the power transmitted by the wall. τ is related to the wall transmission loss (TL) by:

$$TL = 10 \log \frac{1}{\tau} \tag{64}$$

We may characterize any wall by its "transmission impedance", Z_τ, the ratio of the pressure difference across the wall to the normal velocity. For the case of radiation into a "ρc_s termination" (no reflections), τ is related to Z_τ by:[2]

$$\frac{1}{\tau} = \left| 1 + \frac{Z_\tau \cos \theta}{2\rho c_s} \right|^2 \tag{65}$$

ρ is the density of the air. Although the interior of an aircraft does not approximate a ρc_s termination, Eqs (64) and (65) may serve to indicate general trends and changes in noise reduction with variations values of the parameters. When the sound is randomly incident on the wall, we must perform an average over angle, and thereby obtain the average statistical transmission

1. K. Gösele, "Schallabstrahlung von Platten, die zu Biege-Schwingungen Angeregt Sind", Acustica, 3-4, 243-248 (1953).

2. Handbook of Acoustic Noise Control, Vol. I, Supplement 1. WADC TR 52-204 (1955), pp. 82-115.

coefficient, $\bar{\tau}$:

$$\bar{\tau} = 2 \int_0^{\pi/2} \tau \cos\theta \sin\theta \, d\theta \qquad (66)$$

For an infinite plate with no damping:

$$Z_\tau = -i \, 2\pi f m \left(1 - \frac{f^2 \sin^4\theta}{f_{cr}^2}\right) \qquad (67)$$

where m is the mass per unit area of the plate, and f_{cr} is the critical frequency, the lowest value of the sound coincidence frequency, f_c (which occurs for grazing incidence). Combining Eqs (64), (65), and (67) we obtain

$$TL = 10 \log\left[1 + \left(\frac{\pi f m \cos\theta}{\rho c_s}\right)^2 \left(1 - \frac{f^2 \sin^4\theta}{f_{cr}^2}\right)^2\right] \qquad (68)$$

Figure 59 gives contours of equal TL as functions of the angle of incidence θ and of frequency. The results obtained by carrying out the integration of Eq (66) are shown in Fig 60. Here TL is given in terms of the dimensionless ratios f/f_{cr} and $\pi f_{cr} m/\rho c_s$.

For an infinite plate with damping, the expression for TL for an arbitrary angle of incidence is very similar to Eq (68) except that at coincidence Z_τ equals $-i \, 2\pi f m \eta$ and the TL has a non-zero value dependent on the damping factor, η (the ratio of the imaginary part of Young's Modulus to the real part). Reference 2 (p. 110) contains graphical results of TL obtained by carrying out the integration of Eq (66) in this case.

2. Thin Cylindrical Shells

The cylindrical shell motion which is of primary interest in the study of sound transmission is the radial motion which propagates along the shell axis (the Z axis) with a velocity c_z. This is called the flexural motion of the shell. It is convenient to break this motion up into angular modes:

$$U = \sum_n U_n \cos n\phi \exp\left[-2\pi i f\left(t - \frac{z}{c_{z_n}}\right)\right] \qquad (69)$$

where U is the radial velocity, U_n is the velocity amplitude in the nth mode, and ϕ is the angular coordinate.

As we did above for plates, we will first consider the behavior of the velocity c_z, in order to determine the location of coincidences. Coincidences occur where the c_z curve intersects the horizontal line $c_z = c_s$.

Figure 61 is a plot of c_z as a function of frequency, for the primary axially symmetric (n=0) mode. (A secondary branch has not been included, since it does not make an important contribution to the motion.) A cylindrical radius R of 5 ft has been assumed. At the high frequencies the shell acts like a plate, and the results of the previous discussion apply. We may call the coincidence which occurs at high frequencies the "flat plate coincidence". At the low frequencies c_z is independent of frequency and is equal to the velocity of longitudinal waves c_L. (17,000 ft/sec for aluminum or steel). The transition region occurs when:

$$f_o = \frac{c_L}{2\pi R} \qquad (70)$$

With R equal to 5 ft the transition region occurs around 450 cps. This transition gives rise to another coincidence, which we call the "radial coincidence".

Figure 62 gives c_z for the n=1 mode. In the low frequencies, the shell acts like a uniform beam, giving rise to another coincidence, called the "beam coincidence".

Fig 63 gives c_z for the n=2 mode. This case also illustrates the interesting feature of higher order modes. The low frequency behavior is determined by the degree of internal pressurization of the shell. In general, pressurization will tend to eliminate the low frequency beam coincidence found in the n = 1 case.

We must now consider the form of the transmission impedance Z_T for a cylindrical shell. As we might expect, Z_T in this case is far more complicated than the expression of Eq (67) for a flat plate. For large values of θ (near grazing incidence), the expression for Z_T obtained by Smith[3] may be simplified:

$$Z_T = -2\pi i f m \left(\frac{f_o}{f}\right)^2 \left\{ 1 - \left(\frac{f}{f_o}\right)^2 - \frac{(n^2+k^2a^2)(n^2+\nu^2 k^2a^2) + (1-\nu^2)n^2k^2a^2}{(n^2+k^2a^2)^2} \right\} \qquad (71)$$

where ν is Poisson's ratio, k is the wave number of sound in air $\left(\frac{2\pi f}{c_s}\right)$, m is the mass per unit area of the cylinder, and f is much less than f_o. It is possible to substitute Eq (71) (or more complicated expressions, such as those of reference 3) into

3. P. W. Smith, Jr., J. Acoust. Soc. Am., 29, 725 (1957).

Eqs (65), (66), and (64) to obtain an expression for the TL of a cylindrical shell. At present this work has not been carried out. It is probably the next step to be taken in the analysis of sound transmission through cylindrical shells.

SECTION IV

EFFECTS OF RECEIVING-SPACE CONFIGURATION ON NOISE REDUCTION

In Section III we defined acoustical transmission loss (TL) as 10 log $1/\tau$, where τ is the ratio of the transmitted acoustic intensity to the incident acoustic intensity for a given panel or structure. The transmission loss is a more-or-less basic property of a structure, that is, for most cases, TL depends only on panel geometry and panel materials. As we pointed out, there are some more complex cases, expecially cases involving curvature of the panel. In these complex cases the TL of the panel can be dependent upon the type of excitation, e.g., uniform excitation, concentrated excitation, etc. Boundary-layer excitation and other forms of aerodynamic excitation are special cases, also discussed in Section III.

Because intensity and pressure are simply related in a plane wave, we may write the following relation:

$$\frac{1}{\tau} = \frac{I_1}{I_2} = \frac{P_1^2/\rho_1 c_1}{P_2^2/\rho_2 c_2} \tag{72}$$

where the subscripts 1 and 2 refer to conditions external to and within the receiving space, respectively. Now when the ambient conditions are identical on both sides of the panel, we have

$$\rho_2 c_2 = \rho_1 c_1 \tag{73}$$

Thus, Eq (72) becomes:

$$\frac{1}{\tau} = \frac{P_1^2}{P_2^2} \tag{74}$$

from which it follows that

$$TL = SPL_1 - SPL_2 \qquad (75)$$

Although the TL of a structure is an important characteristic, it by no means tells the whole story. In order to estimate the sound pressure levels to be found in a given receiving space behind (or within) a panel or structure, we must take account of the effects of the receiving space on the panel motion and on the distribution of acoustic energy within the space.

The final result toward which we are working here is the development of a Noise Reduction (NR), which will include both the panel TL and the effects of the receiving space. Our resultant value of NR can then be used directly to describe the level difference between the excitation outside the panel and the sound pressure levels in the receiving space.

But, from Eq (75) we see that under certain conditions the transmission loss of a panel may be interpreted simply as a noise reduction, that is as a difference in sound pressure levels. In this report we find it convenient to use this interpretation for transmission loss. We estimate the TL of our panels or structure for room temperature and sea level pressure according to the methods of Section III. This transmission loss for reference condition is referred to as TL_o, a reference transmission loss. For our purposes in this report it becomes a reference noise reduction, the two quantities being indistinguishable for the special case of a perfectly absorbing receiving space at reference ambient conditions.

Our procedure for determining noise reduction in terms of TL_o is therefore to use the following relation:

$$NR = TL_o + C_n + C_a \qquad (76)$$

where

C_n = correction for receiving-space effects
n = 1, 2, or 3 for small, medium, or large receiving space, respectively.

C_a = correction for ambient conditions in the receiving space. (small receiving spaces will have to be treated as a special case).

In Part A of this section we summarize the procedures for determining NR. Parts B and C present discussions of the procedures and of the reasoning leading to their development. The remaining parts contain additional information on special cases, and present an example of the application of the estimating procedures.

A. Summary of Procedures for Estimating Noise Reduction

1. Divide the frequency range of interest into 1, 2, or 3 regions, as required, in accordance with the following definitions of receiving-space size:

small receiving space (low frequencies)	$\frac{L}{\lambda} < \frac{1}{6}$
medium-sized receiving space (mid-frequencies)	$\frac{1}{6} < \frac{L}{\lambda} < 10$
large receiving space (high frequencies)	$10 < \frac{L}{\lambda}$

where λ is the sound wavelength within the receiving space, and L is a typical dimension of the receiving space.

2. For a small receiving space, obtain the correction C_1 to TL_o from Fig 64. The cavity stiffness parameter in this figure is $\frac{1}{2\pi}\frac{\lambda}{V/S}$, where V and S are cavity volume and transmitting panel area, respectively.

3. For a medium-sized receiving space, estimate the amount of absorption in the space as "high", "medium", or "low" according to Figures 66, 67, and 68. These figures describe the average statistical absorption coefficient in terms of the thickness of blanket and percent of wall coverage.

   Determine the correction C_2 to TL_o from the appropriate curve in Fig 69. As with the correction for small receiving spaces, C_2 depends on TL_o. Note that C_2 is the maximum correction. One should expect a range of effective corrections from 0 to C_2.

4. For a large receiving space determine the amount of absorption (high, medium, low) at the appropriate frequencies from Figs 66, 67, and 68 as in 3) above. Calculate S_w/S_2, where

   S_w = area of the transmitting panel
   S_2 = total surface area in the receiving space.

   Read the correction C_3 to TL_o from Fig 70.

5. To correct for ambient conditions in the receiving space, read C_a from Fig 71, for the appropriate receiving-space temperature and altitude (pressure).

   a) For a small receiving space determine ΔC_a from Fig 72 as a function of TL_o, $\frac{1}{2\pi}\frac{\lambda^2}{V/S}$, and C_a.

Calculate

$$C_a' = C_a + \Delta C_a, \tag{77}$$

the net correction for ambient conditions in a small receiving space.

b) For medium-sized and large receiving spaces use C_a, as read directly from Fig 71, as the net correction for ambient conditions.

6. Find the noise reduction NR as follows:

a) Small receiving space

$$NR = TL_o + C_1 + C_a' \tag{78}$$

b) Medium-sized receiving space

$$NR = TL_o + C_2 + (0 \text{ to } C_a) \tag{79}$$

A range of values is expected.

c) Large receiving space

$$NR = TL_o + C_3 + C_a \tag{80}$$

B. Corrections for Receiving-Space Effects

In order to determine the appropriate corrections for receiving-space effects, we divide the frequency range into three regions according to the ratio of L, a typical receiving-space dimension, to λ, the wavelength of sound in the receiving space. In general, we assume that no one of the receiving-space

dimensions is much larger than the other dimensions, that is, that our receiving space is not extremely flat or long and thin. Our three frequency regions are the following:

1. small receiving spaces,

$$\frac{L}{\lambda} < \frac{1}{6}$$

2. medium-sized receiving spaces

$$\frac{1}{6} < \frac{L}{\lambda} < 10$$

3. large receiving spaces

$$10 < \frac{L}{\lambda}$$

These frequencies are not simply related to the six frequency ranges of panel behavior discussed in Section III.

In discussing the physical behavior of the sound waves in the receiving space in each of the three regions, it is convenient to refer to "free-field" receiving conditions. The term free-field simply means that the receiving space is effectively infinite in extent, or that it is perfectly absorptive. Under these conditions the panel TL is adequate to relate the sound pressure level on the receiving side of the panel to the sound pressure level of the waves incident on the outside of the panel. The relation is:

$$SPL_2 = SPL_{incident} - TL$$

Plane waves are assumed so that on each side of the panel the sound pressure level is independent of position. $SPL_{incident}$ does not include pressure doubling at the panel surface.

The effect of the receiving space is almost always to increase the sound pressure level over that observed with free-field receiving conditions. The level increase can therefore be described equivalently as negative corrections to TL to give NR.

1. Small receiving spaces

In this case the receiving space is so small relative to the wavelength of sound that it behaves essentially as a stiffness. As such, it serves to add a stiffness reactance to the acoustic impedance of the panel, limiting the panel motion to some extent.

The acoustic pressure is expected to be more or less uniform throughout the receiving space. The sound pressure in the receiving space will, in general, be higher than the corresponding pressure for free-field receiving conditions. Acoustical absorption in the receiving space is relatively unimportant when the panel itself is stiffness controlled. However, some absorption is useful in controlling undamped resonances that may occur in the panel.

Figure 64 presents the expected level increase due to cavity stiffness for a stiffness-controlled panel. The parameter on the curves involves the effective cavity stiffness, which is expressed in terms of λ, the wavelength of sound, V, the cavity volume, and S, the area of the transmitting panel. The parameter is dimensionless, and any consistent system of units may be used. The upper limit of the effect of receiving-space stiffness is to negate the effect of the panel completely, giving receiving-space levels equal to $SPL_{incident}$ + 6, that is, the total outside level including pressure doubling.

2. Medium-sized receiving spaces

At a number of frequencies in the range for which the receiving space is "medium-sized", we may expect discrete resonances with accompanying standing acoustic waves. At the maxima in these standing waves the acoustic pressures can build up considerably over those for free-field receiving conditions. Only near the minima in the standing wave pattern we can expect to have sound pressures as low as those for free-field conditions.

Acoustical absorption is quite important in controlling the buildup of the standing waves. We characterize the strength of the buildup by the standing-wave ratio, SWR = SPL_{max} - SPL_{min}, that is the level difference from maximum to minimum levels in the standing wave. The standing wave ratio is large in spaces with low absorption and small in spaces with high absorption.

The following table summarizes our categorization of spaces on a scale of acoustical absorption and standing wave ratio, SWR:

Absorption in Space	Average Statistical Absorption Coefficient $\bar{\alpha}_{stat}$	Standing Wave Ratio, SWR (db)
High	0.40	8 - 18
Medium	0.25	15 - 23
Low	0.13	23 - 30

Figure 65 shows the approximate statistical absorption coefficient, α_{stat}, for several thicknesses of unfaced aircraft-type acoustical blanket with no airspace behind the blanket.

When an absorbing blanket is faced with an impervious septum (say, for example, a flexible plastic sheet weighing about 0.05 lb/ft^2) the absorption changes appreciably. We may say qualitatively that the low-frequency absorption is enhanced as though the blanket absorption curve were simply shifted downward. (The downward shift is about one octave for a 1.5-inch blanket with a septum weighing 0.05 lb/ft^2).

The effect of the septum is to reduce the high-frequency absorption sharply, so that the absorption coefficient reaches its peak value and falls off (on a logarithmic scale) just about as fast above the peak as it does below.

The average absorption coefficient in a receiving space depends both on the type of surface treatment used and on the fraction of the total surface that is treated. Figures 66, 67, and 68 show approximate average statistical absorption coefficients, $\bar{\alpha}_{stat}$, for receiving spaces treated with varying amounts of blankets of thickness 1, 2, and 4 inches, respectively. Curves are shown for 25%, 50%, 75%, and 100% surface coverage. The absorption-coefficient scale has been divided into Low, Medium, and High absorption ranges, according to the information presented in the table above.

Figure 69 presents C_2, the maximum correction to TL_o giving NR at resonance, for varying amounts of receiving-space absorption (SWR). At frequencies other than resonance frequencies we can expect corrections less than those shown in Fig 69. In any case throughout this frequency range there will be a distribution of levels ranging from approximately the levels for free-field receiving conditions at the standing-wave minima up to the maximum values calculable from the information in Fig 69. Therefore we apply a range of values in our estimate

of TL.

At resonance the maximum pressures are to be expected at the surfaces and corners in the receiving space as well as along the pressure anti-node lines. In a standing-wave pattern the pressure maxima are considerably broader than the pressure minima. Therefore, the space-average sound pressure level in a cavity at resonance will be closer to the maximum values than to the minimum or free-field values.

3. Large receiving spaces

In the frequency range where our receiving space may be called "large", the typical dimension of the receiving space is many times the wavelength of sound. Under these conditions we may expect reasonably diffuse sound fields in the receiving space, and standard room-acoustic techniques may be used to estimate the sound pressure levels.* The expected correction C_3 to TL_o to account for reverberation in the receiving space is presented in Fig 70 as a function of receiving-space absorption. Once again we may use Figures 66 through 68 to characterize the receiving-space absorption.

We expect the sound pressure level to be more or less uniform throughout the receiving space, especially for spaces having low absorption. However, there will be some pressure rise as one approaches the walls or the transmitting panel.

---

*See, for example, L. L. Beranek, Acoustics, McGraw-Hill Book Co. Inc., New York, N. Y. (1954).

P. M. Morse and R. H. Bolt, "Sound Waves in Rooms", Rev. Mod. Phys. 16, 2, (April 1944).

C. Corrections to Noise Reduction Due to Changes in Ambient Conditions

When the characteristic impedance, ρc, of the air either inside or outside the panel or both, varies from its value at room temperature and at sea level, we must include a correction for this fact in our estimate of noise reduction. Actually the effect of a variation in characteristic impedance is twofold:

a) The transmission loss of the panel is altered, and a different amount of acoustic power would be radiated into a completely absorbing receiving space for a given acoustic pressure wave incident on the outside of the panel.

b) The relations between acoustic pressure and intensity (i.e., power flow) are altered, and account must be taken in correcting the effective noise reduction for the effects of receiving-space geometry and absorption.

For our purposes here, where we are concerned principally with sound pressure levels, it is most convenient to lump the two corrections together. We then apply the correction C_a to the reference transmission loss, TL_o, together with the correction C_n for the character of the receiving space (see Section IV-B) to give an effective noise reduction. Thus

$$NR = TL_o + C_n + C_a \qquad (76)$$

Figure 71 presents the correction C_a to transmission loss for various ambient conditions in the receiving space. Curves for various pressure altitudes are plotted as a function of temperature. The ordinate scale gives a number to be added to TL_o as one step in determining NR.

We point out that the altitude to be used in reading Fig 71 is the effective pressure altitude in the receiving space. Thus, in a pressurized aircraft, the correction to be applied to panel TL will depend upon whether or not the particular receiving space in question is pressurized. Note that significant differences in NR can exist even at moderate altitudes. The altitude effect is the predominate one, the temperature dependence being only slight.

The correction C_a applies directly for large and medium-size receiving spaces. However, because of the peculiar nature of the phenomenon occurring in a small receiving space, an adjustment to C_a must be made. This adjustment ΔC_a is presented in Fig 72 as a function of the TL_o of the panel (assumed stiffness-controlled), the receiving-space stiffness parameter $\frac{1}{2\pi}\frac{\lambda^2}{V/S}$, and the magnitude of C_a. A quantity χ also enters into the calculation and is obtained from the nomogram at the top of the figure. The adjusted correction for ambient conditions in small receiving spaces is then

$$C_a' = C_a + \Delta C_a \qquad (77)$$

We note that the receiving-space stiffness parameter $\frac{1}{2\pi}\frac{\lambda^2}{V/S}$ depends on the wavelength of sound in the receiving space at the actual ambient conditions. Therefore, theoretically one should correct $\frac{1}{2\pi}\frac{\lambda^2}{V/S}$ for changes in receiving-space temperature (the wavelength at a given frequency is dependent on temperature only). However, this correction is a minor one for the temperature range shown in Fig 71, and we neglect it.

Example: A stiffness-controlled panel is backed by a small receiving space with stiffness parameter $\frac{1}{2\pi}\frac{\lambda^2}{V/S} = 4$.

The panel TL as determined for a particular reference condition is 20 db. What is the effective noise reduction for this configuration when the pressure altitude of the receiving space is 40,000 ft and the temperature in this space is 100 degrees F?

Solution: From Fig 71 we read for 40,000 ft and 100°F a correction C_a equal to +15 db. From Fig 72 we now determine for C_a = 15 db, TL_o = 20 db, and $\frac{1}{2\pi}\frac{\lambda_2}{V/S} = 4$, an adjustment ΔC_a of -2 db. Thus, the net correction due to ambient conditions is

$$C_a' = C_a + \Delta C_a = 15 - 2 = 13 \text{ db} \qquad (81)$$

In addition we read from Fig 64, for TL_o = 20 db and $\frac{1}{2\pi}\frac{\lambda_2}{V/S} = 4$, a correction C_1 of -10 db to TL. The resultant noise reduction is therefore

$$NR = TL_o + C_1 + C_a'$$

$$= 20 - 10 + 13 = 23 \text{ db} \qquad (82)$$

D. Noise Levels Due to a Sound Source within the Receiving Space

In considering noise within flight vehicles, it is sometimes important to be able to estimate the sound pressure levels expected from a noise source contained within the receiving space. One important example is the question of ventilation-system noise within crew compartments, especially in cockpit areas.

In analyzing this type of situation, let us assume that our principal concern is with a frequency range in which the dimensions of the receiving space are greater than several wavelengths of the sound involved. For example, our concern with ventilating-system noise might well be in the speech-interference range, where

the mean wavelength is about 7 inches. Under these circumstances, any crew space should meet our size requirements. The following relation is appropriate to this case*:

$$SPL \doteq PWL + 10 \log \frac{4(1-\bar{\alpha})}{S\bar{\alpha}} \qquad (83)$$

where S is the total surface area (in sq ft) of the receiving space with average absorption coefficient $\bar{\alpha}$.

Equation 83 assumes that the noise source is non-directional and is confined to a relatively small region, so that we may say that the sound diverges more or less spherically from the source. The PWL of the ventilation-system air jet noise source is estimated according to the procedure described in Part C of Section II and presented in Fig 45.

It is probably a reasonable approximation to say that, at the high frequencies generally encountered in ventilation-system noise, "medium-high" absorption (average statistical absorption coefficient $\bar{\alpha}_{stat}$ about 0.35) describes the situation in small crew spaces such as cockpits. For larger crew spaces $\bar{\alpha}_{stat} = 0.25$ is probably a good estimate. Thus, we may estimate the reverberant field sound pressure level by the following equations:

$$SPL \doteq PWL - 10 \log S + 9 \quad \text{for } \bar{\alpha}_{stat} = 0.35 \qquad (84)$$

$$SPL \doteq PWL - 10 \log S + 11 \quad \text{for } \bar{\alpha}_{stat} = 0.25 \qquad (85)$$

*The subject of noise fields in large enclosures is discussed in detail in L. L. Beranek, Acoustics, McGraw-Hill Book Co. Inc., New York, N. Y., (1954), Chap. 10.

The direct-field sound pressure level is given by the following relation:

$$SPL \doteq PWL - 10 \log 4\pi r^2 \qquad (86)$$

where r is the source-receiver distance (in feet).

We combine the direct and reverberant field by determining the direct field as a function of distance from the source. Then we superpose the reverberant-field levels, never allowing the estimated SPL's in the crew space to fall below the reverberant field level.

We realize that the estimating procedure that we have just outlined is necessarily approximate in nature. Crew spaces differ too widely to submit to a uniform, simple analysis. However, we feel that the procedure as presented will give a reasonable estimate of the ventilation-system noise level to be expected. The use of measured source levels rather than estimated source levels, when measured data are available, will, of course, improve the quality of the estimate. The procedure we have outlined is presented in Example 4 in Section V.

E. Example: Estimation of NR for the Fuselage Structure of a Passenger Aircraft.

In Part G of Section III we described a fuselage sidewall structure for a hypothetical passenger aircraft. Now we wish to estimate the NR for this fuselage structure. Assume the following regarding the configuration:

a) Length of cabin of interest ≐ 10 ft.

b) Perimeter of cabin cross section:

fuselage sidewall, approximately 230° of arc, or 20 ft length, assumed to be all noise-transmitting surface.

floor about 9 ft wide assumed to transmit no noise.

Thus for a cabin section 10 ft long

$S_w = 200\ ft^2$, area of transmitting wall

$S_F = 90\ ft^2$, floor area, non-transmitting

$S_2 = S_w + S_F = 290\ ft^2$

$$\frac{S_w}{S_2} = \frac{200}{290} \doteq 0.7$$

c) Assume that the ends of our 10 ft cabin section neither absorb nor transmit noise.

d) Passenger seats: 12 seats in our 10-ft long cabin section (3 rows, 4 seats each). The seats are large and fully upholstered, and therefore represent an appreciable amount of absorption in addition to wall absorption. Assume the following amounts of absorption for each seat:

f (cps)	100	200	400	800	≥1600
$S\alpha_{stat}(ft^2)$ (each seat)	5	5	5	5	5

e) Cabin floor: assumed covered with carpet having absorption coefficient as follows:

f (cps)	100	200	400	800	1600	3200	6400
α_{stat}	0.2	0.2	0.3	0.4	0.5	0.7	0.8

f) Interior trim. Partly impervious, partly porous. Assume the following average absorption coefficients for about a 4-in. blanket faced with a septum weighing 0.05 lb/ft^2:

f (cps)	100	200	400	800	1600	3200	6400
α_{stat}	0.4	0.8	0.7	0.4	0.3	0.2	0.15

g) Estimate total and average absorption in the cabin section. Tabulate values of $S\alpha$(ft^2)

Item f(cps)	100	200	400	800	1600	3200	6400
walls(200 ft^2)	80	160	140	80	60	40	30
floor(90 ft^2)	18	18	27	36	45	63	72
seats, 12	60	60	60	60	60	60	60
Total $S\alpha$	158	238	227	176	165	163	162
$\bar{\alpha} = \frac{S\alpha}{S_2}$	0.55	0.8	0.6	0.55	0.55	0.55	0.55
$\frac{\bar{\alpha}}{1-\bar{\alpha}}$	1.2	4.0	4.0	1.3	1.2	1.2	1.2

We note that the average absorption coefficient is quite high especially at low frequencies. Our procedures assume a value $\bar{\alpha} = 0.4$ for a space with "high absorption" ($\bar{\alpha}/(1-\bar{\alpha}) = 0.67$). Now, the reverberant-field SPL varies with 10 log $\bar{\alpha}/(1-\bar{\alpha})$.*

*See L. L. Beranek, Acoustics, McGraw-Hill Book Co. Inc., New York, N. Y., (1954).

Therefore we should make a correction to NR for extra-high absorption encountered in this case. This correction $\Delta NR = 10 \log (\bar{\alpha}/(1-\bar{\alpha})/0.67)$, is as follows:

f (cps)	100	200	400	800	1600	3200	6400
ΔNR(db)	+2.5	+8	+8	+3	+2.5	+2.5	+2.5

(We note from (2) below that this correction is to be used only above 1000 cps.)

h) Take L = 10 ft, the typical dimension of the receiving space. Thus we have

f (cps)	100	200	400	800	1600	3200	6400
λ(ft) (approx)	10	5	2.5	1.25	0.63	0.31	0.16
$\frac{L}{\lambda}$	1	2	4	8	16	32	64
	Medium-sized receiving space				Large receiving space		

where the size of the receiving space is as defined in this section.

i) The cabin is pressurized to sea level pressure, and the temperature is 70°F.

1. Determine the correction C_2 for frequencies below 1000 cps (Medium-sized space).

From Fig 69 read C_2 (somewhat above the "high absorption" curve. (See g) above). Refer to Fig 55 noting that we are always concerned with $TL_o \geq 15$ db.
$\therefore C_2 \doteq -6$ db for the whole frequency range.

2. Determine the correction C_3 for frequencies above 1000 cps (large space).
From Fig 70 read $C_3 = -6$ db for $\frac{S_w}{S_2} = 0.7$. Combine with ΔNR from (g) above to give $\left[C_3\right]_{net}$

f (cps)	1600	3200	6400
$\left[C_3\right]_{net}$ (db)	-4	-4	-4

3. Determine NR from TL_o. No correction (C_a) is required for ambient conditions in the receiving space.

Plot TL_o on Fig 73 from Fig 55. Apply C_2 and C_3 to get NR.

We have compared the estimated NR in Fig 73 with the results of acoustical measurements on aircraft with similar fuselage sidewalls. It appears that the estimate of NR differs in several respects from "observed" NR. The estimated NR appears somewhat low in the region near the major resonance. Also our estimate may be high in the high frequencies. However, we must realize that our model was a greatly simplified version of a passenger aircraft (without windows, extra stiffening, etc.).

Several comments are in order:

a) NR was estimated for the case where <u>all</u> of the exterior surface was transmitting surface. This case is probably realistic for boundary layer noise, but is not appropriate for more localized disturbances like propeller or exhaust noise. For a localized excitation the ratio $\frac{S_w}{S_2}$ becomes smaller, tending to increase

the noise reduction in the large-space (high-frequency) region. A similar adjustment may be appropriate in the medium-sized space region, although the estimating procedures do not include it.

b) There are usually sources of noise inside the aircraft (especially ventilation systems) that can mask or override noise received from the outside. Such sources have not been considered in this example, and would reduce the apparent NR. The noise from air-conditioning-type sources can be estimated by procedures illustrated in Example 4 of Section V.

c) Our estimation procedures are perhaps most uncertain in the region near and below major resonances. More work, both theoretical and experimental, is required to improve the accuracy of the procedure in this region.

d) Flanking paths are particularly difficult to account for. It appears likely that the TL increase as presented for acoustical blankets in Fig 51 is optimistic in the light of current practical methods of blanket installation. Further study would help to clarify this question and the general subject of flanking transmission.

SECTION V

EXAMPLES

The five examples considered in detail in this section, together with the examples contained in the text of the report, illustrate the use of the procedures developed in the report. We hope that the examples will provide some idea of the various ways in which the procedures may be adapted to practical problems.

Example 1

Find the maximum SPL occurring on the wing of a heavy jet bomber during ground run-up operation. The bomber has eight engines arranged in groups of two. The exit velocity of each engine is about 1850 ft/sec. The wing surface is located three jet diameters (about 6 ft) above the centers of the exhaust nozzles of the engines.

From the overall contours of Fig 16 we follow a line drawn a radial distance of 3 D from the jet center line. Along this line we find that the maximum occurs approximately 8 D downstream from the jet nozzle. The value of the maximum at this point is about 156 db. We must allow for the fact that there are two engines in each group and therefore the overall SPL (free-field) on the wing will be about 156 + 2 = 158 db*. We must also add 3-6 db for "pressure

* Recent measurements indicate that the level due to two closely spaced jet engines is about 2 db (rather than 3 db) higher than the level due to one engine alone. This effect may be related to the induction of secondary air between the adjacent jet streams.

doubling" effects at the wing surface. Thus the maximum overall SPL is 161 - 164 db.

Interpolating in Fig 19 for eight diameters downstream we find the shape of the SPL spectrum. The peak frequency f_{max} is given by Eq (12), and is about 200 cps. Therefore, the octave band containing f_{max} is the 150-300 cps band. The SPL in this band is about 5 db below the overall SPL, i.e., 156-159 db.

Example 2

Heavy jet bomber, M = 1.2, at 50,000 ft.
Estimate fluctuating pressure level at a location on a large pod, and determine the SPL in an instrumentation compartment in the pod at this location.

Assume:

Pod diameter - 6 ft
Pod length - 60 ft
Position of compartment - 40 ft from pod nose
Dimensions of compartment - panel 1 ft high x 2 ft long
depth 2 ft
Panel construction - 0.063 in. aluminum alloy, no damping, 0.88 lb/ft^2
Frequency range of interest - 500-4000 cps
Acoustical treatment in compartment - 50% of area, 2 in. acoustical blanket. Inside of panel is covered.
Pressure in compartment = outside pressure, 50,000 ft pressure altitude
Temperature in compartment = 40° F

A. Estimate Boundary-layer Fluctuating Pressure Level
From Fig 34, Q = 240 lb/ft^2
From Eq (37), $SPL_{overall}$ = 134 db (re 0.0002 microbar)
Calculate Reynolds Number defined in Eq (39),

Kinematic viscosity $\nu = \frac{\mu}{\rho}$

At 50,000 ft, $\nu = 8.2 \times 10^{-4}$ ft^2/sec

$\therefore$ $Re_d = 5.3 \times 10^7$

From Fig 35, $\frac{\delta}{d} = 0.01$

$\delta = 0.4$ ft

From Eq (40), $f_{max} \doteq 1100$ cps

From Fig 33, obtain relative octave band spectrum shape ($SPL_{overall}$ is 5 db above peak SPL at f_{max}.)

See Table below:

Mean frequency of Octave Band (cps)	550	1100	2200	4400
SPL in Band (db re 0.0002 microbar)	124	129	123	116

B. Estimate SPL Inside Compartment

Assume skin panel clamped at 4 edges.

From Appendix A, estimate fundamental resonance, $f_1 \doteq 100$ cps.

From Fig 56 estimate sound coincidence frequency,

$f_c \doteq 7000$ cps.

From Eq (60) determine hydrodynamic coincidence frequency

$f_c \doteq 6400$ cps.

Estimate TL:

f_1 is well below range of interest.

f_c is above range of interest.

Therefore mass-law TL for the panel applies over the range of interest. At 550 cps, TL = 22 db (from Fig 46). TL increases 6 db per octave at higher frequencies. From Fig 67, in frequency range of interest, space has high absorption.

Typical dimension of receiving space, $L = (2 \times 2 \times 1)^{\frac{1}{3}} \doteq 1.5$ ft

f	550	1100	2200	4400
$\lambda = \frac{c}{f}$	2.0	1.0	0.5	0.25
$\frac{L}{\lambda} \doteq \frac{1.5}{\lambda}$	0.75	1.5	3	6

For the frequency range of interest

$$\frac{1}{6} < \frac{L}{\lambda} < 10$$

$\therefore$ space is "medium sized".

f (cps)	550	1100	2200	4400
Mass law TL (db)	22	28	34	40
ΔTL for Blankets	2	9	16	23
TL_o	24	37	50	55*
C_2 (from Fig 69)	-8	-8	-8	-8
C_a (from Fig 71)	19	19	19	19
$NR = TL_o + C_2 + C_a$	35	48	60*	60*
From Step A:				
SPL (outside)	124	129	123	116
SPL_2 (compartment)	89	81	63	56

* Assumed to be flanking limited

Example 3

Find the SPL in an octave band centered around 10 cps, at 30 ft upstream from the nozzle of a rocket. The mass flow is 700 lbs/sec, jet velocity is 5000 ft/sec, and exhaust nozzle diameter is approximately 3 ft. The rocket is to be launched vertically, with a "bucket" turning the jet stream horizontal about 20 ft below the exhaust nozzle.

From the given data the stream power $1/2\ mv^2$ is calculated to be approximately 4×10^8 watts. From Fig 21 we obtain 10 log η = -20 db. Equation (13) therefore gives a PWL of 196 db. From Fig 22 we obtain an average source location of 12 diameters, or 36 ft, from the jet nozzle for the frequency band around 10 cps. The Strouhal number corresponding to this case is 6×10^{-3}. From the geometry shown in Fig 74, the distance R is found to be 53 ft. Using this information and Figs 23 and 24, we obtain:

$$SPL_o = PWL - 36 \text{ db}$$

$$kR = 3.0$$

$$10 \log G^2 = 2 \text{ db}$$

Combining this information with Eq (16), we obtain a value for the SPL in the octave band around 10 cps of 128 db.

Example 4

Jet fighter, M = 3.0 at 50,000 ft
Estimate cockpit noise levels in frequency range 1000 - 10,000 cps.
Assume:

Exit velocity at ventilation-defroster system jets - 500 ft/sec

25 jets, total area 1 sq in. (each jet diameter 0.23 in.)

Cockpit pressurized to 5,000 ft

Total surface area in cockpit 50 sq ft.

A. Mechanical Power in Air Jet Stream (see Part C, Section II)

$$W = \frac{1}{2} mv^2 = \frac{1}{2} \rho A_{total} v^3$$

$$= 1.2 \times 10^3 \text{ watts}$$

$$PWL = 10 \log W + 88 = 119 \text{ db}$$

$$f_{max} = 0.2 \frac{v}{D} = 6000 \text{ cps}$$

From Eq (84)

$$SPL_{overall} = PWL_{overall} - 10 \log S + 9$$

$$= 111 \text{ db}$$

From above, and Fig 45

Octave Band Center Frequency	1500	3000	6000
$SPL_{reverb.}$	94	101	106

B. Make a rough estimate of boundary layer noise to see if it contributes significantly.

Use results for Example 2 above, and scale Q

$$10 \log \frac{Q_{M = 3.0}}{Q_{M = 1.2}} = 10 \log \frac{1400}{240} = 8 \text{ db}$$

By adding 8 db to SPL_2 for Example 2, we see that boundary layer noise is probably not a major contributor in the present case. Therefore, $SPL_{reverb.}$ are the desired levels.

Example 5

Turbojet transport at take-off.
Estimate the maximum noise levels occurring on the fuselage in the frequency range below 400 cps.

Assume:

4000 HP, power to propeller
1000 rpm
13.5 ft propeller diameter, 18 in. propeller blade width
14 in. tip clearance
4 blades
$L_{0.7} \doteq 5$ in.
$V_t = \frac{1000}{60} \pi D = 700$ ft/sec
$M_t = \frac{V_t}{c} = 0.7$

From Fig 2, $L_1 = 142$ db

From Fig 3, $L_2 = +2$ db for fuselage surface ($\frac{Z}{D} = 0.086$) and $M_t = 0.7$

From Eq (3), $SPL_{overall} = L_1 + L_2 + 20 \log \frac{3}{m}$

$= 142 + 2 - 2 = 142$ db

From Fig 5, for $W/D^2 = 22$ HP/sq ft, overall vortex noise is 21 db below overall rotational noise, or 121 db.

A. Rotational Noise

From Eq (5), $f_1 = 4 \frac{1000}{60} = 67$ cps.

From Fig 6

Rotational Noise Spectrum

Harmonic	1	2	3	4	5
cps	67	133	200	267	333
SPL	140	135	130	126	119

B. Vortex Noise

Overall vortex noise level = 121 db

From Fig 7

$$f_{max} \doteq 0.13 \frac{V_t}{L_{0.7}} = 0.13 \frac{700}{5/12} = 220 \text{ cps}$$

Vortex Noise Spectrum

Octave Band Center Frequency	110	220
SPL	111	116

BIBLIOGRAPHY ON PROPELLER NOISE

1. I. E. Garrick and C. E. Watkins, National Advisory Committee for Aeronautics, TN 3018 (1953). (This reference contains a good bibliography on propeller noise.)

2. L. Gutin, National Advisory Committee for Aeronautics, TM 1195 (1958).

3. H. H. Hubbard and A. A. Regier, National Advisory Committee for Aeronautics Report No. 996 (1950).

4. H. H. Hubbard and L. W. Lassiter, National Advisory Committee for Aeronautics TN 3202 (1954).

5. H. H. Hubbard, National Advisory Committee for Aeronautics TN 2968 (1953).

6. S. J. Lukasik, A. W. Nolle, and the Staff of Bolt Beranek and Newman Inc., Wright Air Development Center Technical Report 52-204 (1955).

7. A. A. Regier and H. H. Hubbard, National Advisory Committee for Aeronautics, RM L7H05 (1947).

8. H. W. Rudmose and L. L. Beranek, Jour. Aero. Sci., 14-2, 79 (1947).

9. A. W. Vogeley and M. C. Kurbjun, National Advisory Committee for Aeronautics, TN 3147 (1955).

10. H. E. von Gierke, "Aircraft Noise Sources", Chapter 33 in Handbook of Noise Control, C. M. Harris, Ed., McGraw-Hill Book Co., Inc., New York (1957).

11. E. Y. Yudin, National Advisory Committee for Aeronautics, TM 1136 (1947).

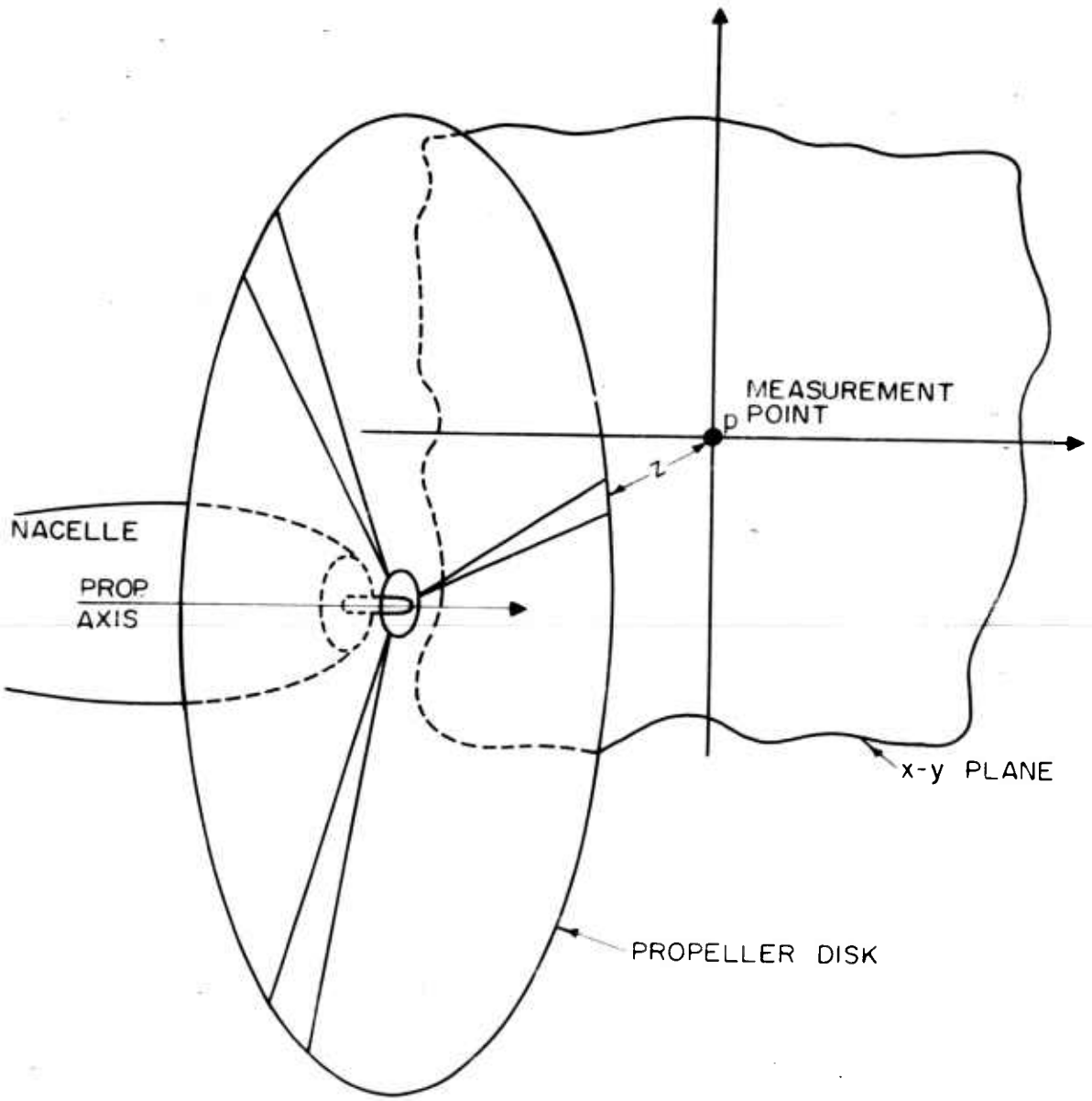

FIG. 1 PROPELLER GEOMETRY PERTINENT TO NEAR FIELD PROPELLER NOISE CHARTS.

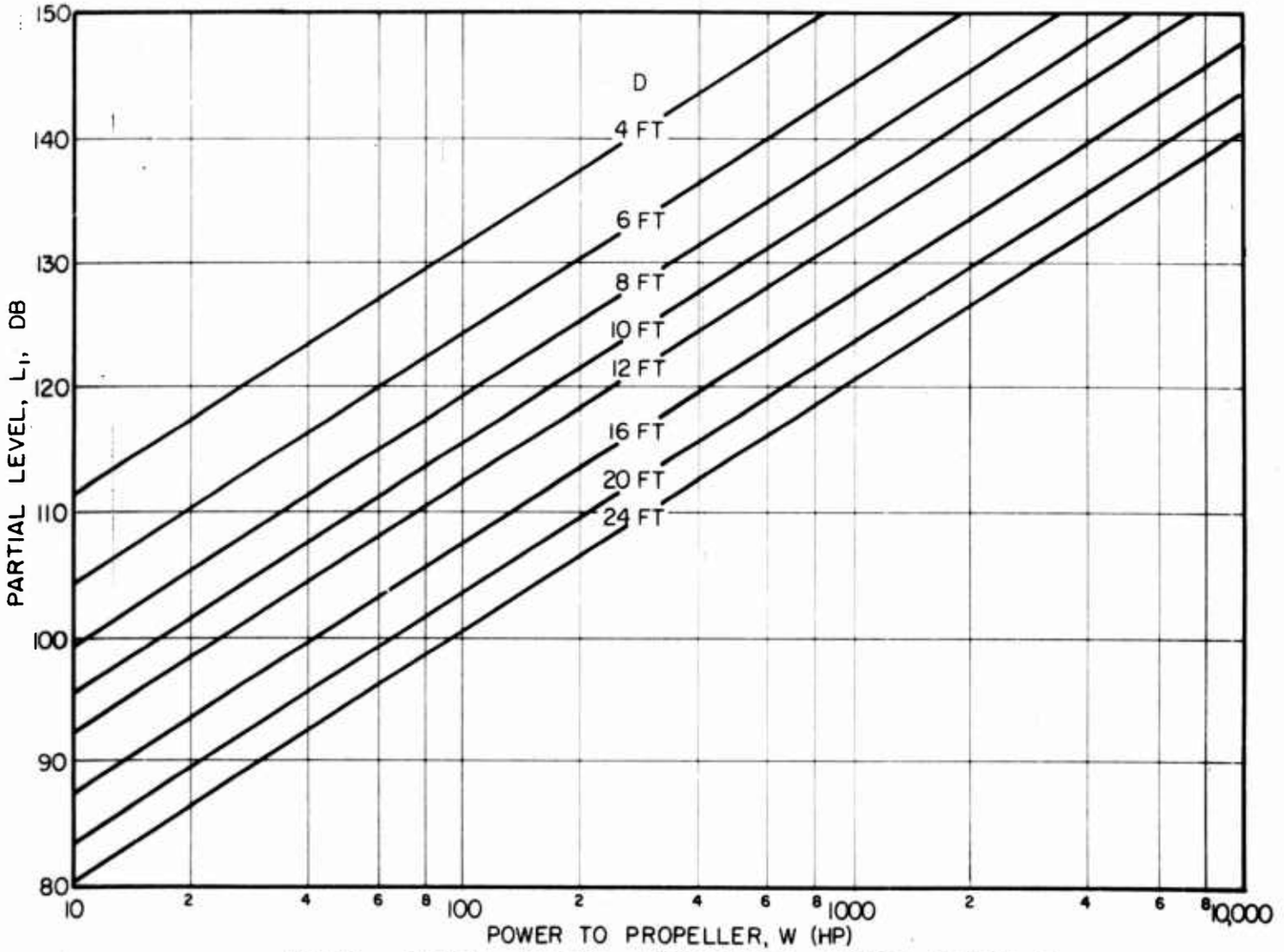

FIG. 2 NEAR FIELD PROPELLER NOISE CHART - 1.
DEPENDENCE OF OVERALL, FREE-SPACE SOUND PRESSURE LEVEL ON POWER DELIVERED TO PROPELLER, W, AND ON PROPELLER DIAMETER, D, FOR 3-BLADED PROPELLERS. AIR TEMPERATURE = 68° F.

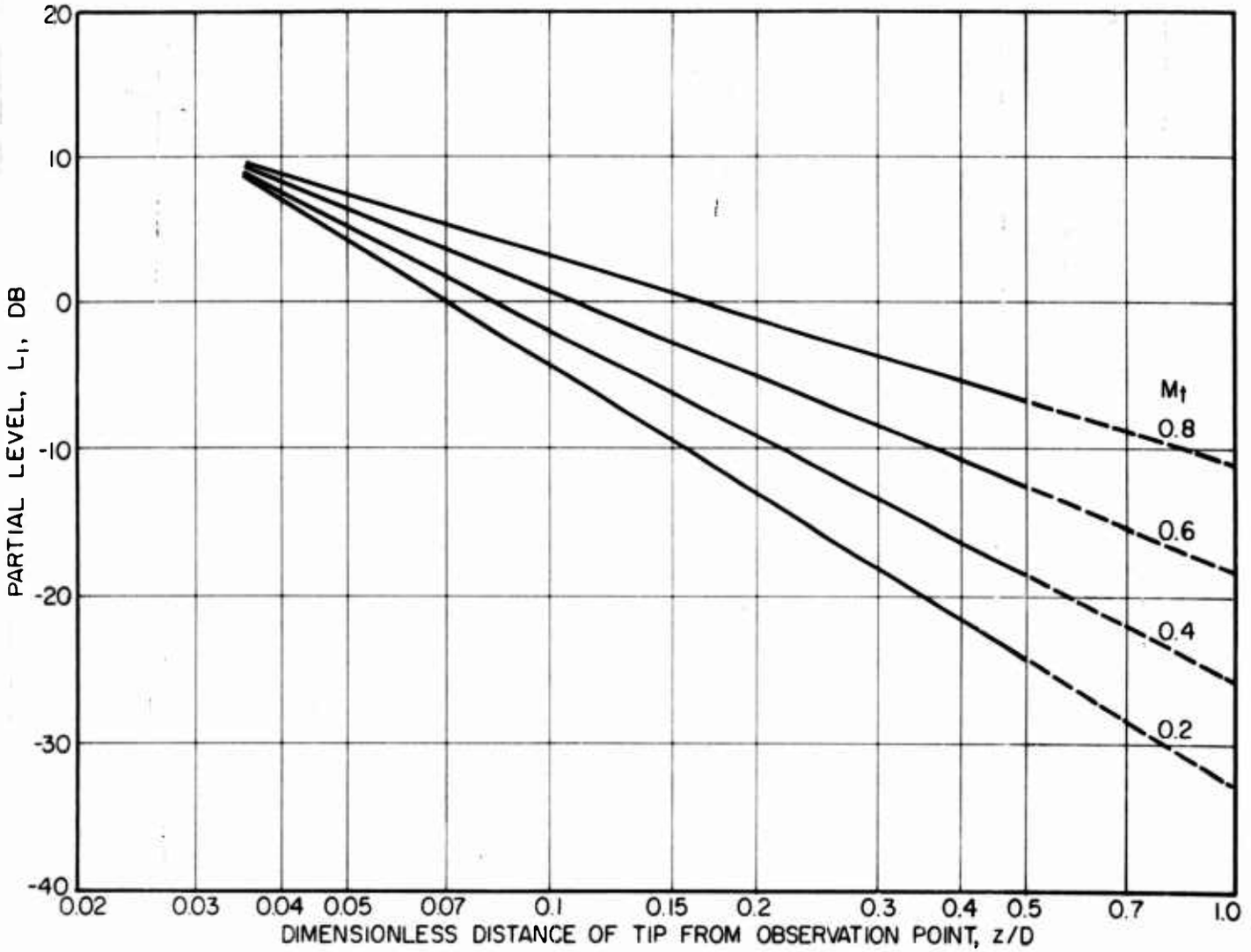

FIG. 3 NEAR FIELD PROPELLER NOISE CHART - 2.

DEPENDENCE OF OVERALL, FREE-SPACE SOUND PRESSURE LEVEL ON z/D, AND ON ROTATIONAL TIP MACH NUMBER, M_t, FOR 3-BLADED PROPELLERS; AIR TEMPERATURE = 68° F.

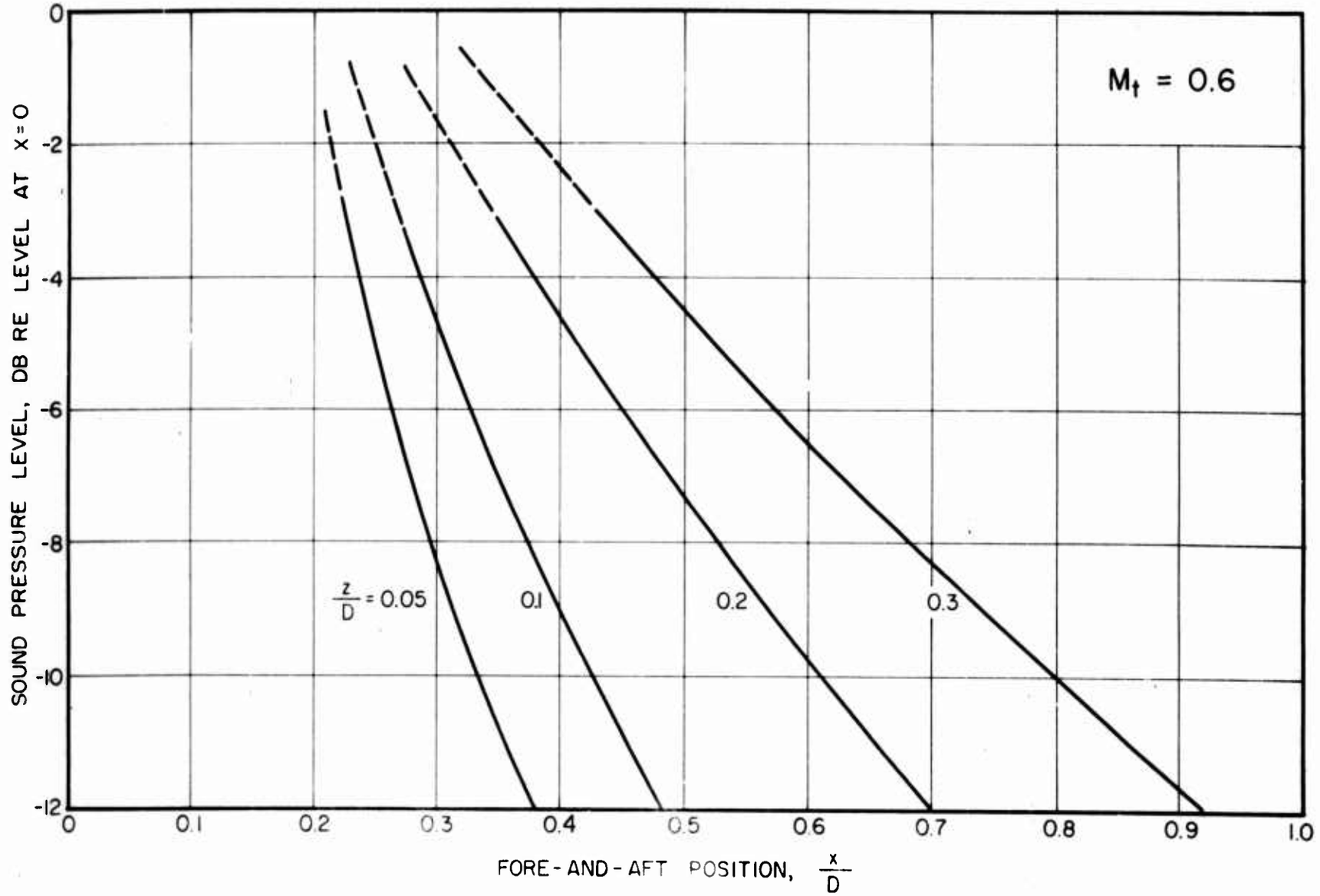

FIG. 4 VARIATION OF OVERALL, FREE-SPACE PROPELLER NOISE LEVELS WITH AXIAL POSITION FORE AND AFT OF PROPELLER PLANE.

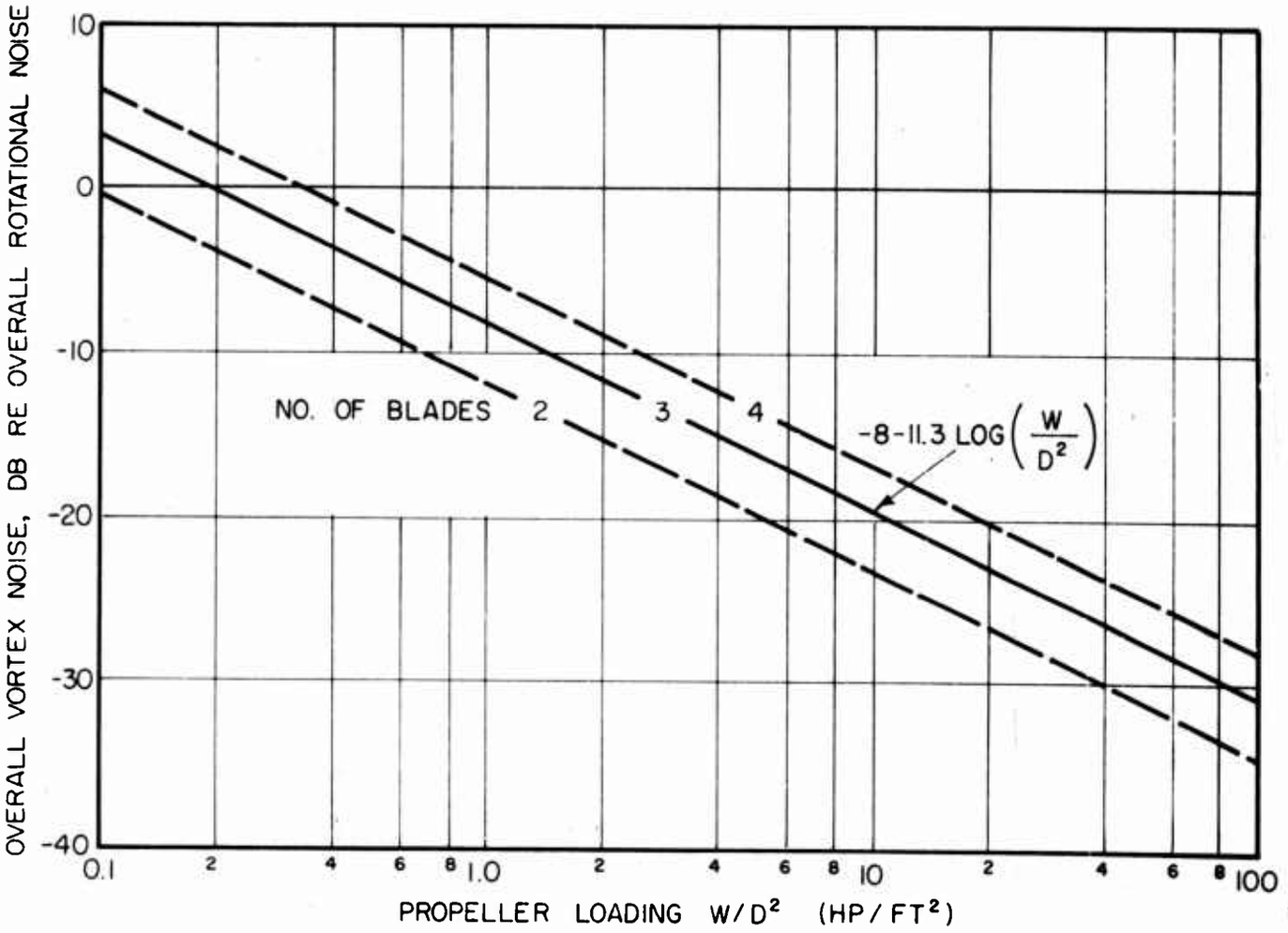

FIG. 5 NEAR FIELD PROPELLER NOISE SPECTRA - I.
RELATIVE CONTRIBUTION OF VORTEX AND ROTATIONAL SOURCES.

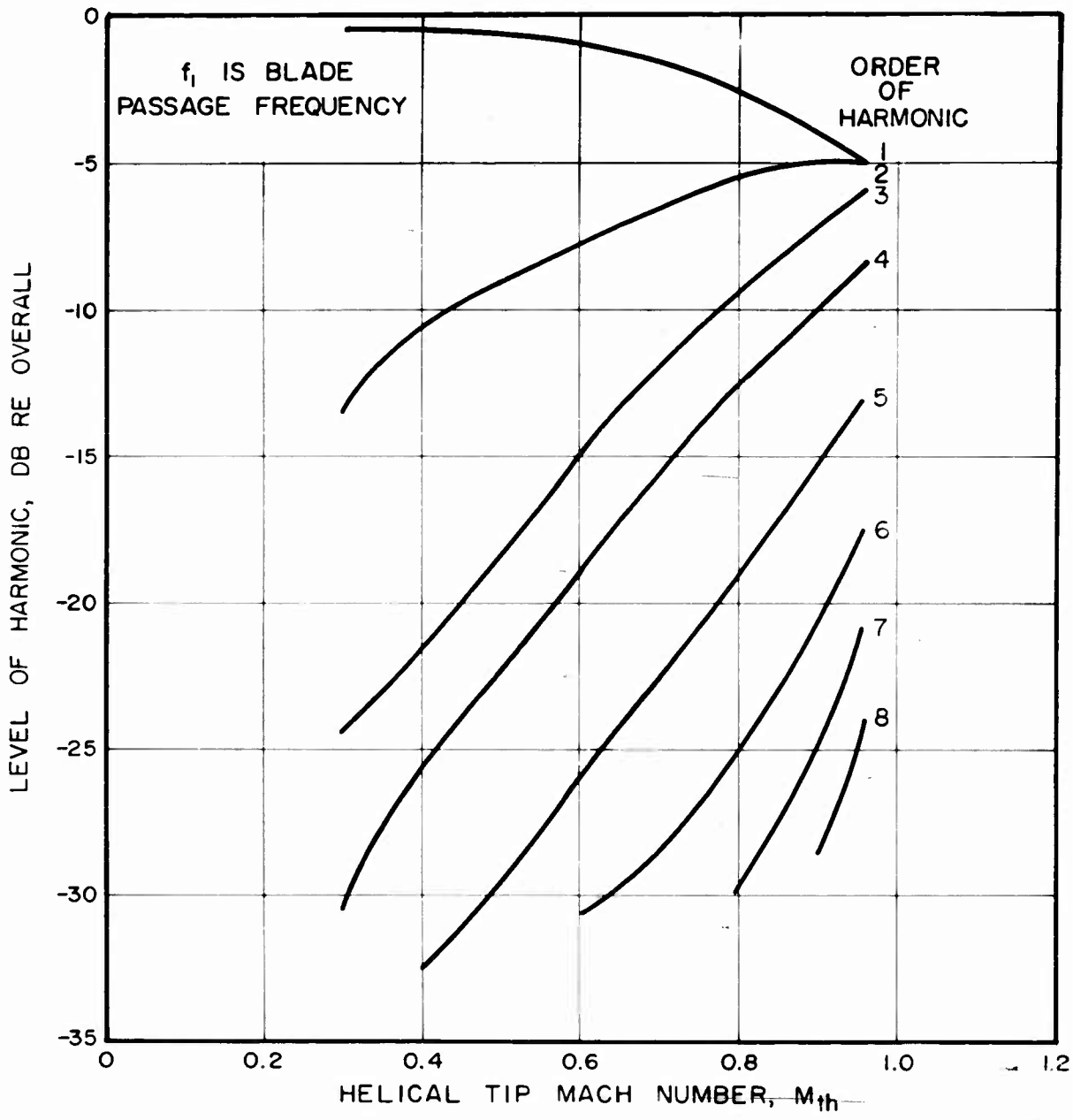

FIG. 6 NEAR FIELD PROPELLER NOISE SPECTRA – 2. ROTATIONAL NOISE.

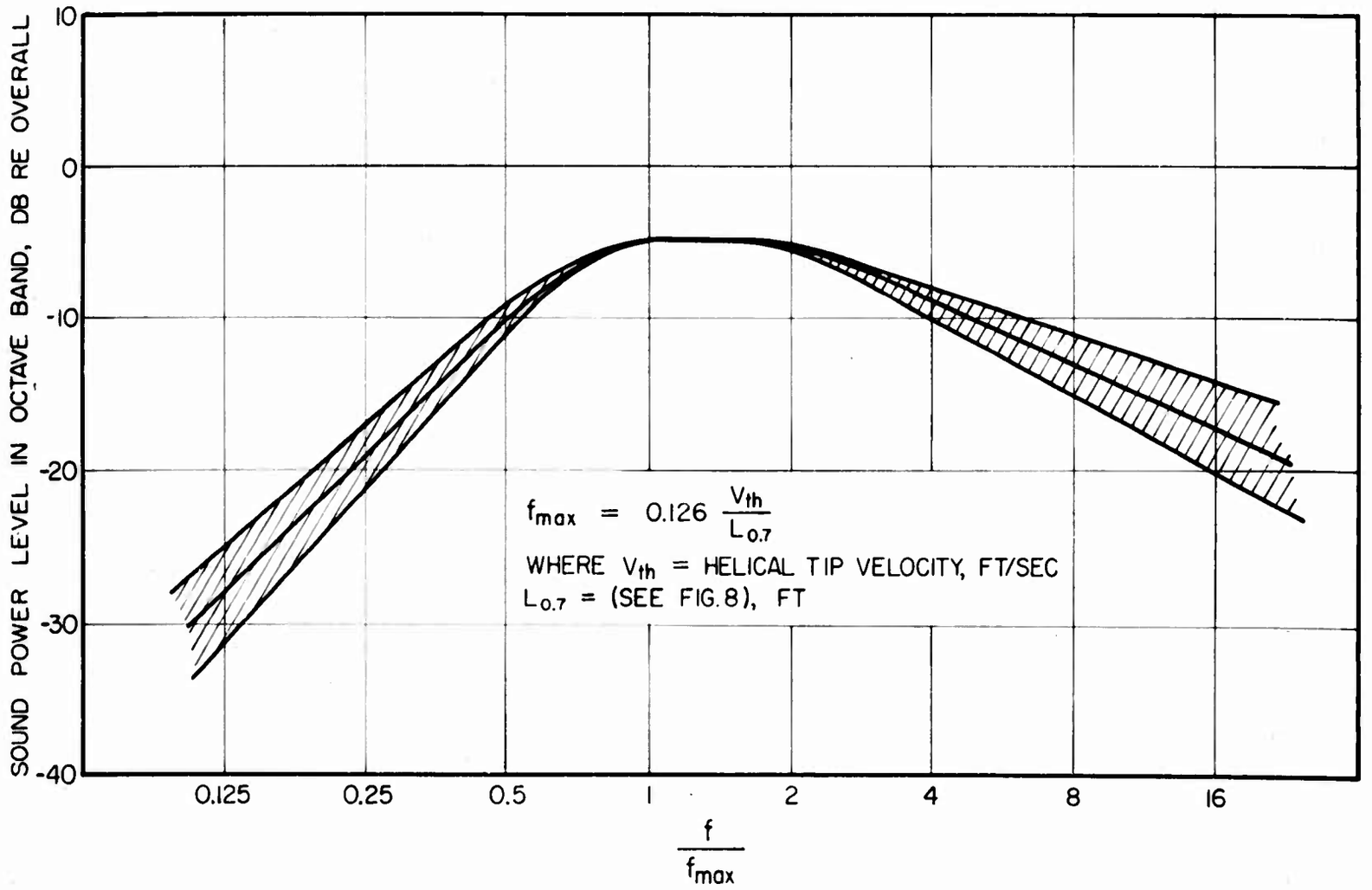

FIG. 7 NEAR FIELD PROPELLER NOISE SPECTRA - 3, VORTEX NOISE.

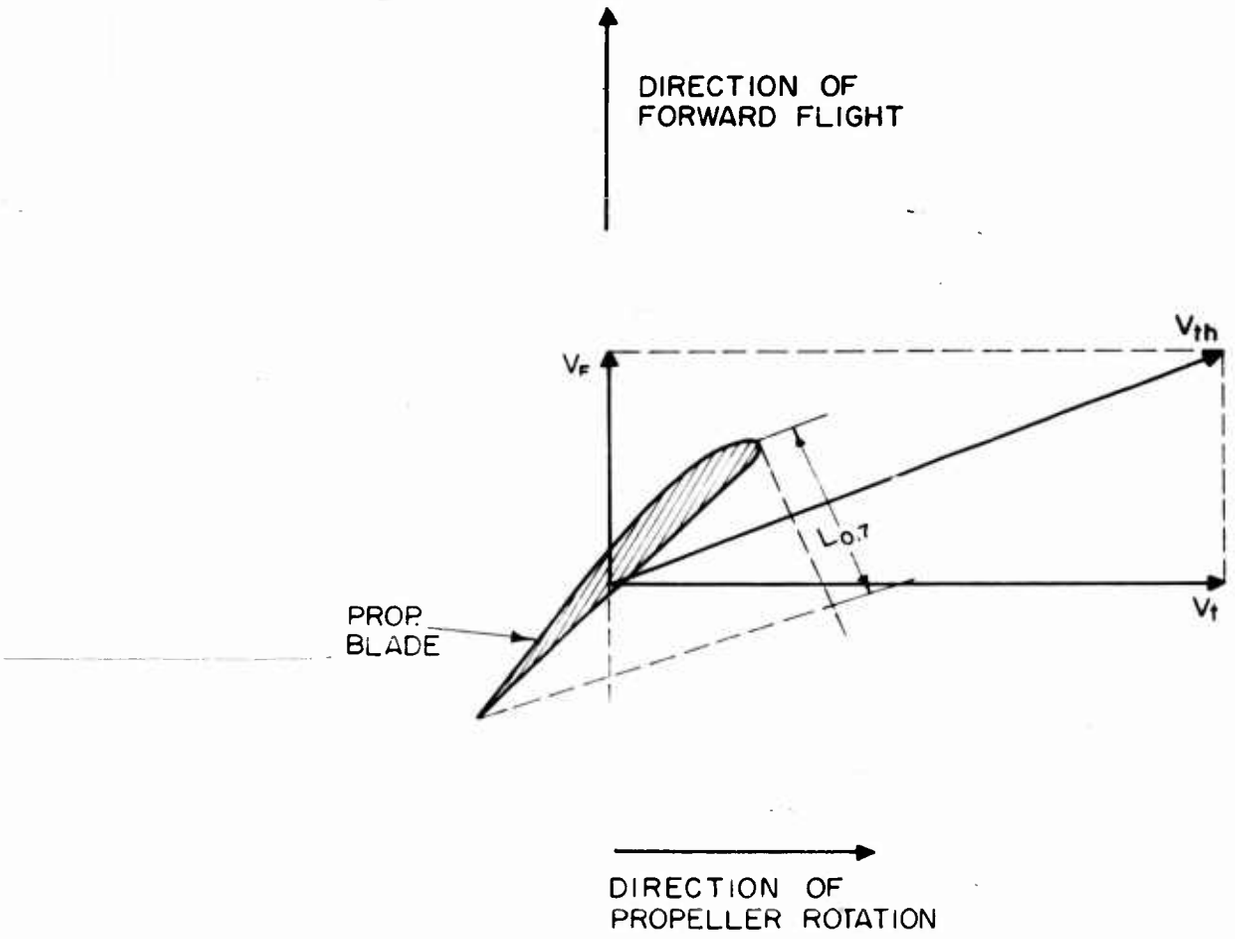

FIG. 8 GEOMETRICAL PROCEDURE FOR DETERMINING $L_{0.7}$
(REF. FIG. 7)

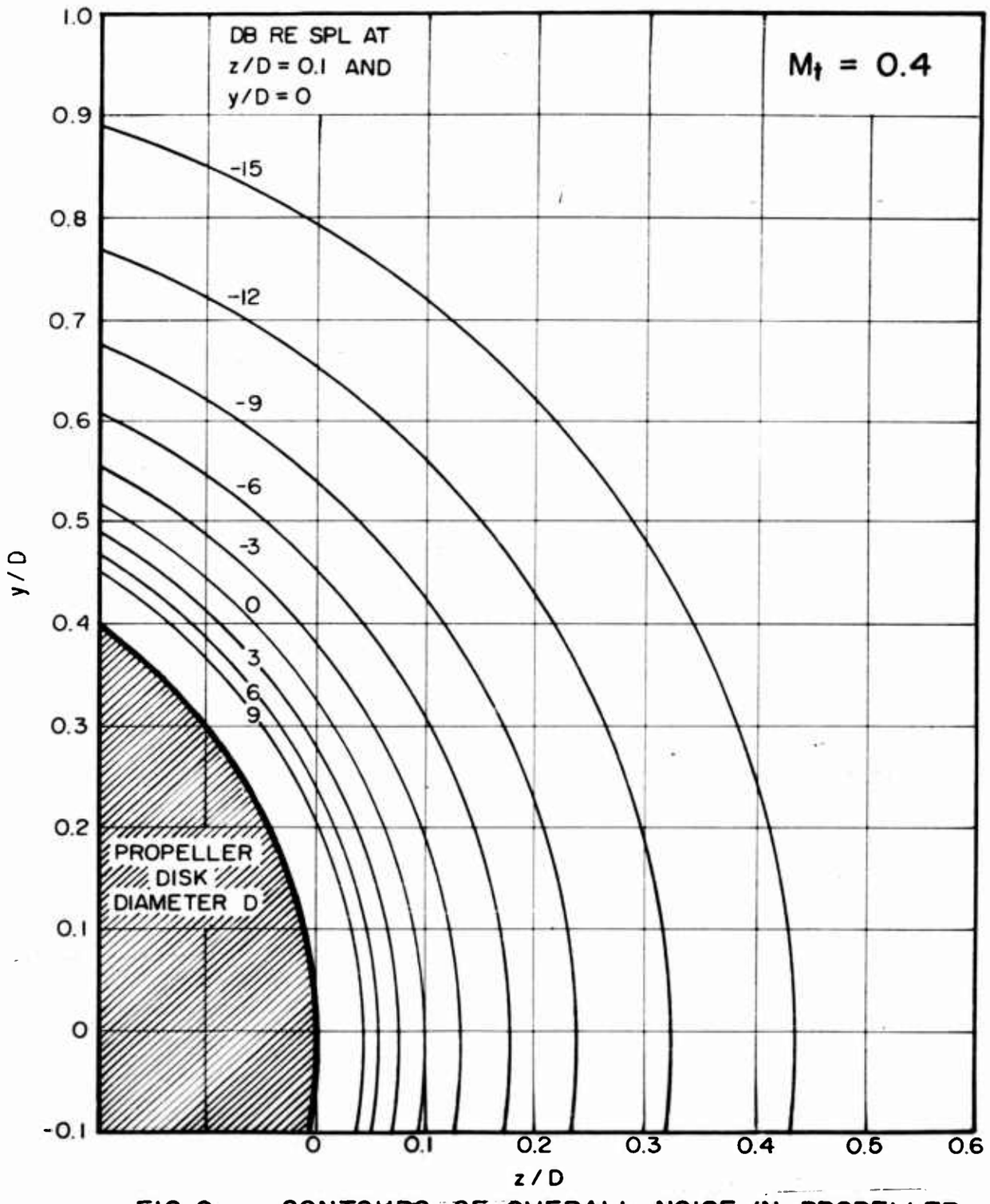

FIG. 9 CONTOURS OF OVERALL NOISE IN PROPELLER PLANE, M_t = 0.4

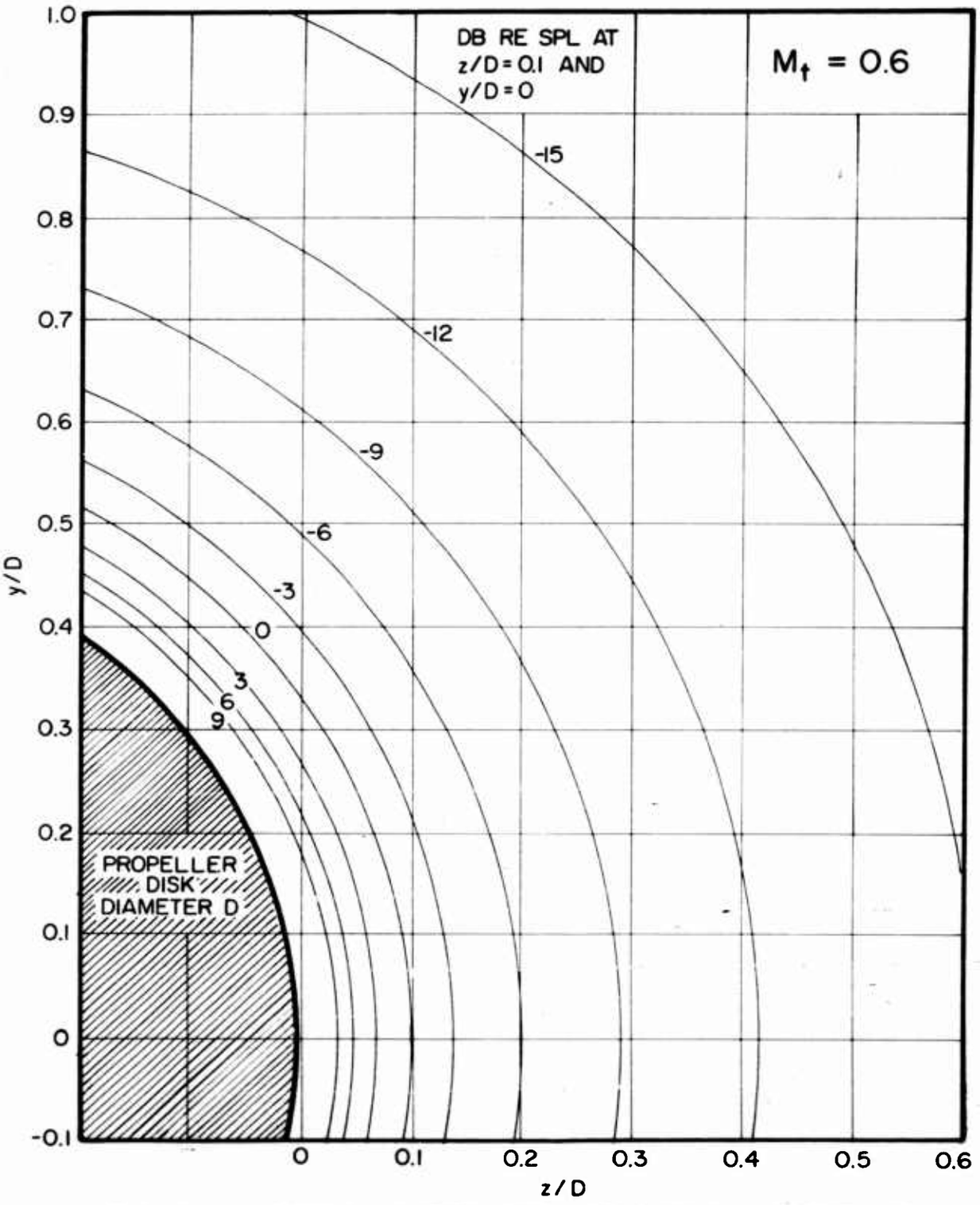

FIG. 10 SPATIAL DISTRIBUTION OF OVERALL PROPELLER NOISE IN PROPELLER PLANE, $M_t = 0.6$.

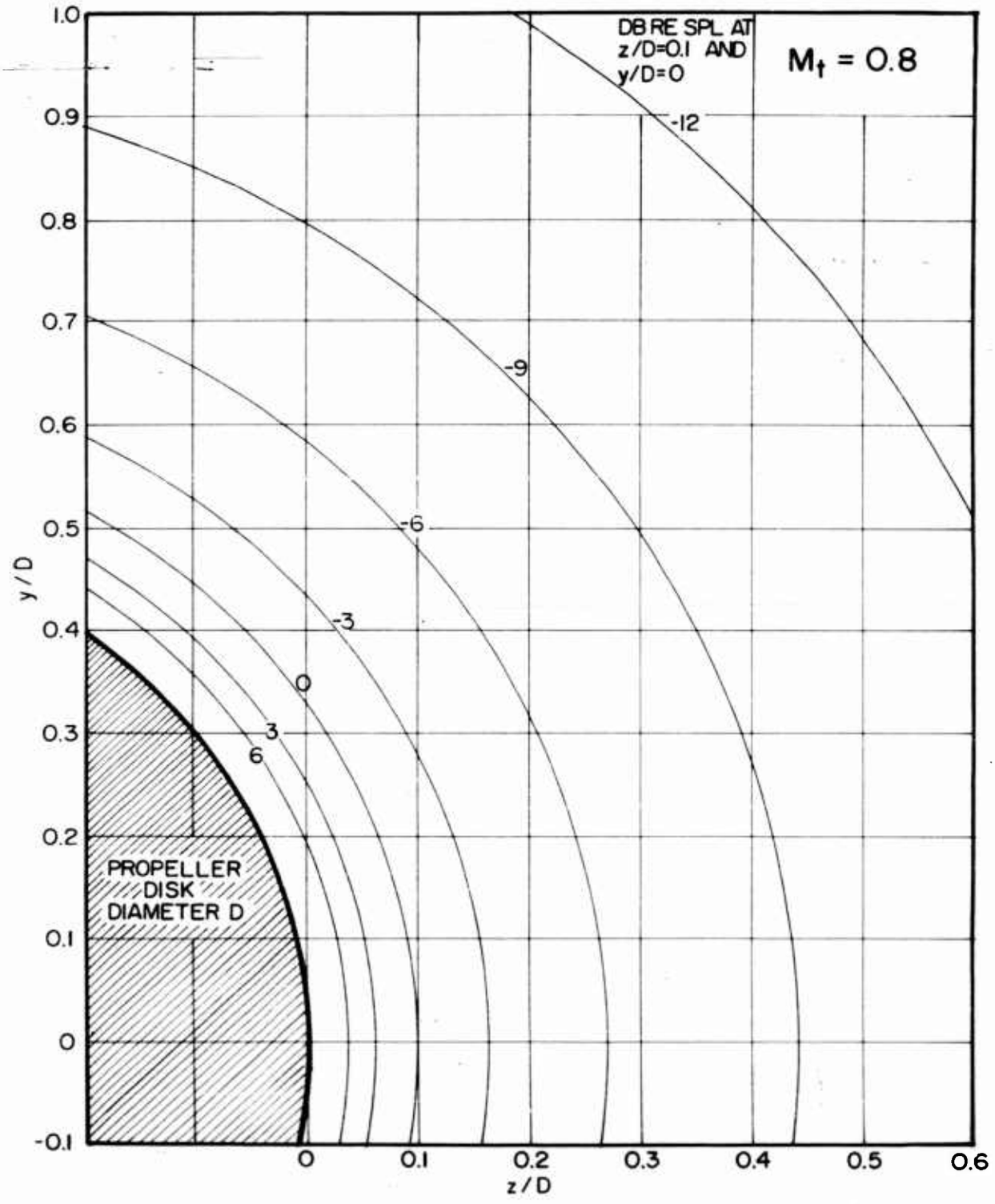

FIG. 11 SPATIAL DISTRIBUTION OF OVERALL PROPELLER NOISE IN PROPELLER PLANE, $M_t = 0.8$

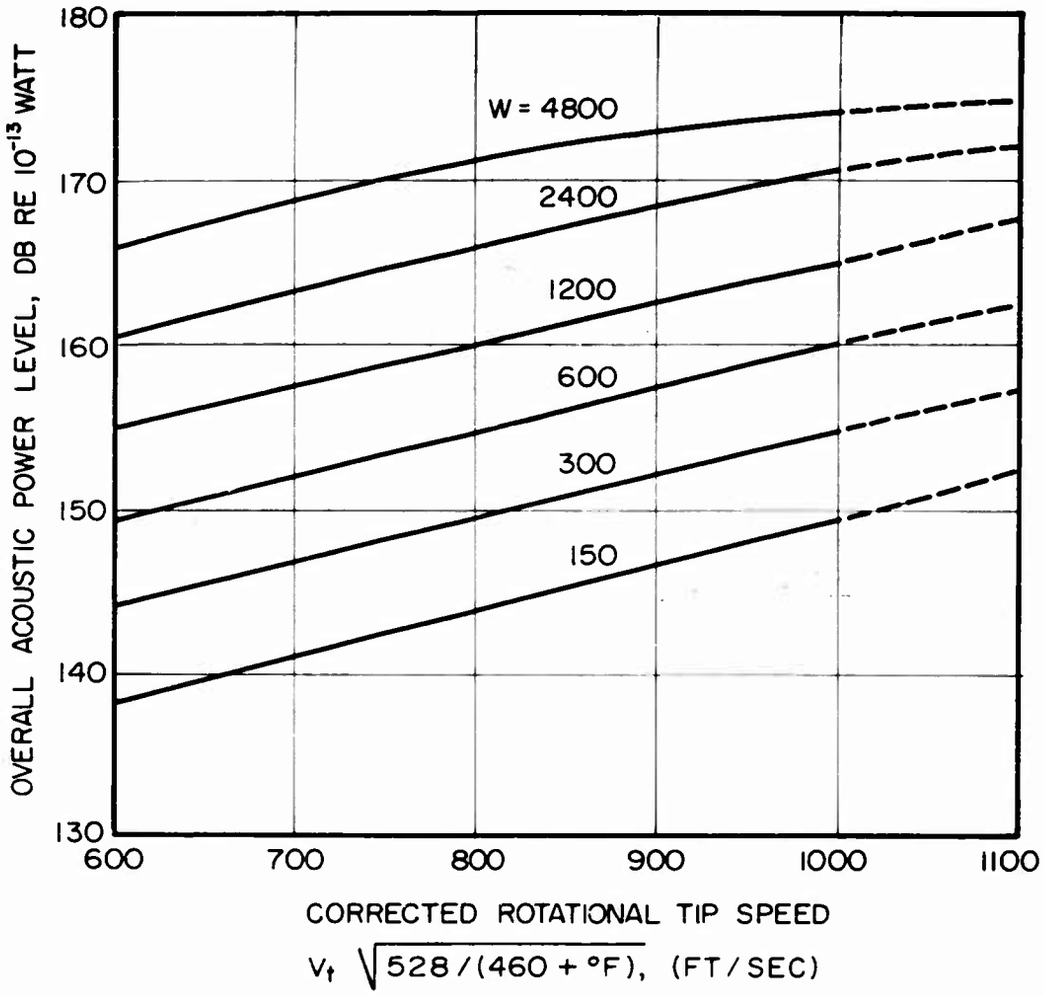

FIG. 12 OVERALL ACOUSTIC POWER LEVEL OF FAR-FIELD NOISE OF 3-BLADED PROPELLERS. DEPENDENCE ON TOTAL POWER, W, DELIVERED TO PROPELLER AND ON CORRECTED TIP SPEED. FOR 2-BLADED PROPELLERS ADD 2 DB; FOR 4-BLADED PROPELLERS SUBTRACT 2 DB.

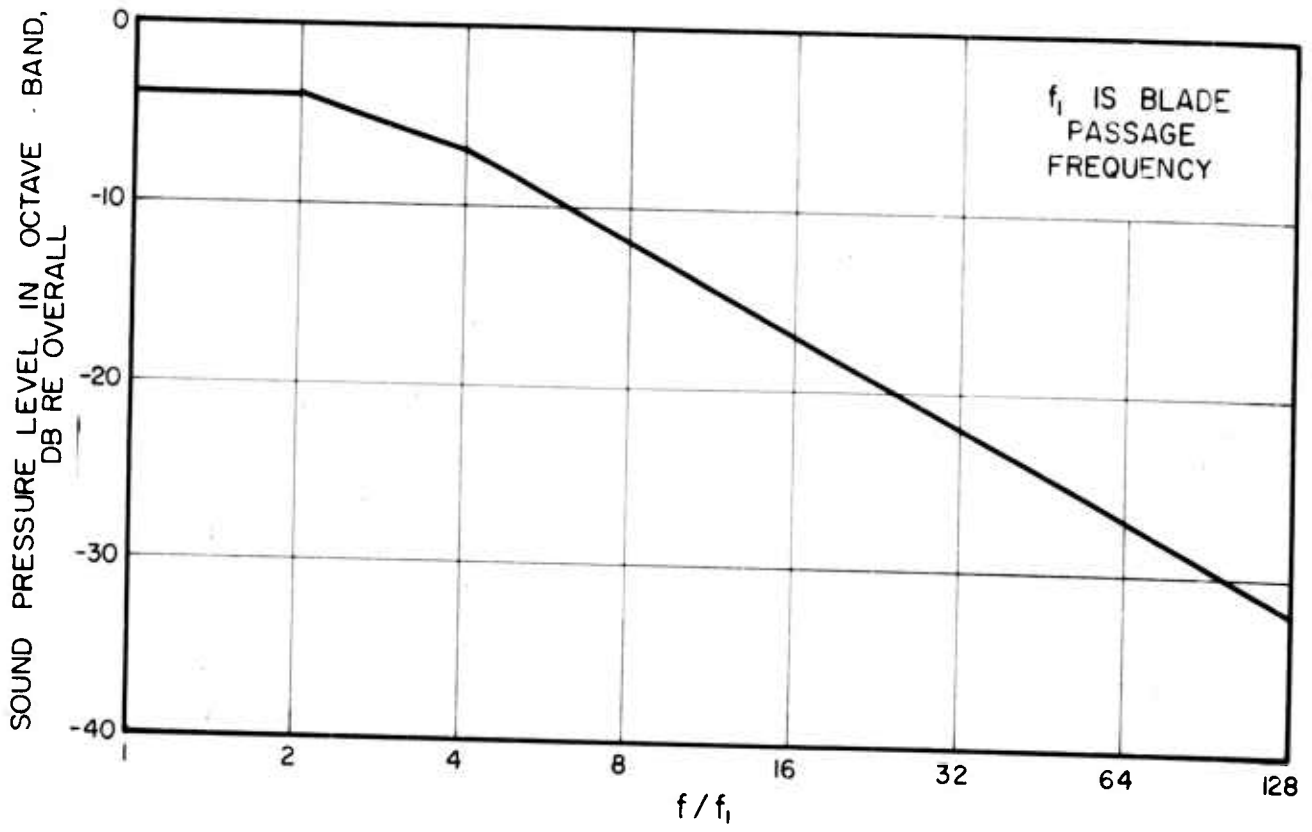

FIG. 13 FAR FIELD PROPELLER NOISE SPECTRUM.

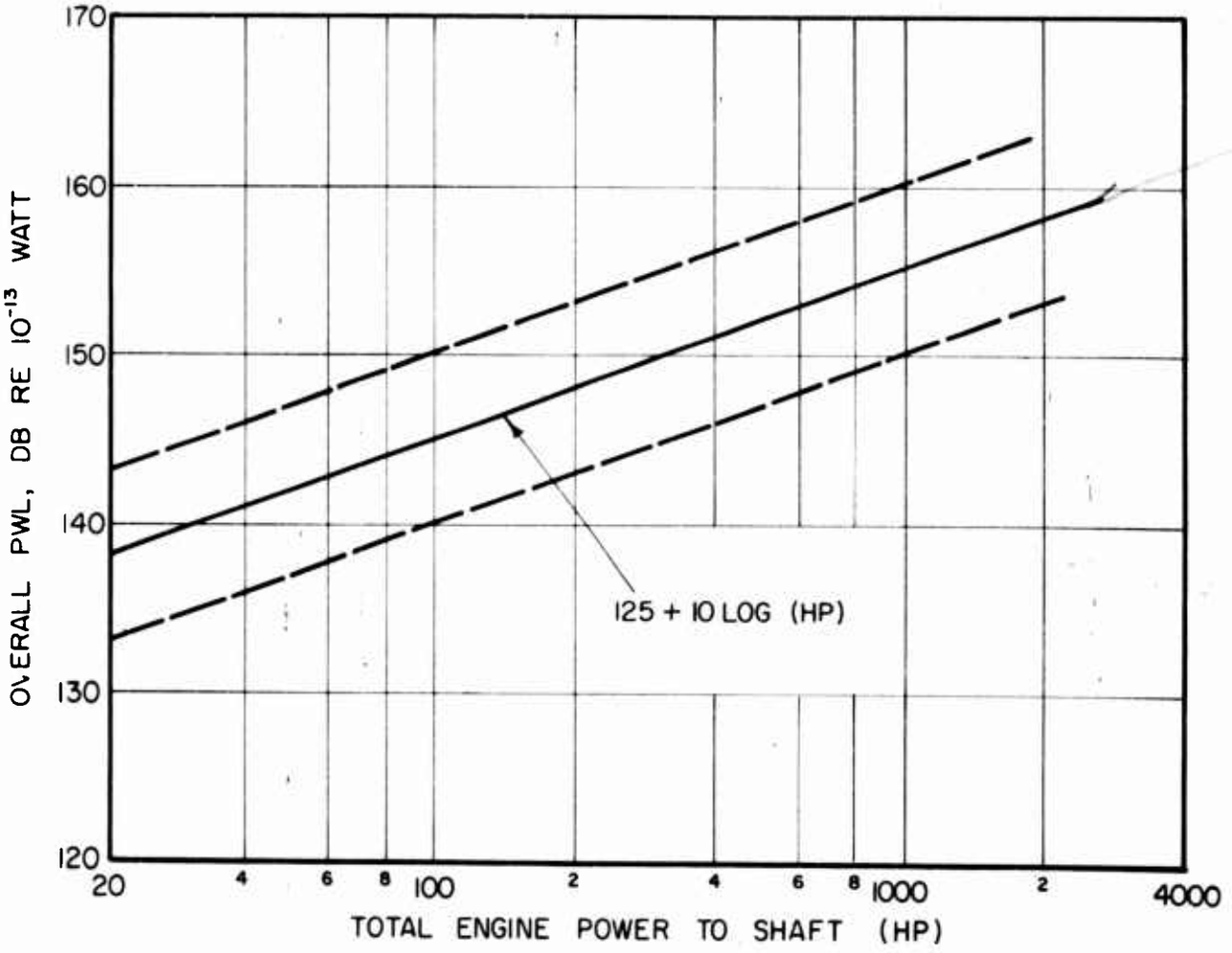

FIG. 14 OVERALL ACOUSTIC POWER LEVEL OF EXHAUST NOISE OF TYPICAL INTERNAL COMBUSTION ENGINES.

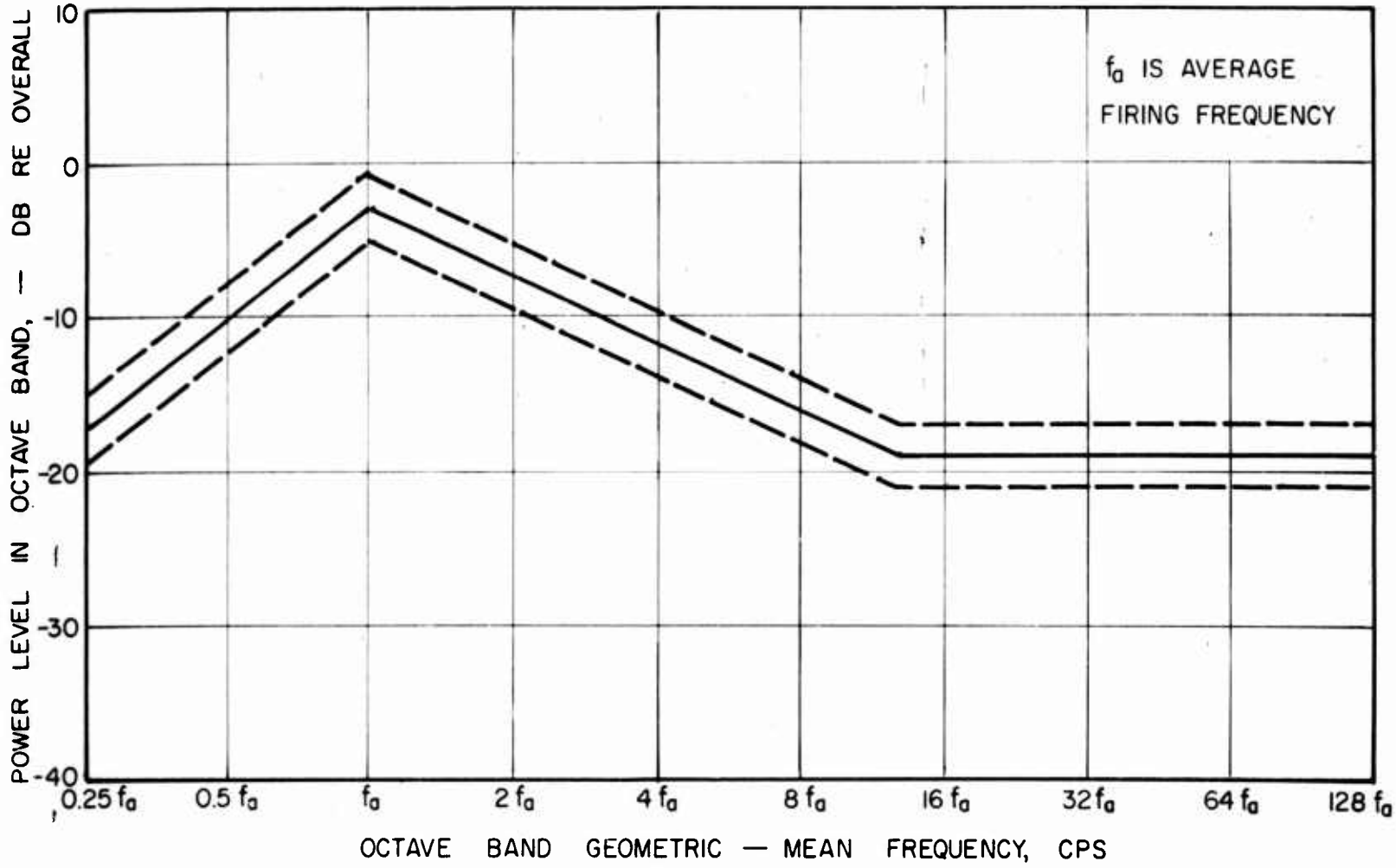

FIG. 15 SPECTRUM OF EXHAUST NOISE OF TYPICAL INTERNAL COMBUSTION ENGINE.

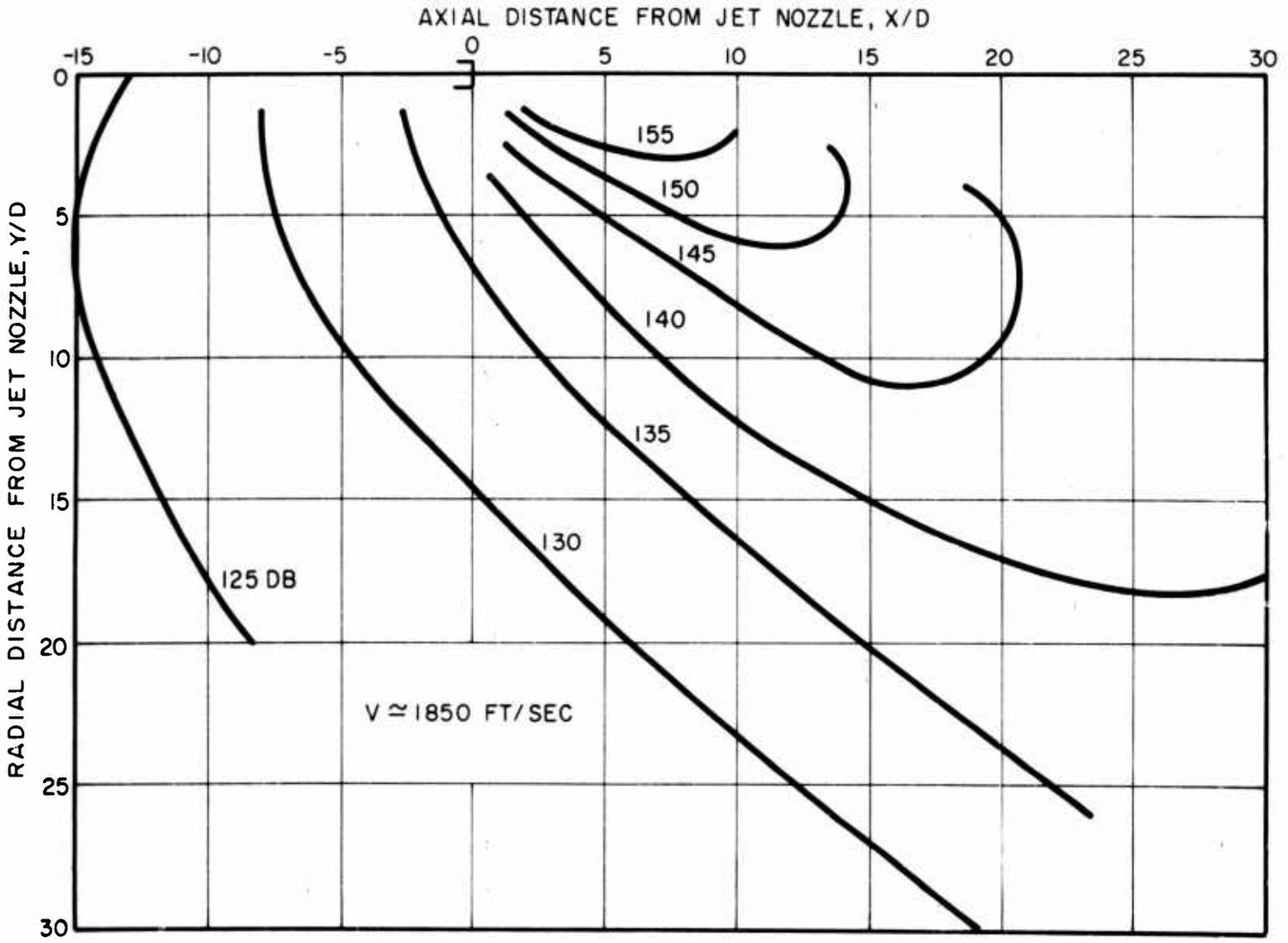

FIG. 16 NEAR SOUND FIELD OF A TURBOJET

REFERENCE CONTOURS OF OVERALL SOUND PRESSURE LEVEL

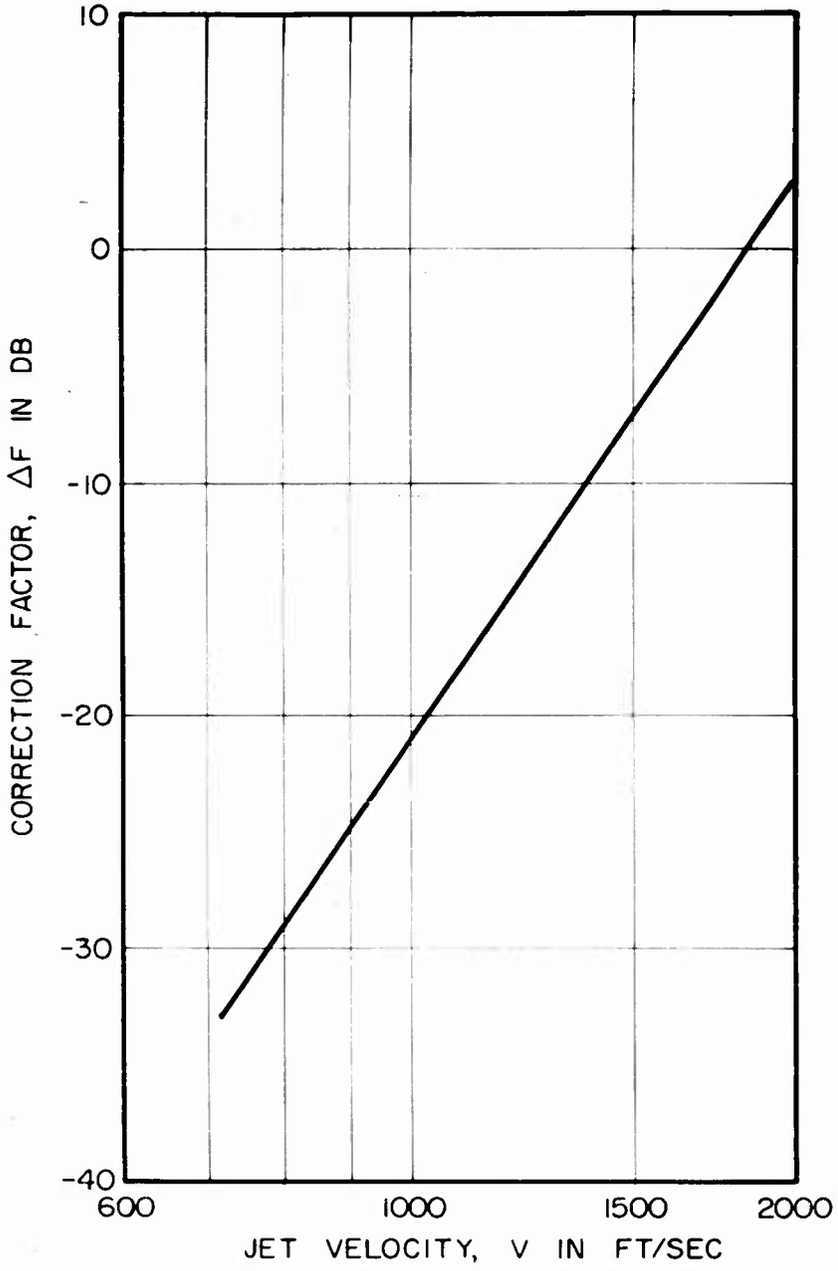

FIG. 17 VELOCITY DEPENDENCE OF NEAR FIELD CONTOUR VALUES

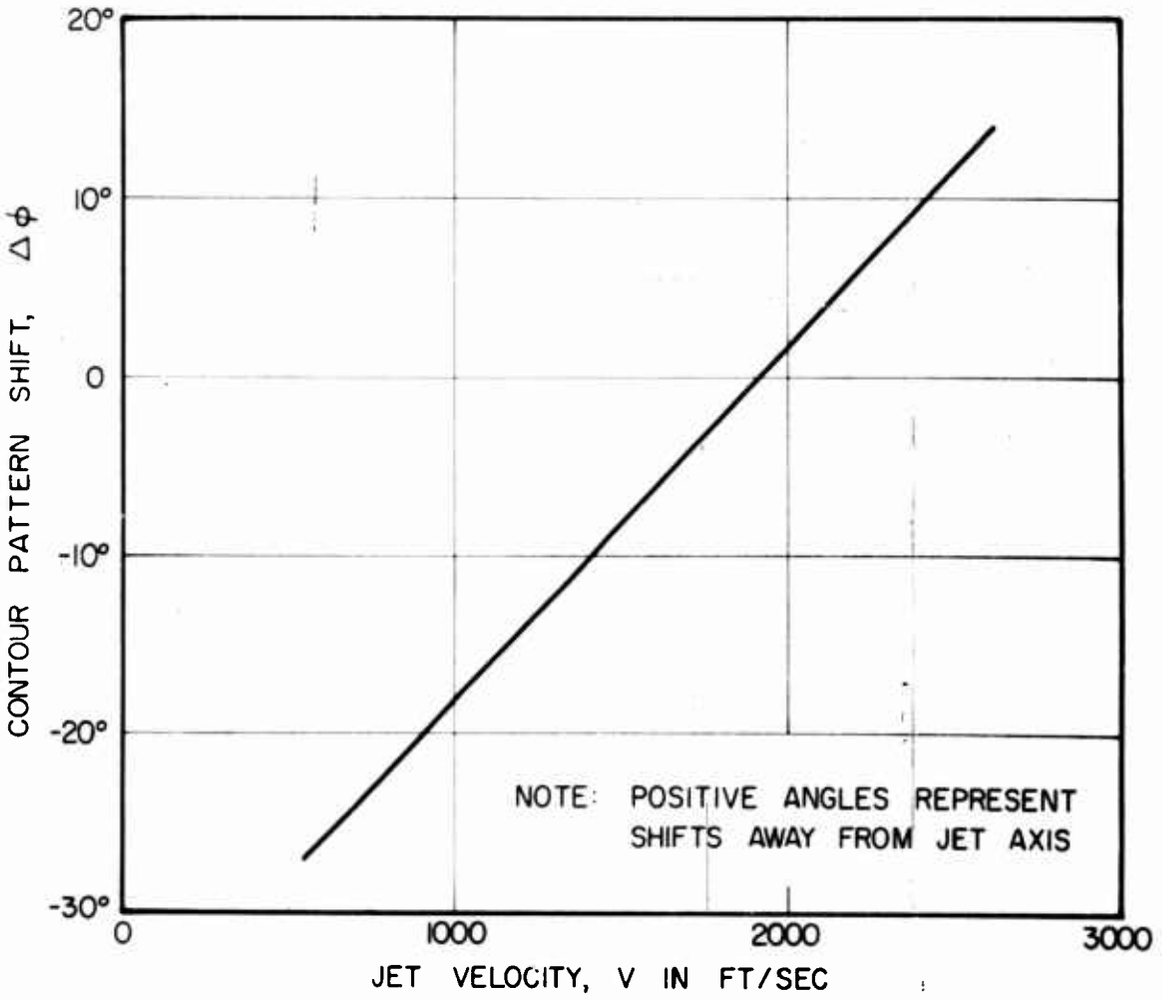

FIG. 18 VELOCITY DEPENDENCE OF OVERALL SPL CONTOUR PATTERN.

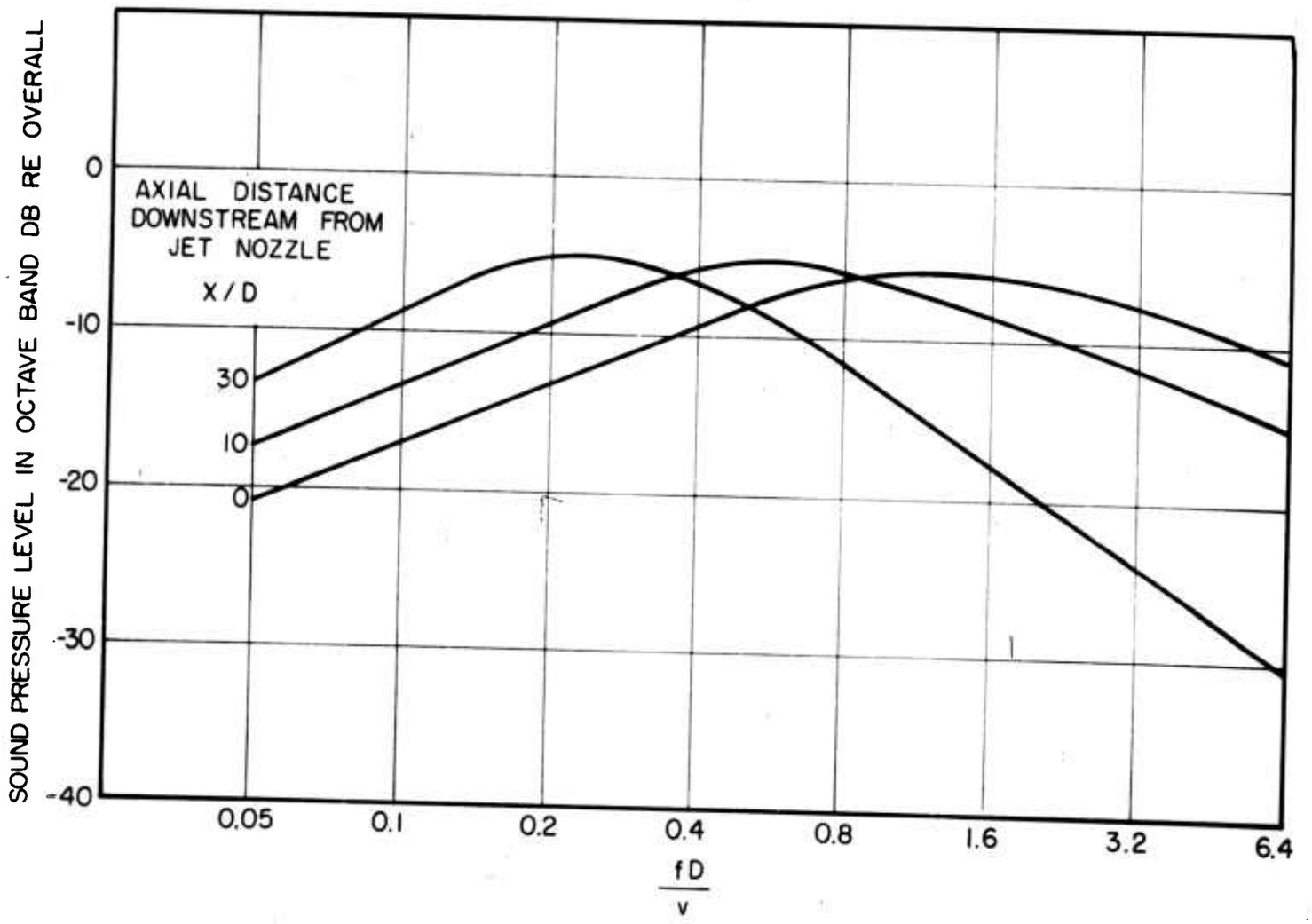

FIG. 19 SPECTRUM OF JET NOISE NEAR FIELD.

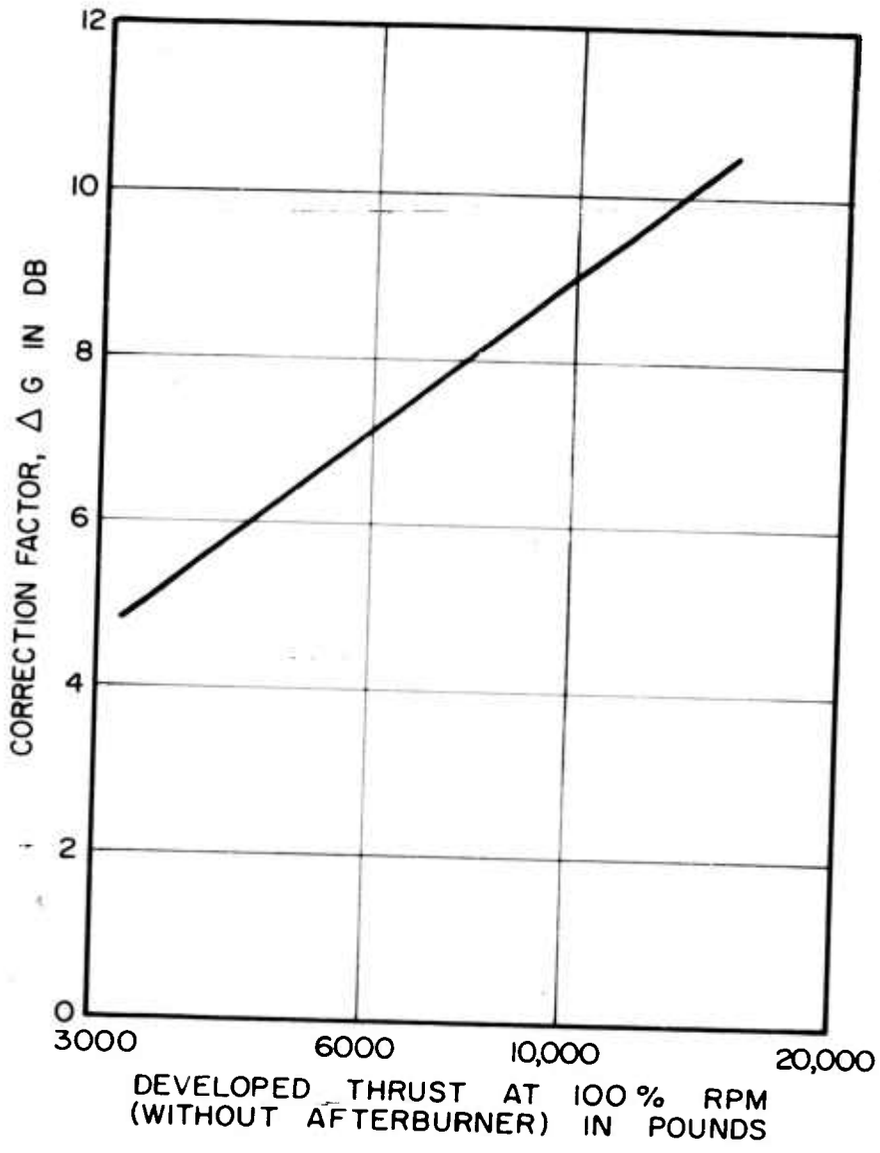

FIG. 20 NEAR FIELD CONTOUR VALUE CORRECTION FOR FULL AFTERBURNER OPERATION.

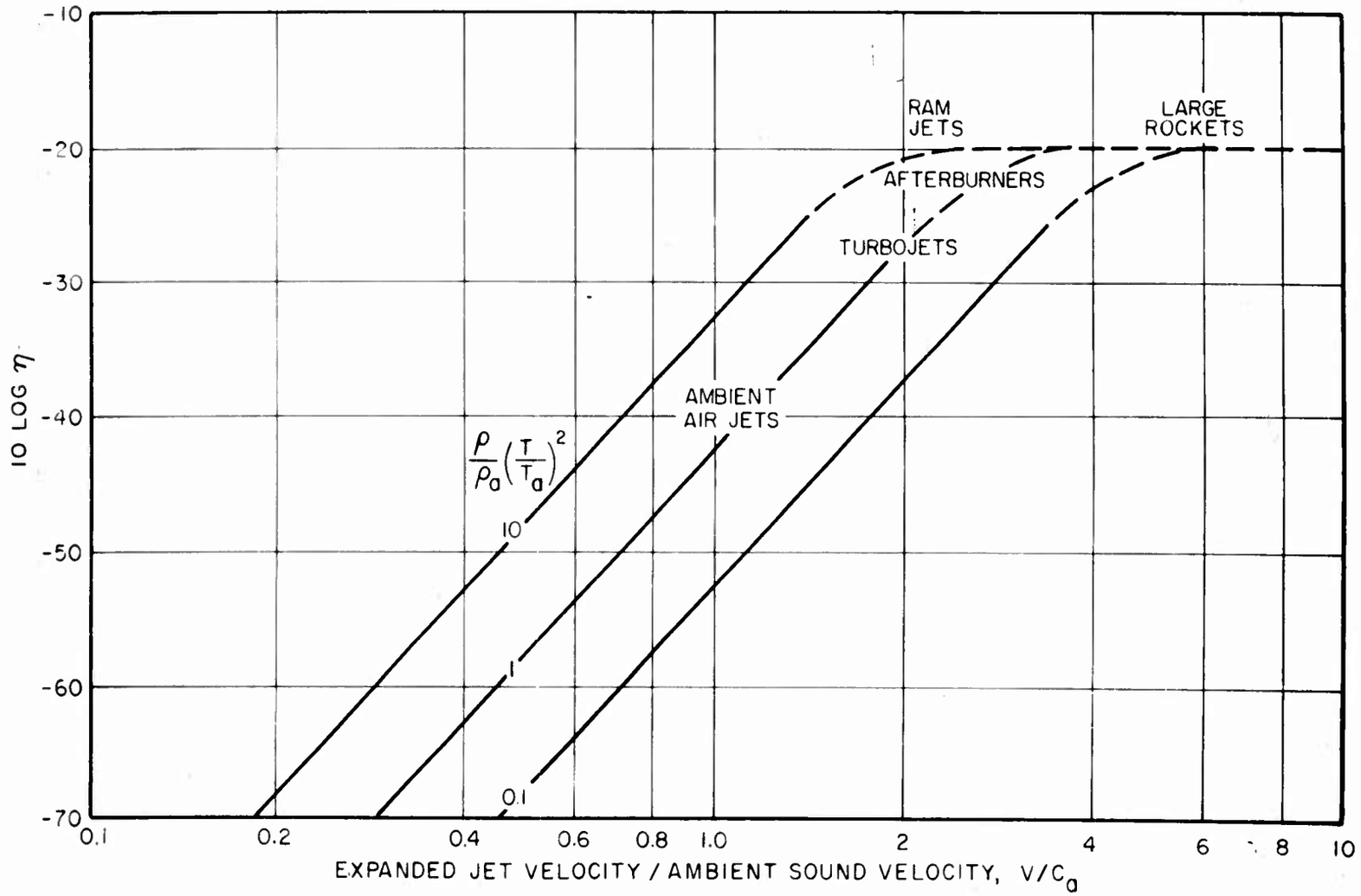

FIG. 21 EFFICIENCY FOR JET NOISE

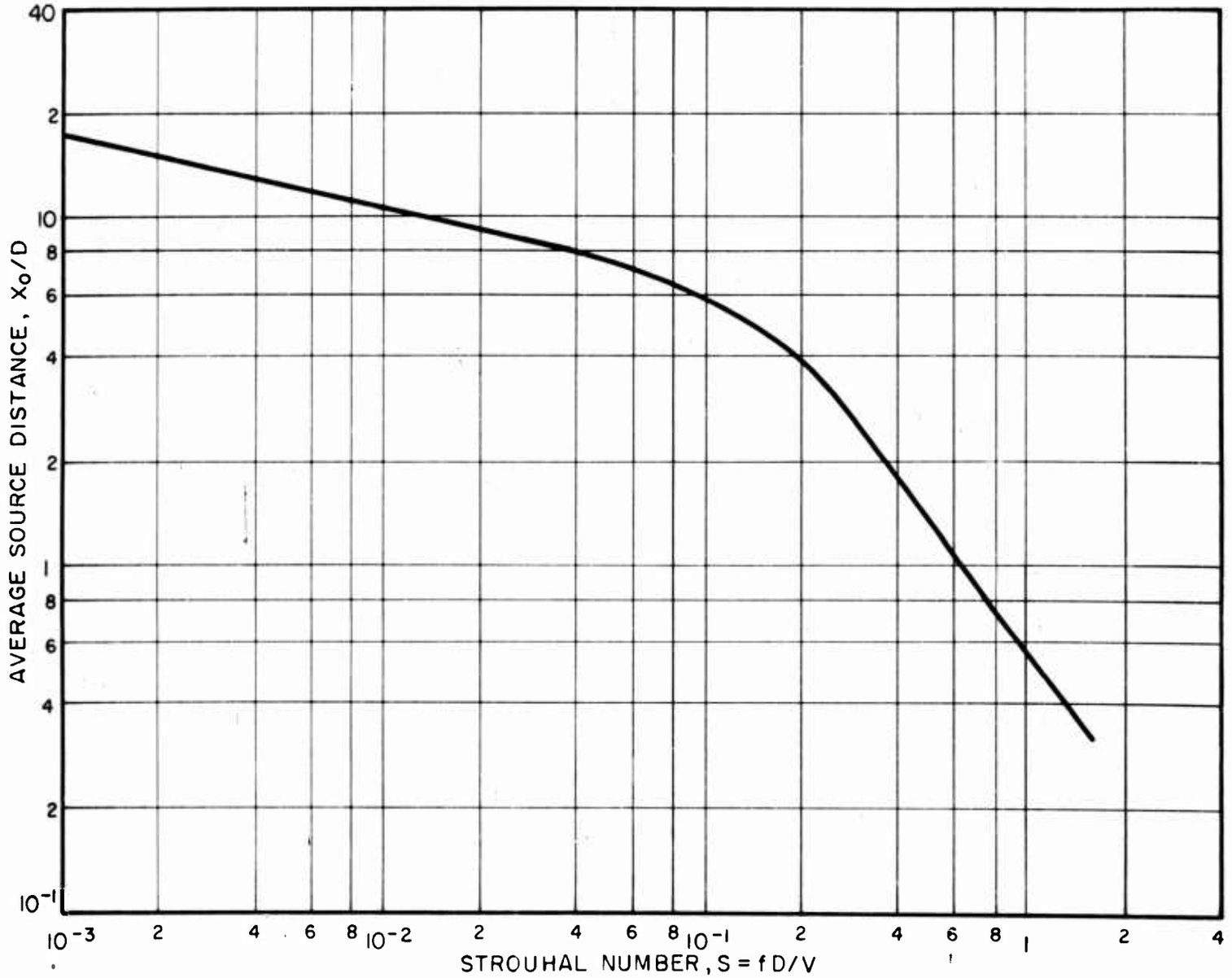

FIG. 22 SOURCE LOCATION AS A FUNCTION OF STROUHAL NUMBER

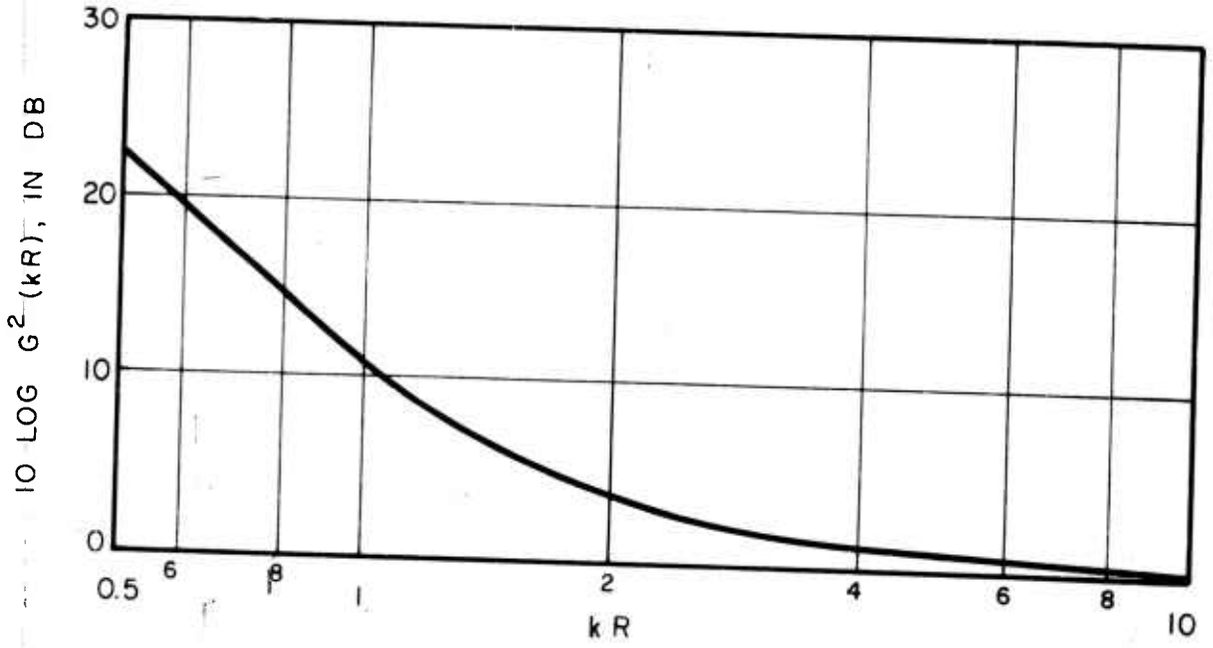

FIG.23 NEAR FIELD TERM

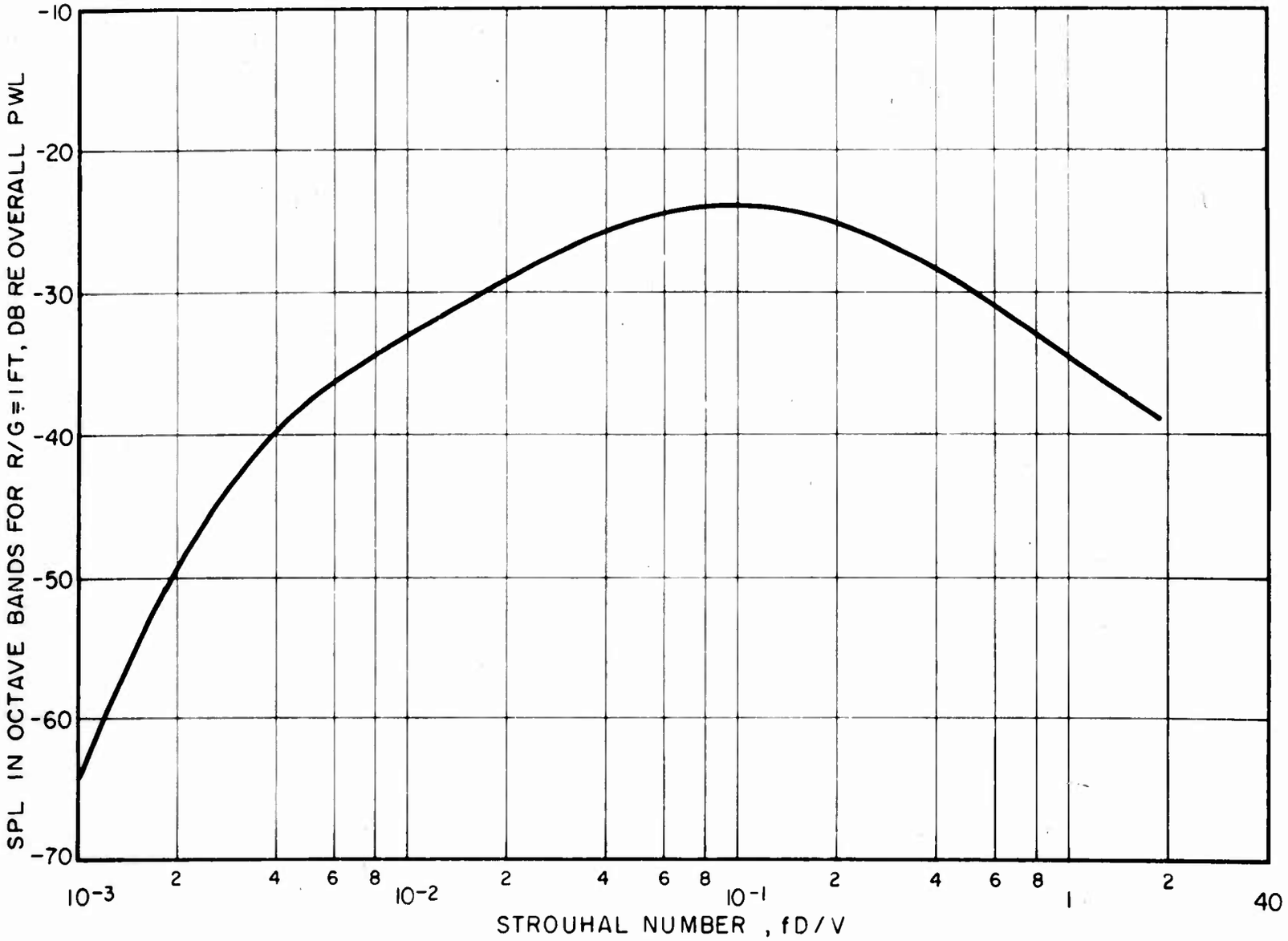

FIG.24 REFERENCE SOUND PRESSURE LEVEL MEASURED OVER MISSILE SURFACE

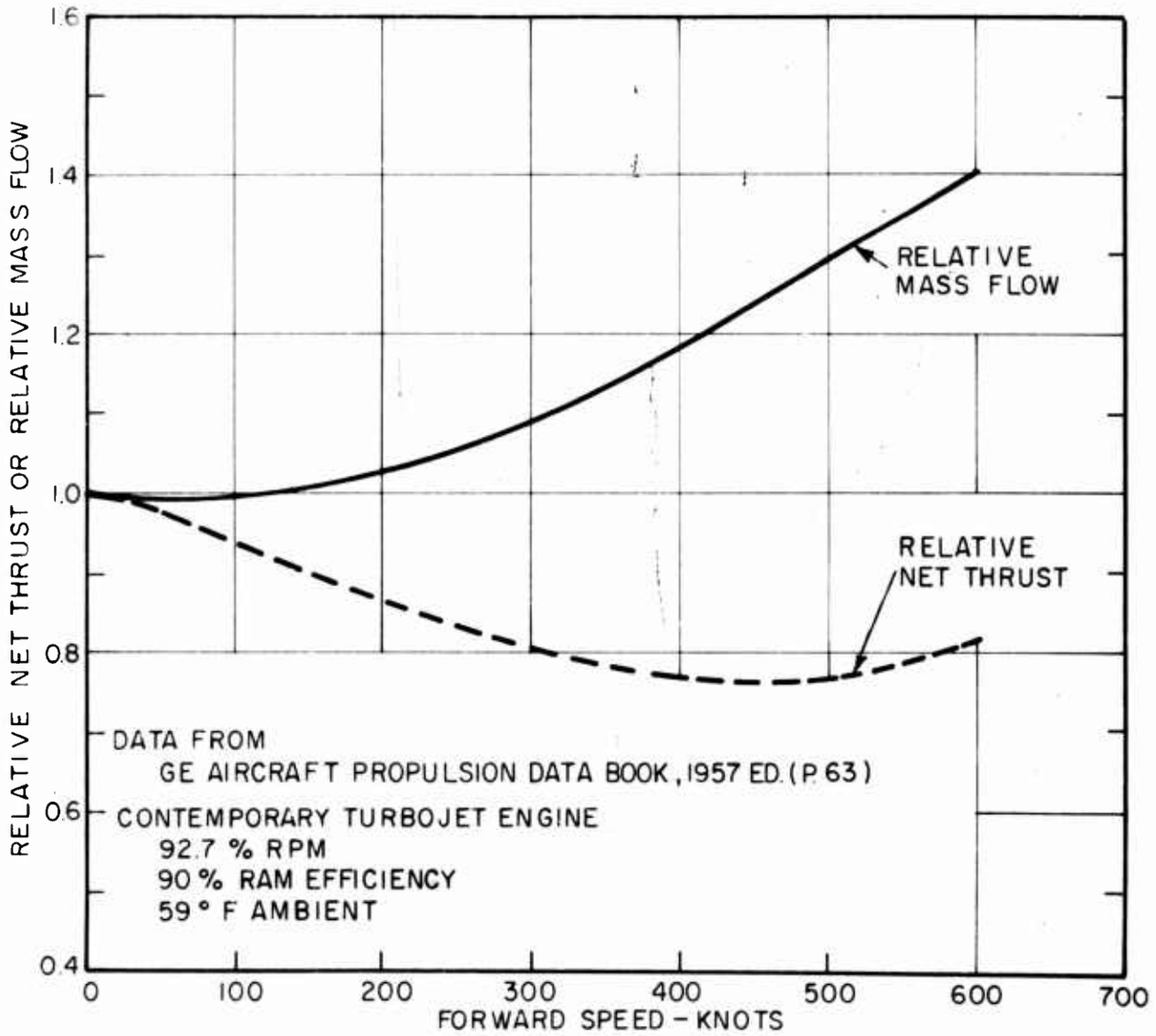

VARIATION OF ENGINE OPERATING PARAMETERS WITH FORWARD SPEED

FIGURE 25

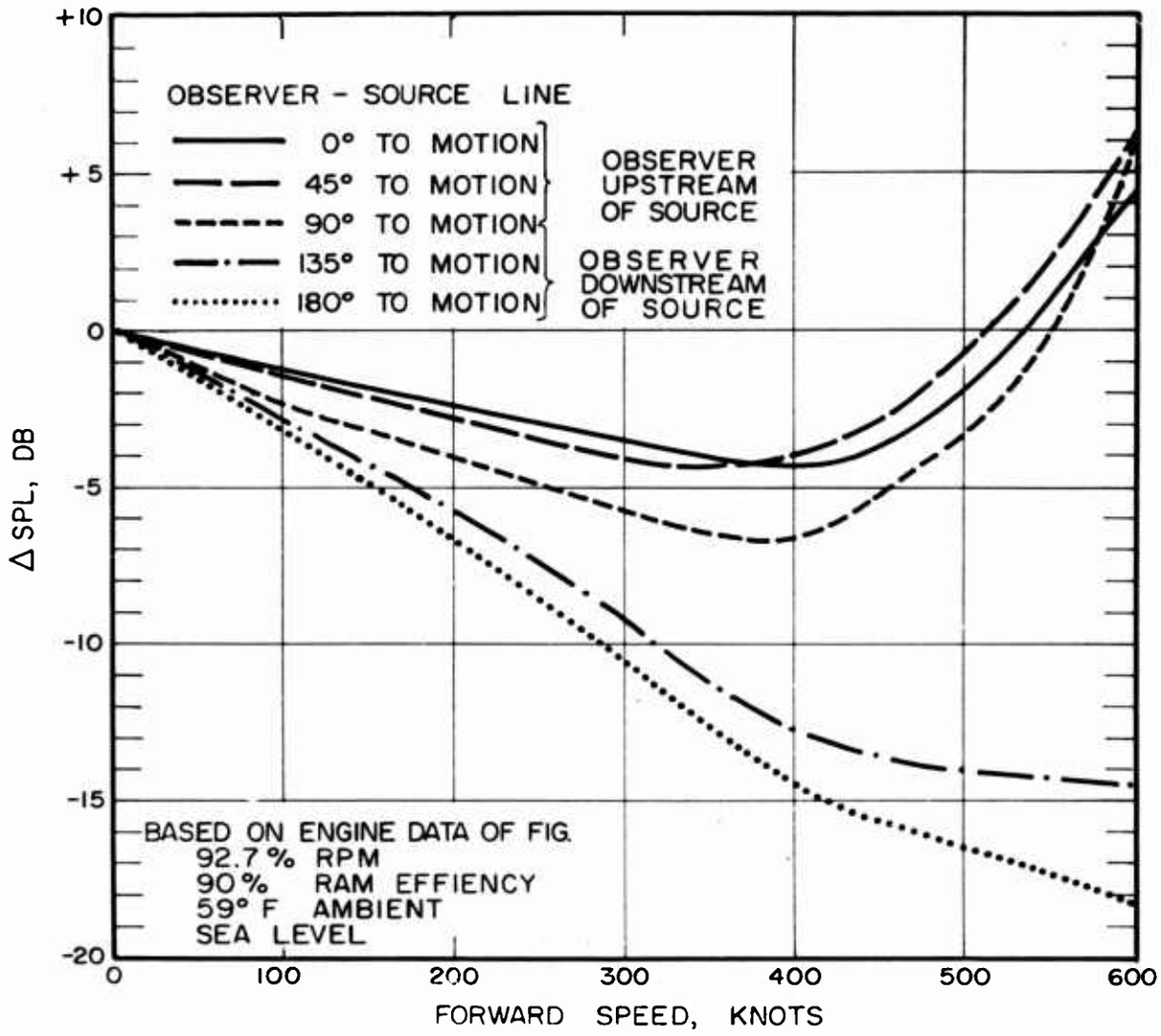

FIG. 26 EFFECT OF FORWARD SPEED ON OVERALL SPL.

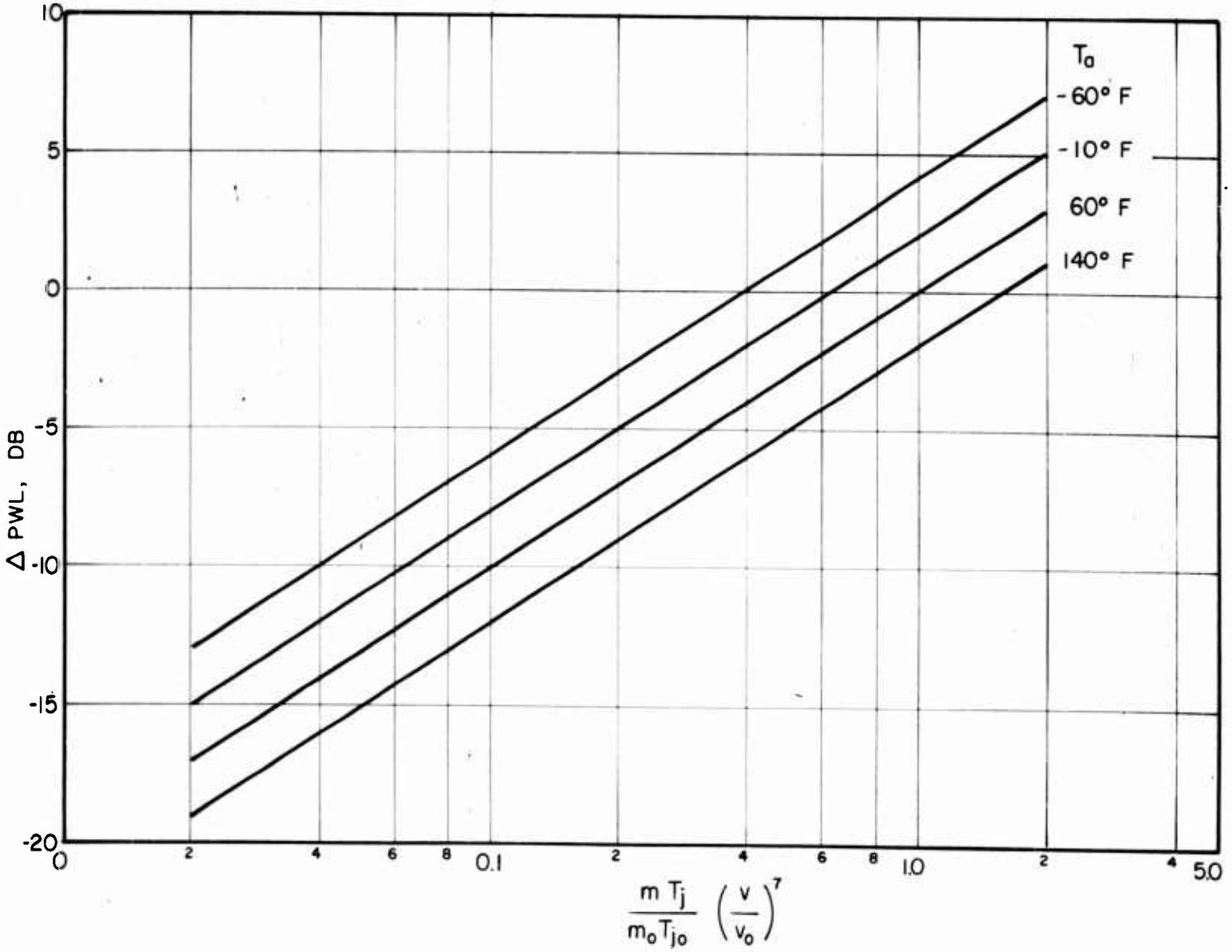

FIG. 27 CHANGE IN SOUND POWER RADIATED BY CONTEMPORARY TURBOJET ENGINES.

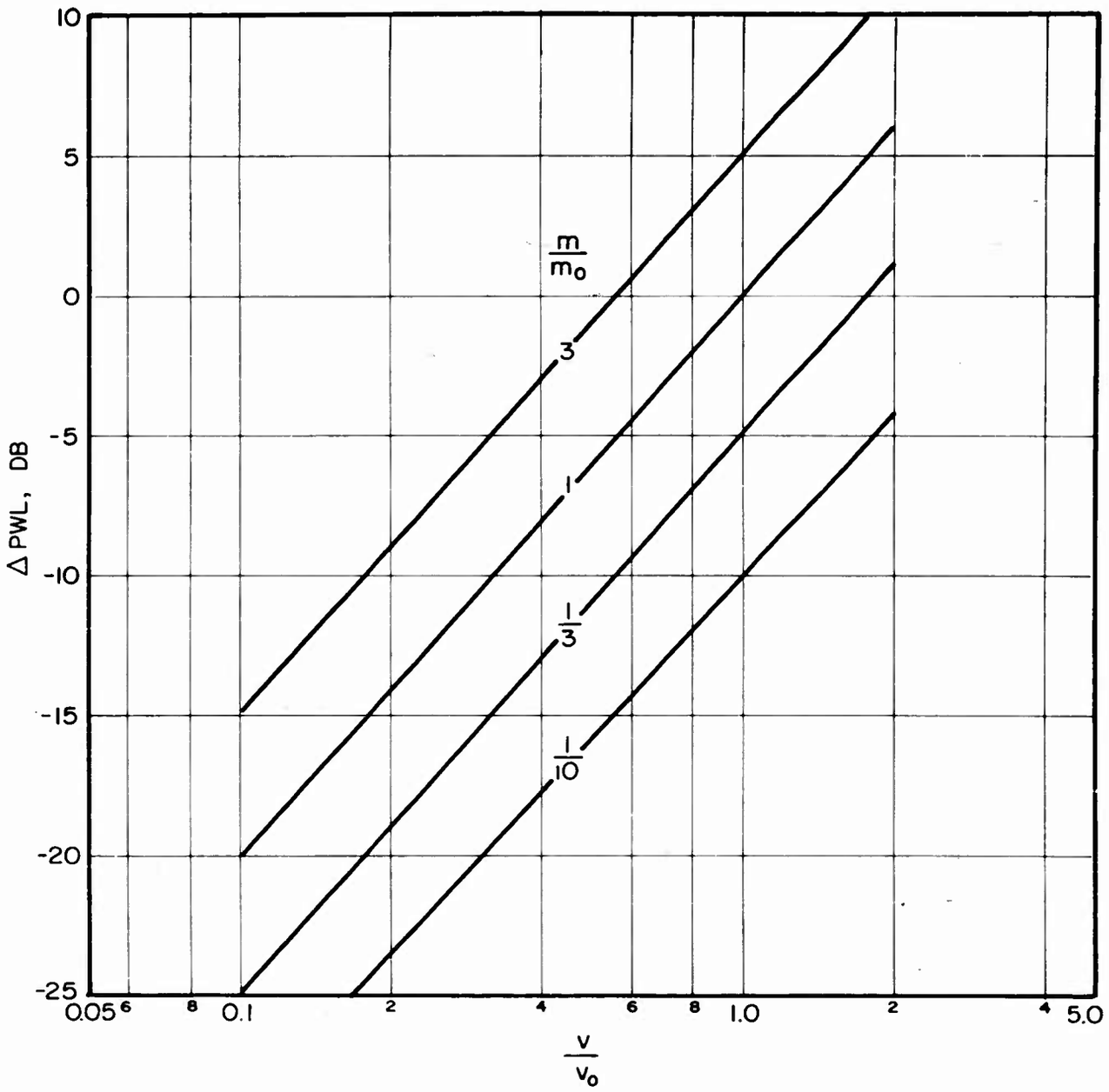

FIG. 28 CHANGE IN SOUND POWER RADIATED BY LARGE ROCKETS.

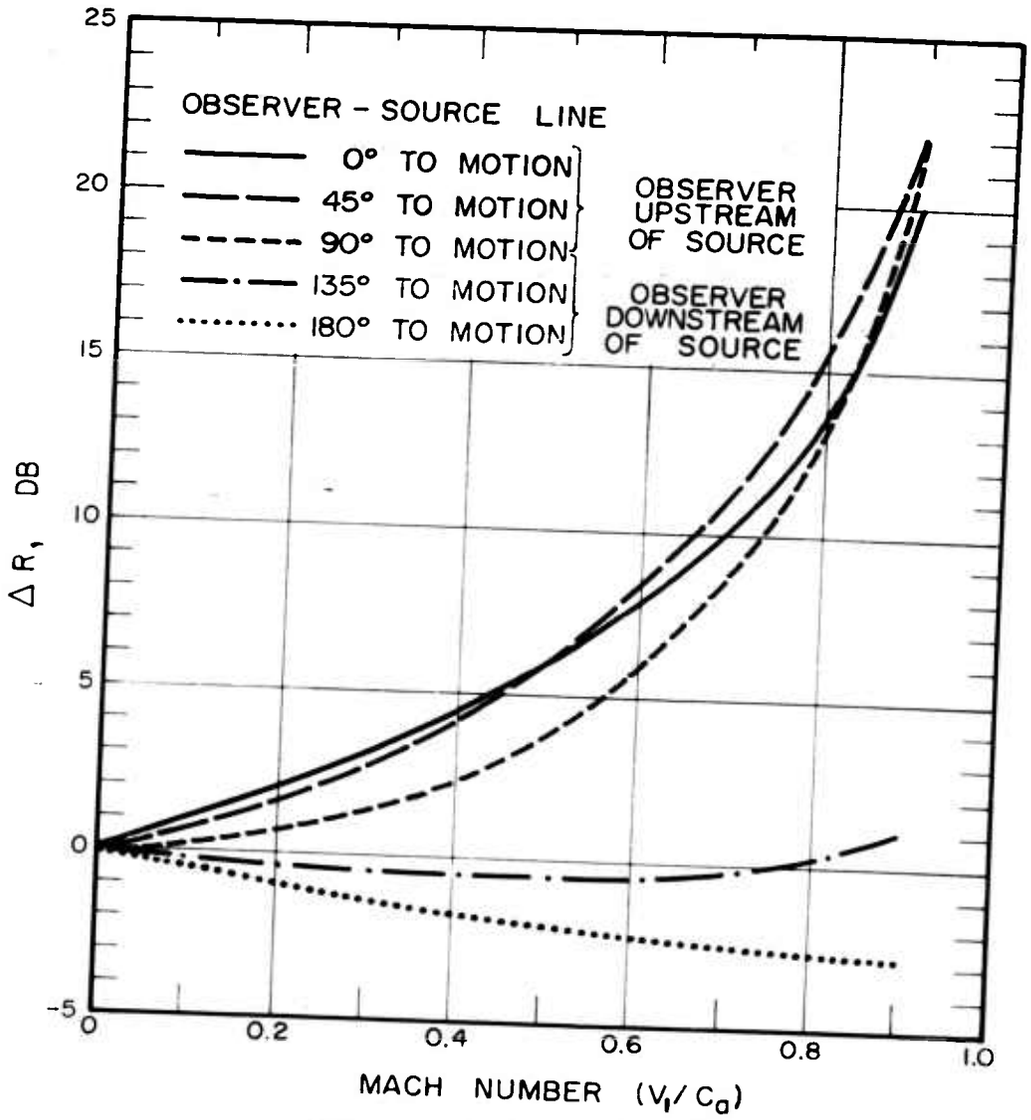

FIG. 29 CORRECTION FACTOR FOR MOVING MEDIUM.

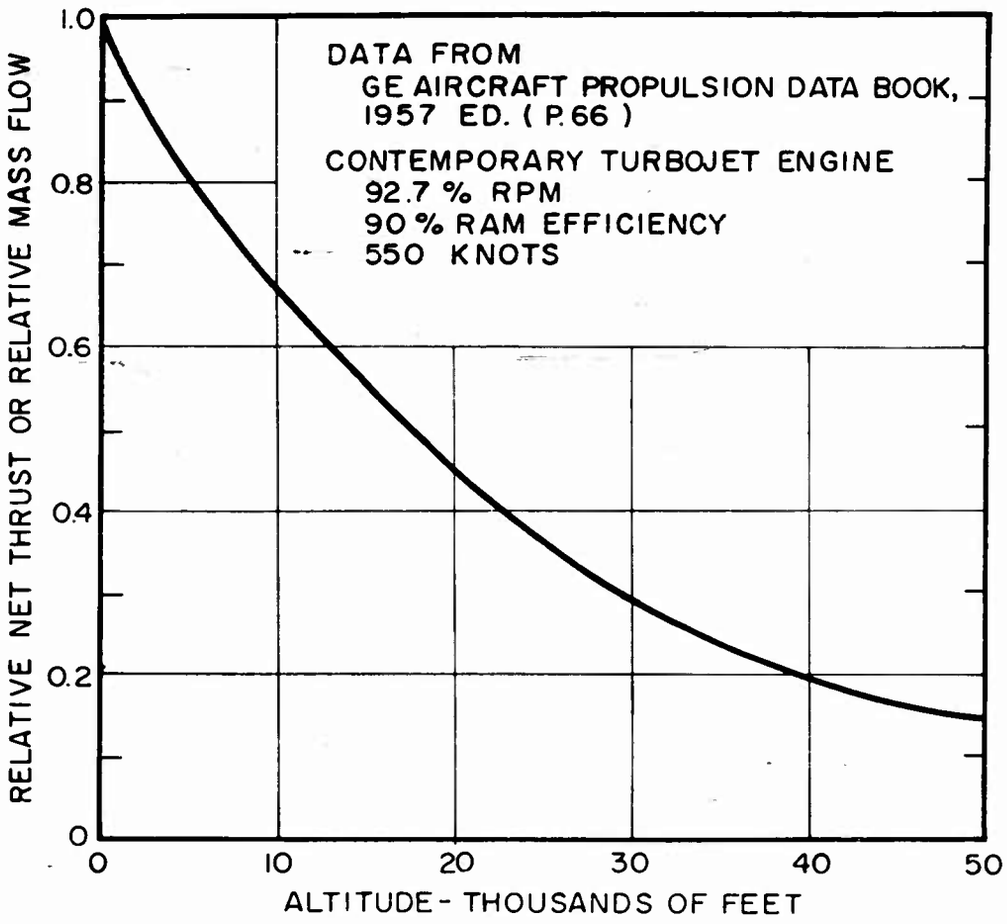

FIG. 30 VARIATION OF ENGINE OPERATING PARAMETERS WITH ALTITUDE

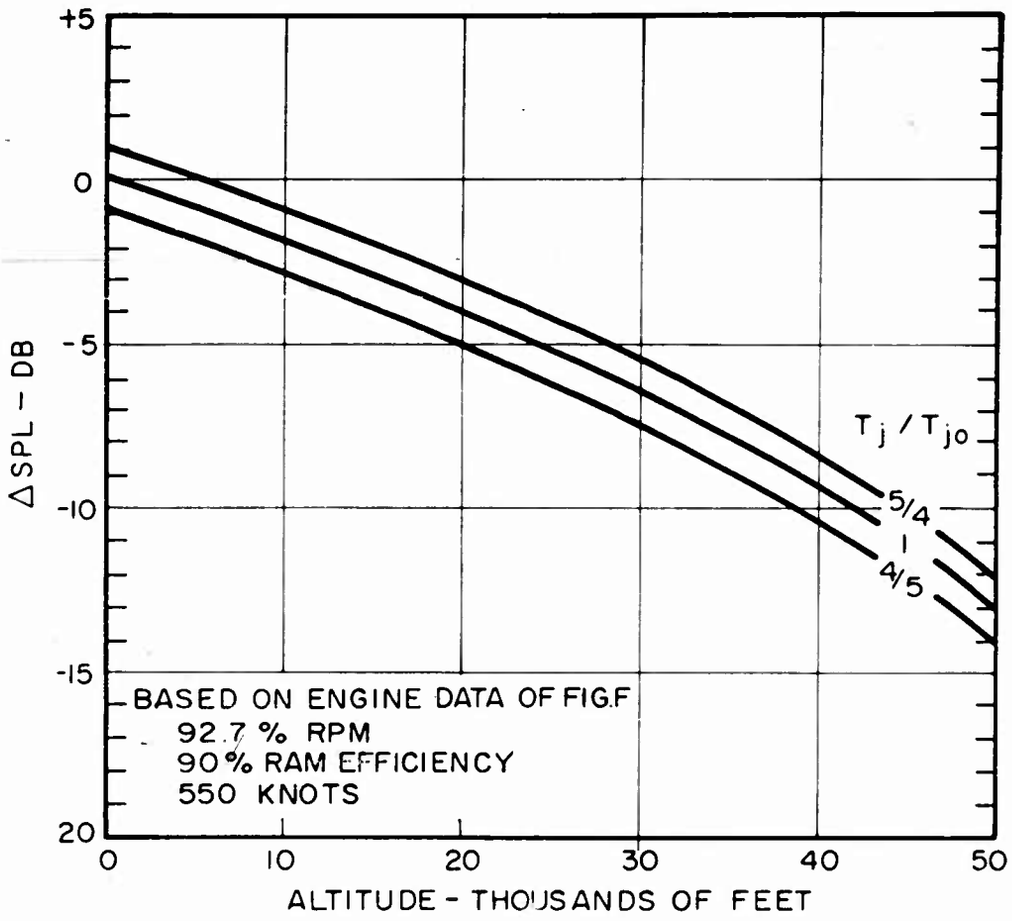

FIG. 31 EFFECT OF ALTITUDE ON OVERALL SPL.

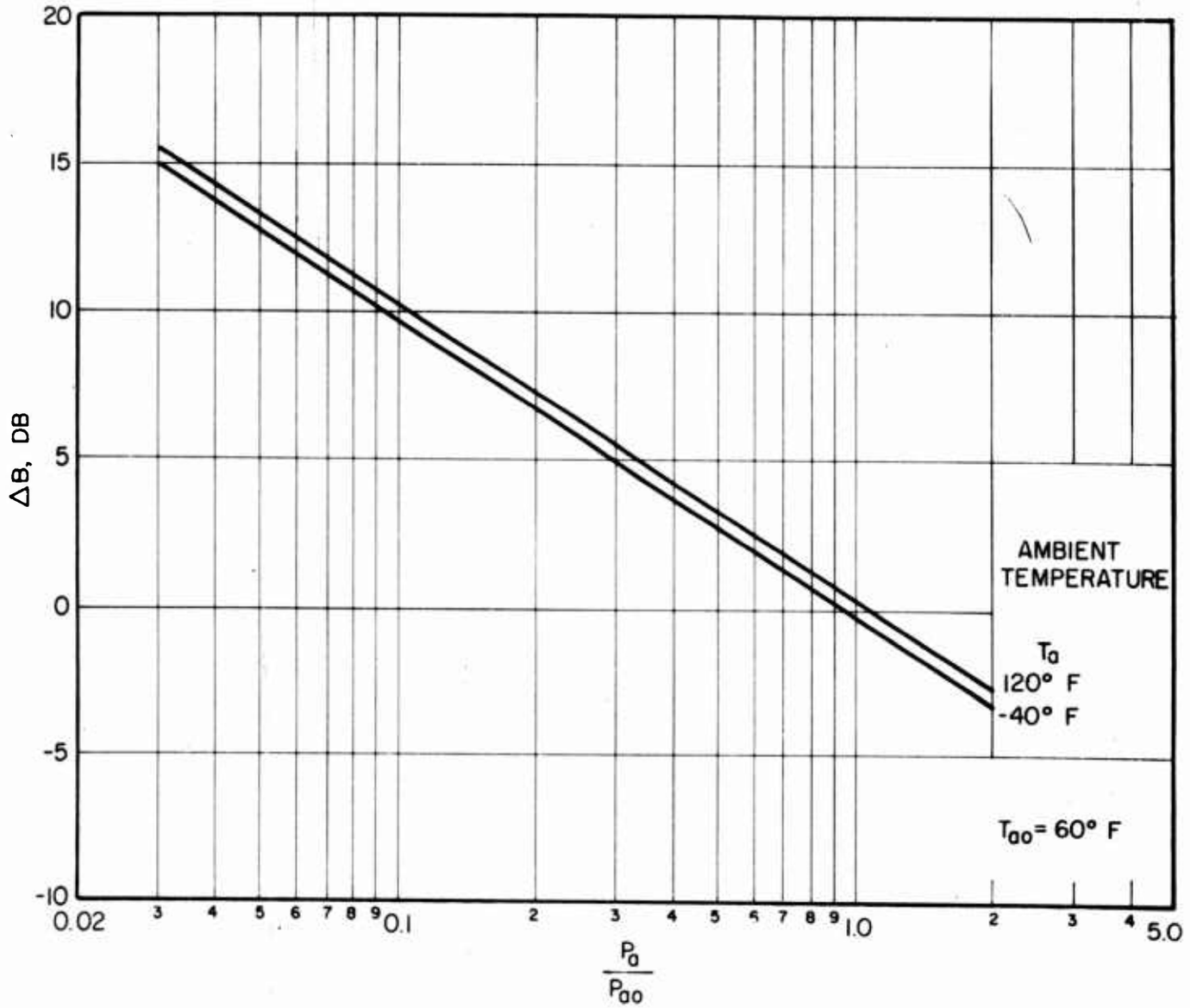

FIG. 32 CONVERSION FACTOR RELATING Δ PWL AND Δ SPL.
(Δ SPL = Δ PWL − Δ B)

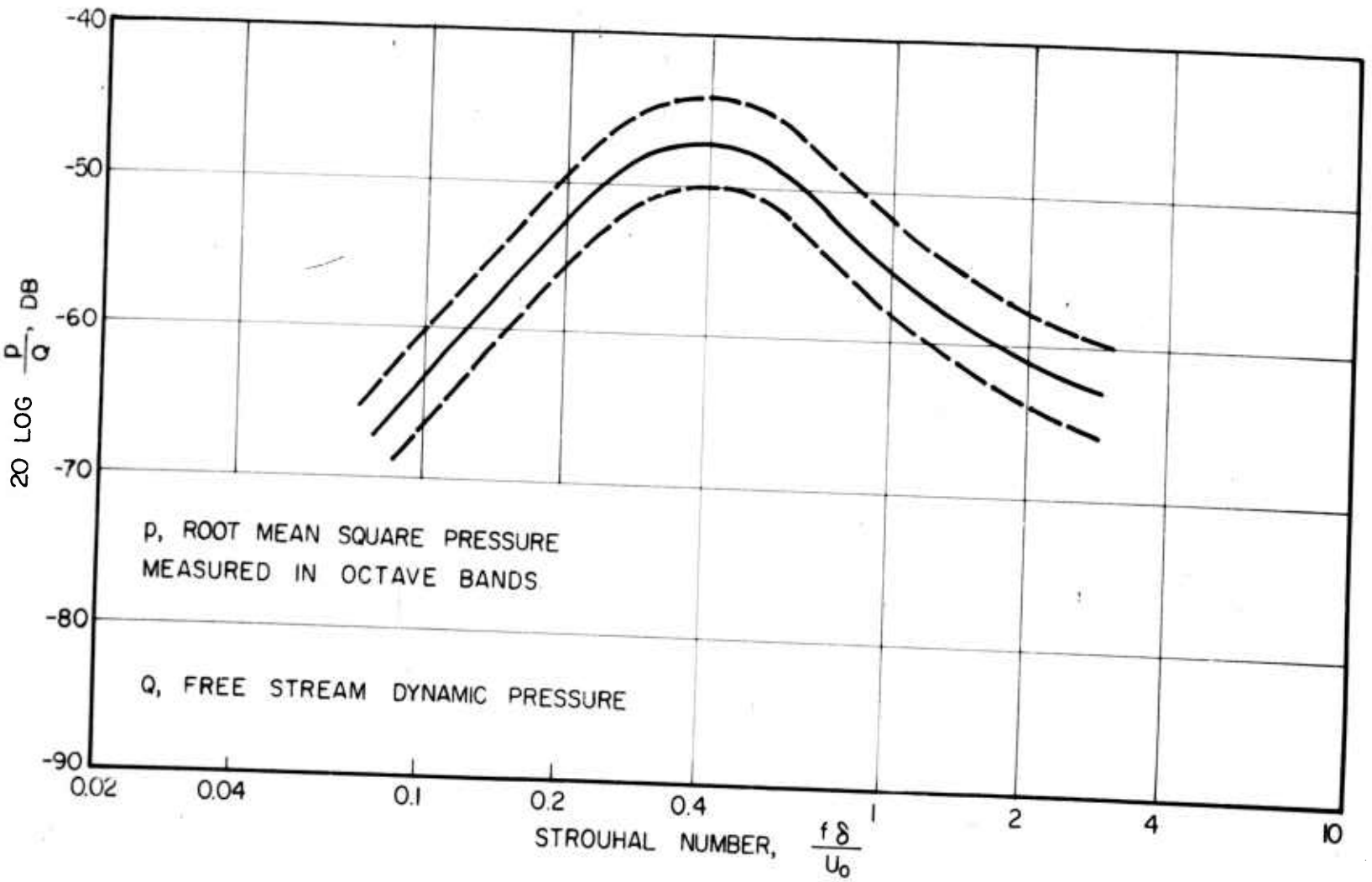

FIG. 33 APPROXIMATE BOUNDARY LAYER PRESSURES FROM MEASUREMENTS IN SUBSONIC AIRCRAFT.

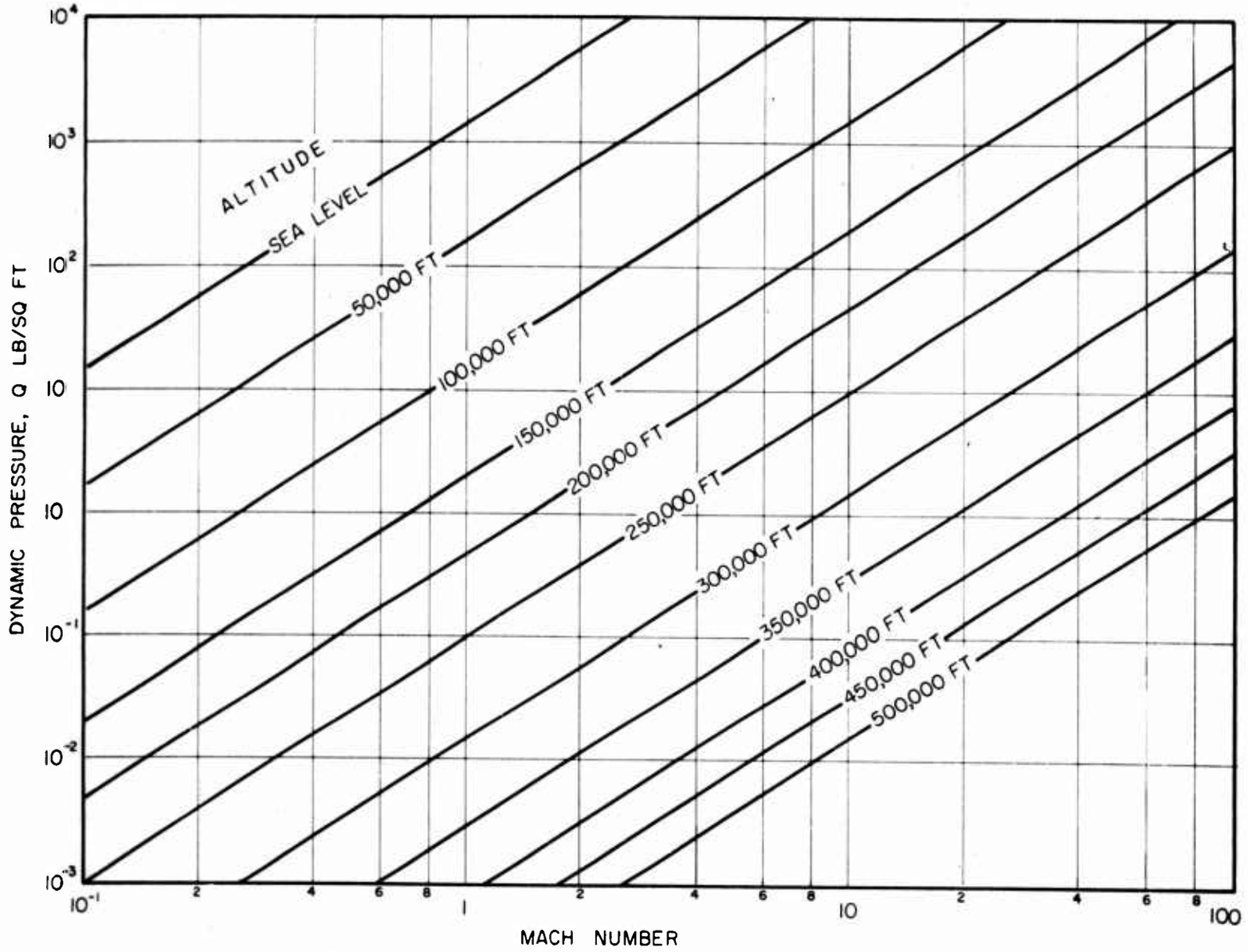

FIG. 34 DYNAMIC PRESSURE AS A FUNCTION OF MACH NUMBER AND ALTITUDE.

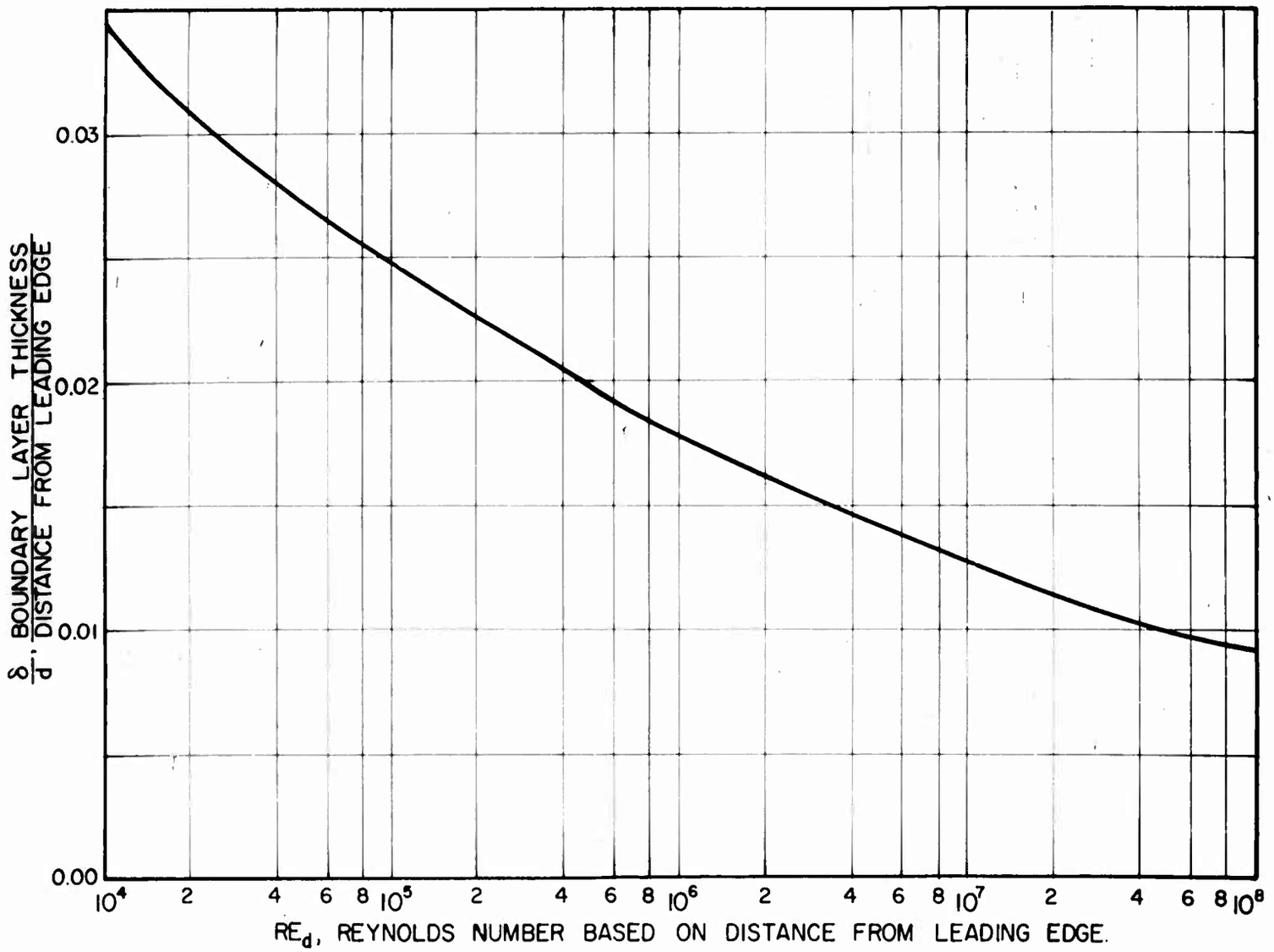

FIG. 35 ESTIMATE OF BOUNDARY LAYER THICKNESS.

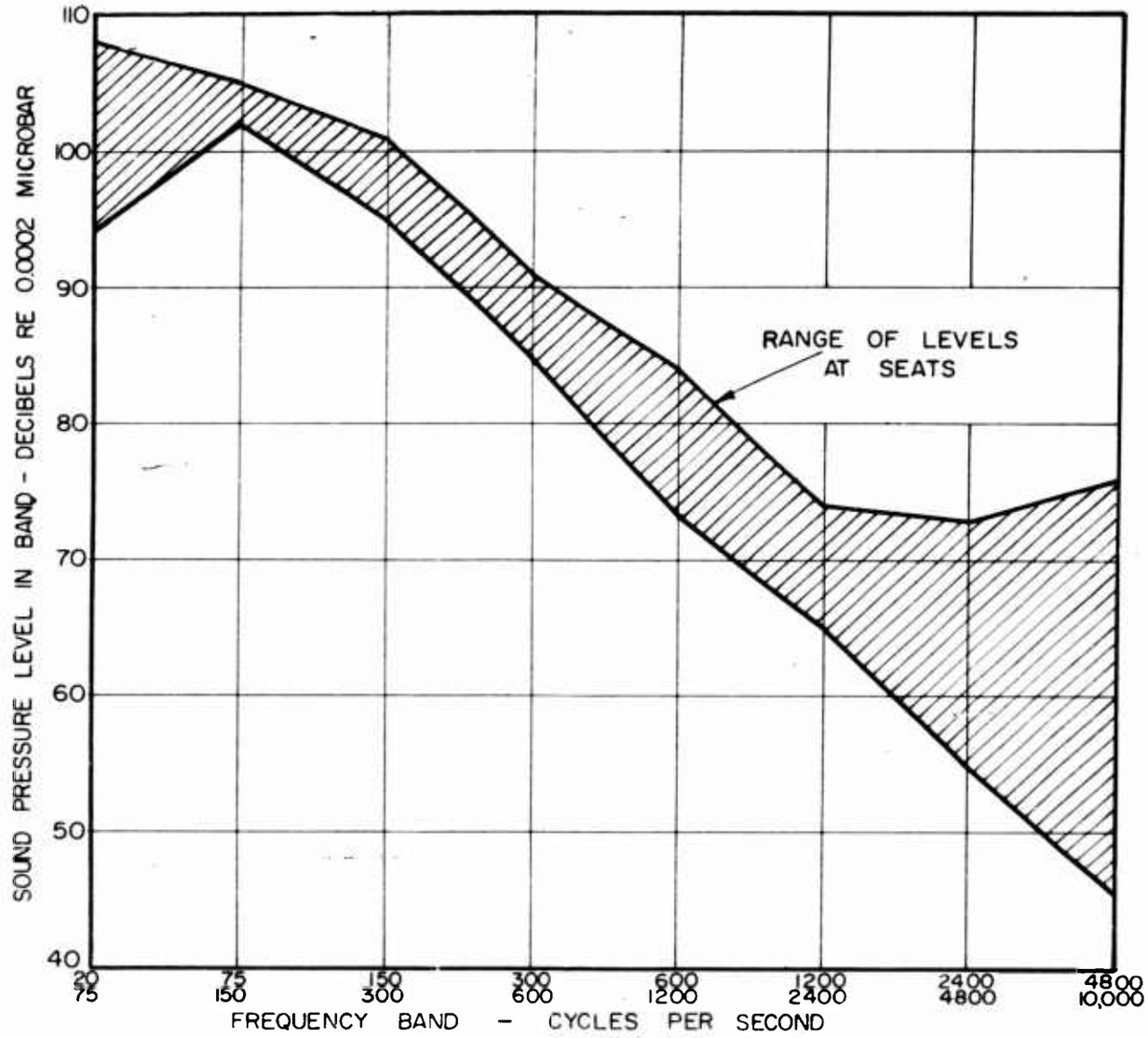

FIG. 36 TYPICAL SPL IN BUSINESS AIRCRAFT.

TWIN RECIPROCATING ENGINE BUSINESS PLANES,
CRUISE CONDITIONS
APPROXIMATE IAS 140 KNOTS
APPROXIMATE ALTITUDE 10,000 FT

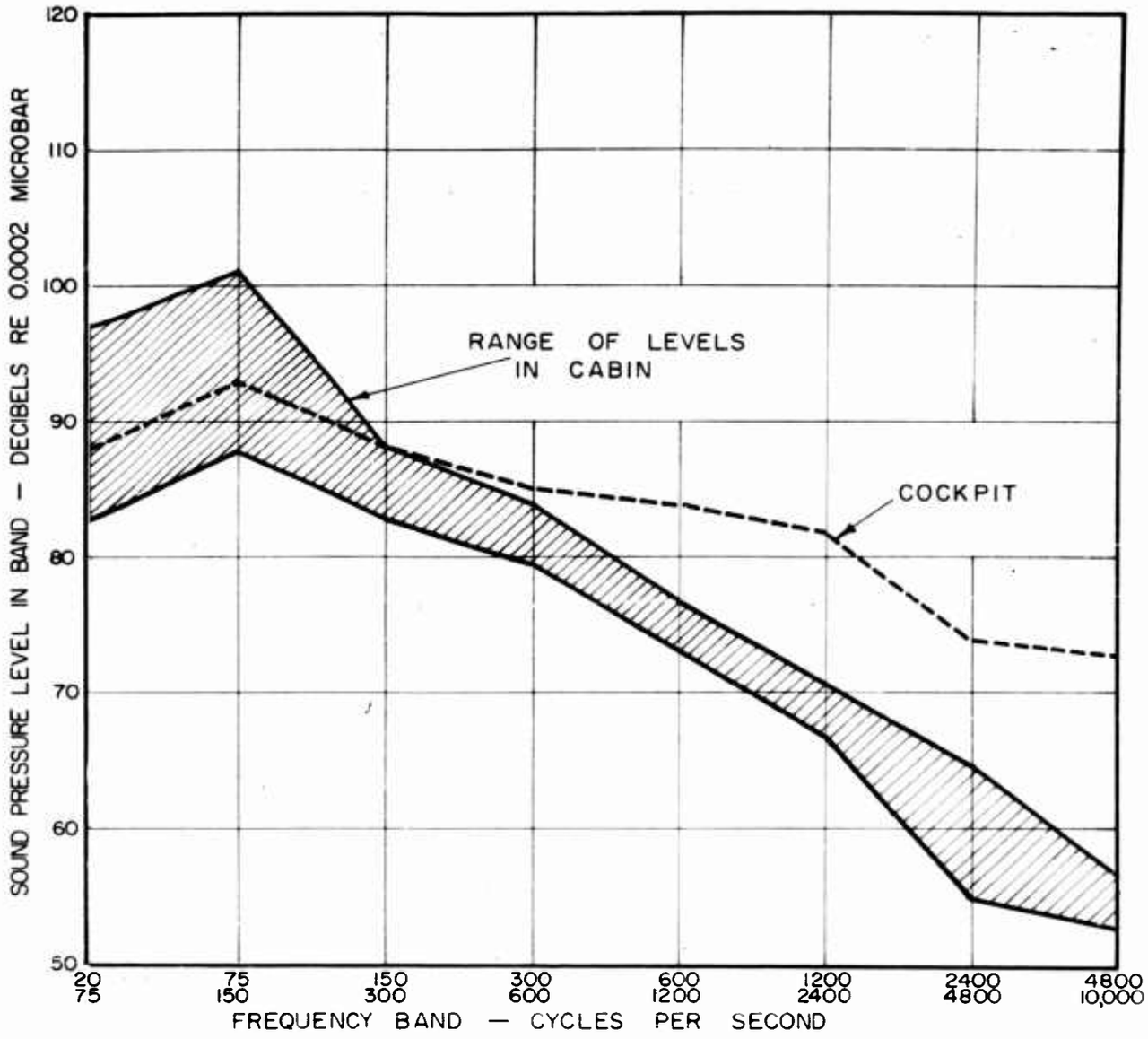

FIG. 37 TYPICAL SPL IN COMMERCIAL AIRCRAFT.

VISCOUNT, CRUISE CONDITIONS
AIRSPEED NOT GIVEN
ALTITUDE 25,000 FT

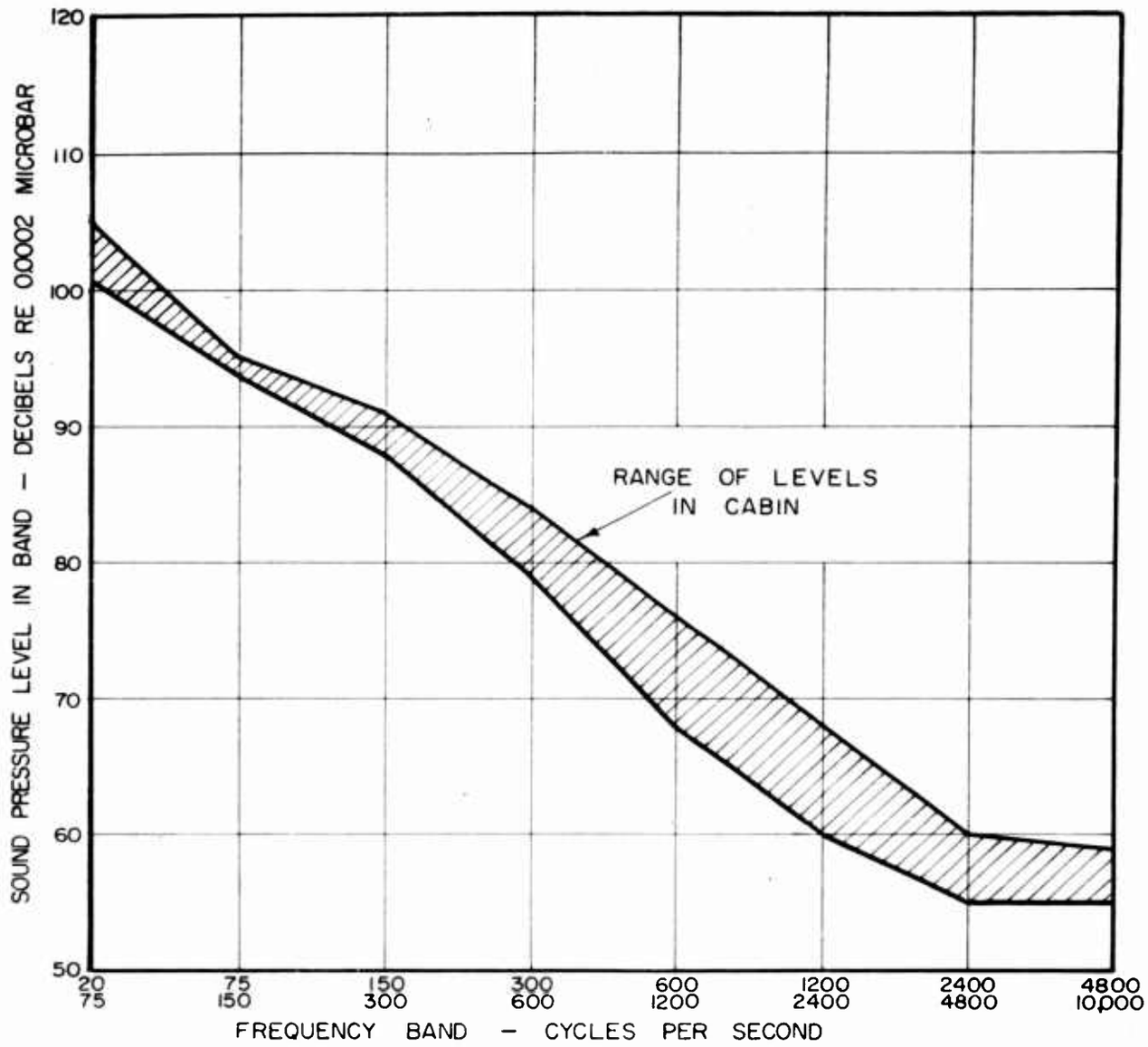

FIG. 38 TYPICAL SPL IN COMMERCIAL AIRCRAFT.

CONVAIR 440
IAS 165 KNOTS
ALTITUDE 10,000 FT

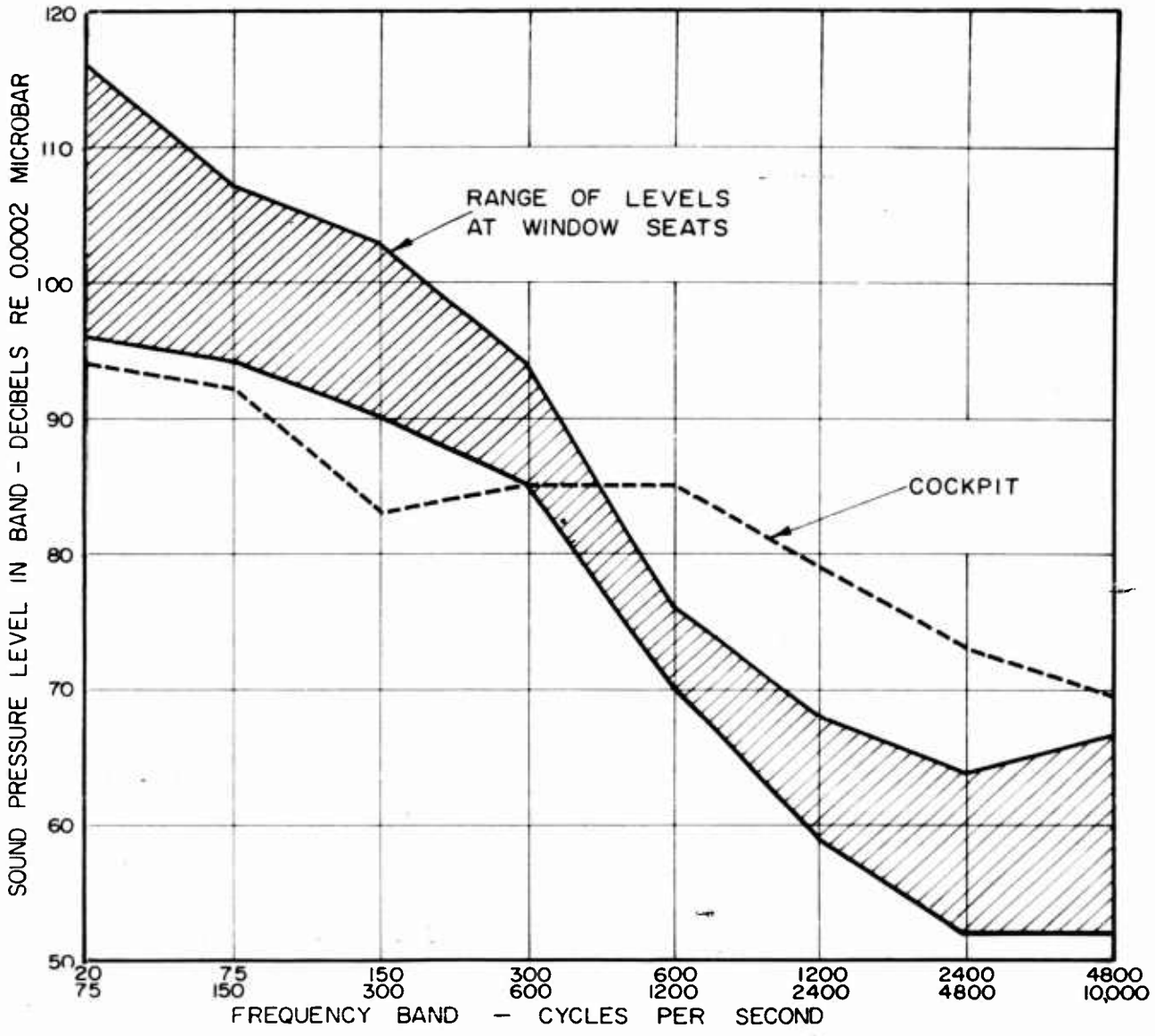

FIG. 39 TYPICAL SPL IN COMMERCIAL AIRCRAFT.

SUPER-6 CONSTELLATION
IAS 220 KNOTS
ALTITUDE 18,000 FT

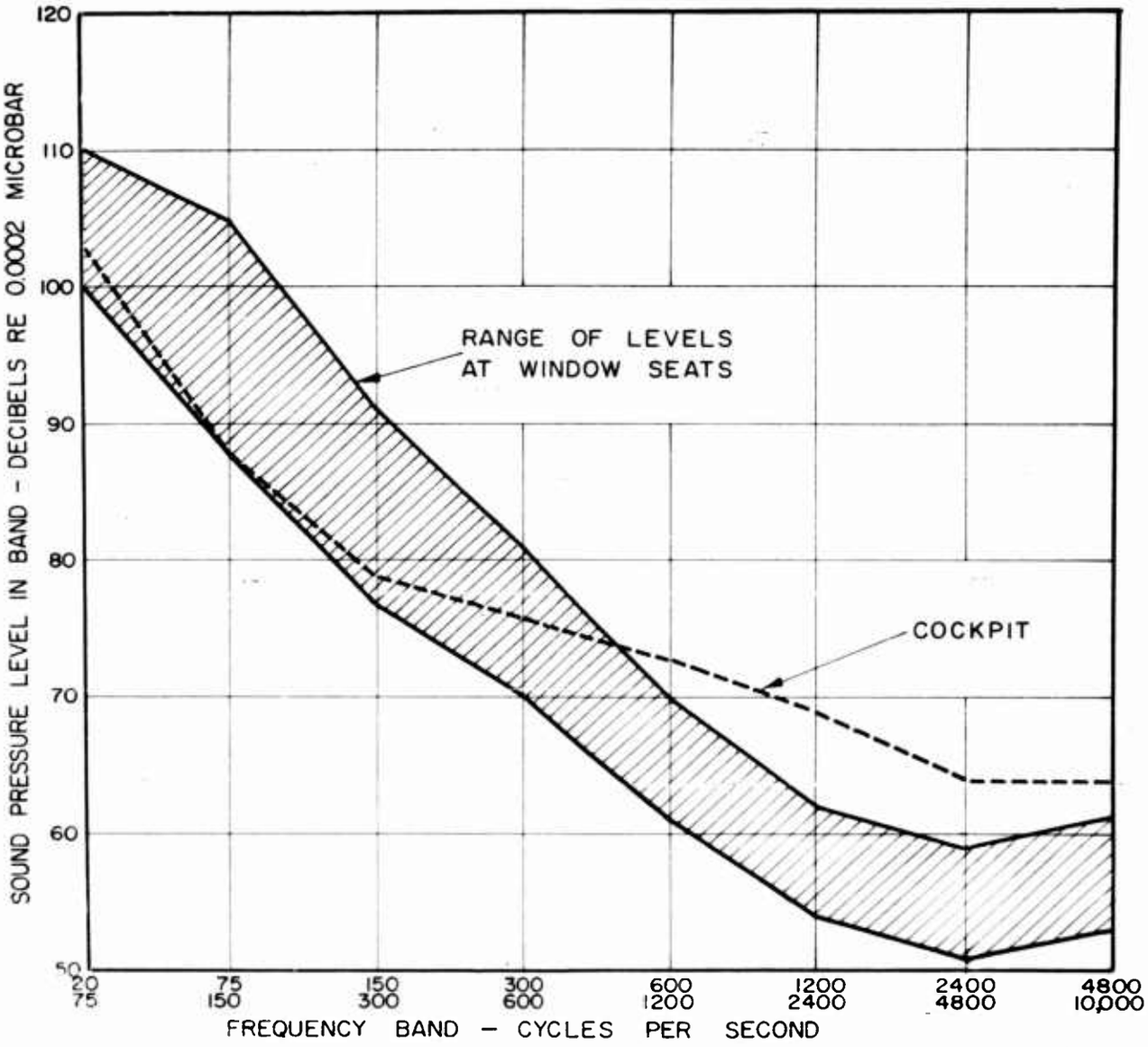

FIG. 40 TYPICAL SPL IN COMMERCIAL AIRCRAFT.

STRATOCRUISER, CRUISE CONDITIONS
APPROXIMATE IAS 230 KNOTS
ALTITUDE 18,000 FT

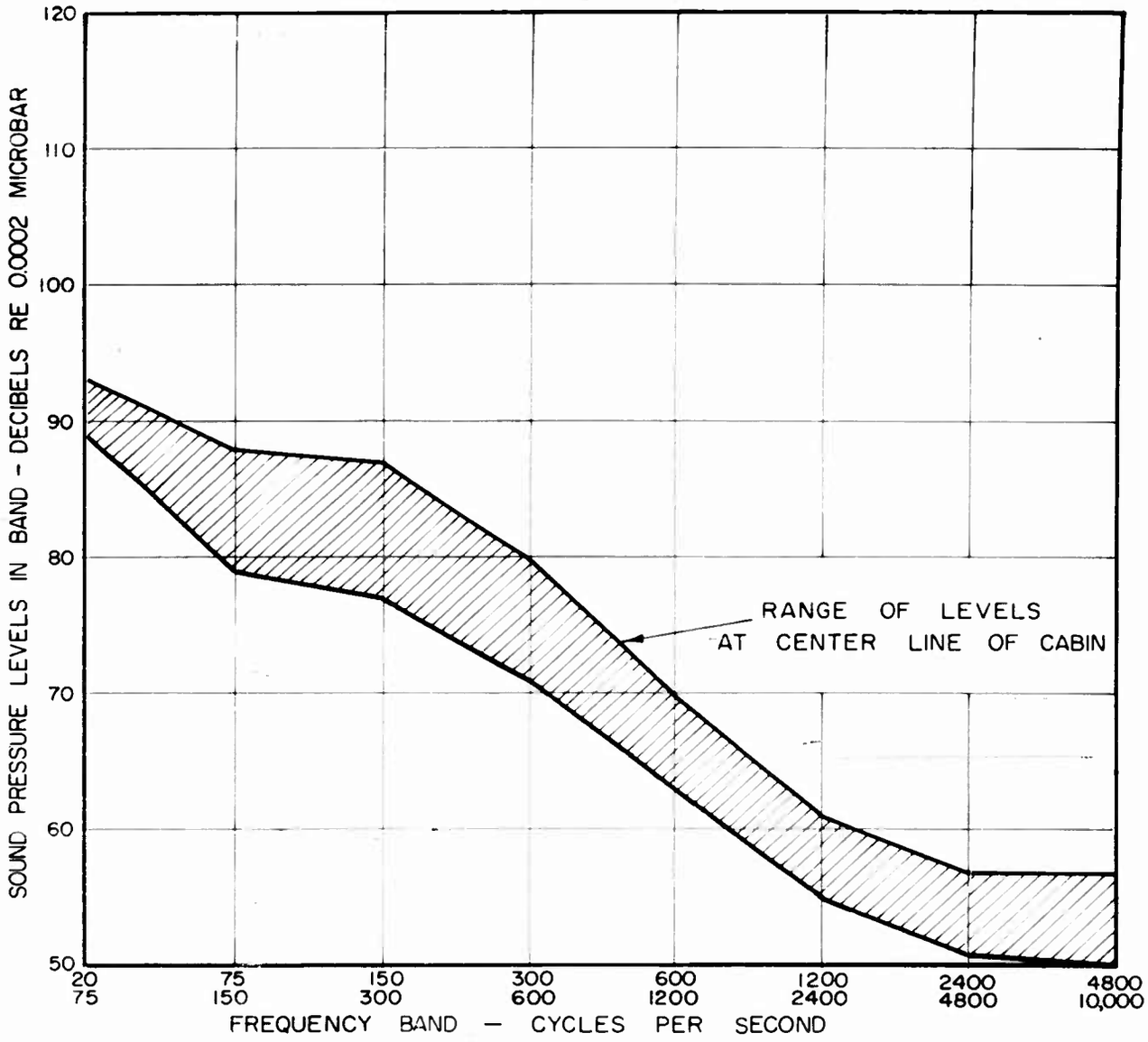

FIG. 41 TYPICAL SPL IN COMMERCIAL AIRCRAFT.

STRATOCRUISER, CRUISE CONDITIONS
APPROXIMATE IAS 230 KNOTS
ALTITUDE 18,000 FT

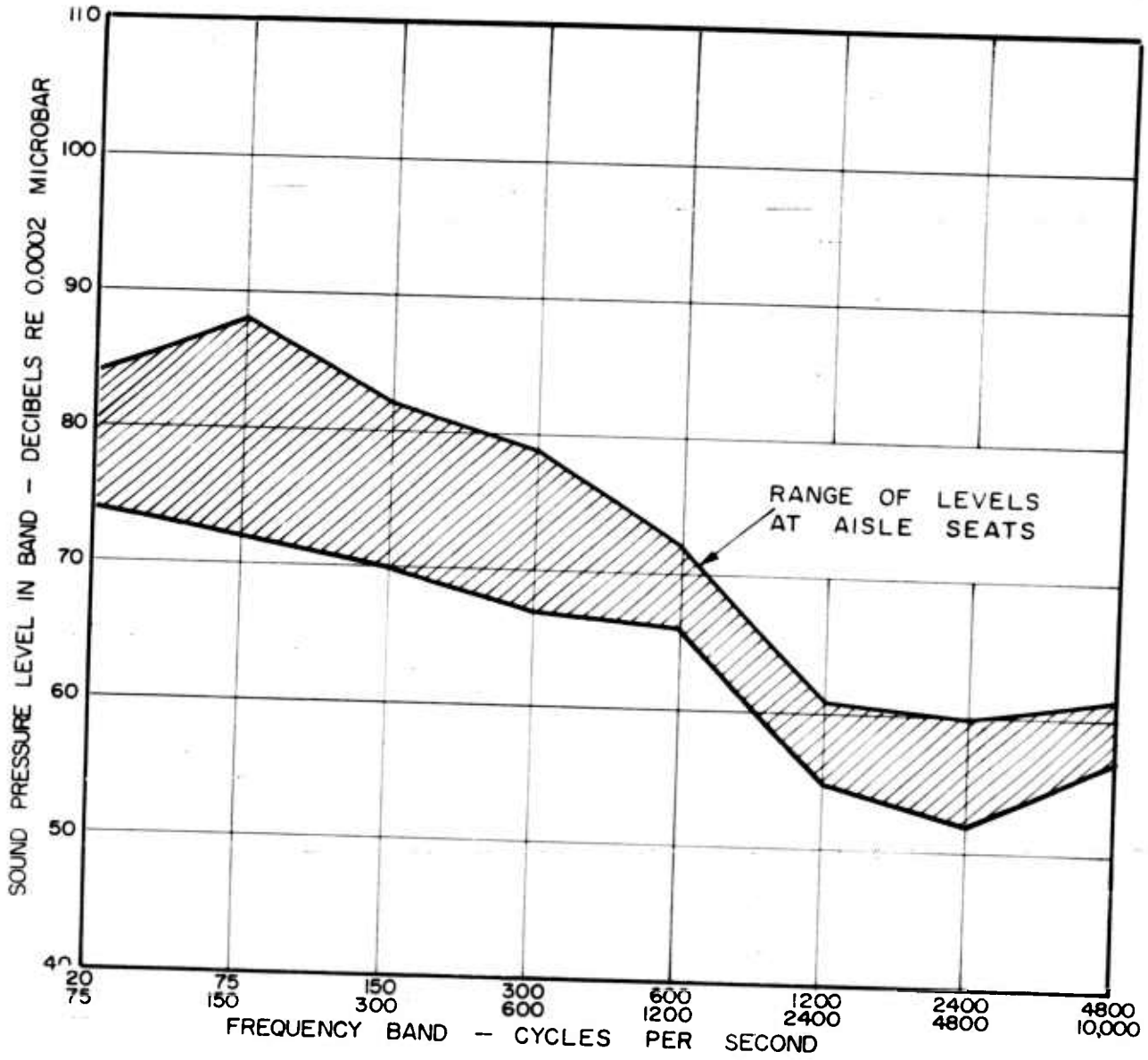

FIG. 42 TYPICAL SPL IN COMMERCIAL AIRCRAFT.

CARAVELLE, CRUISE CONDITIONS
IAS 255 KNOTS
ALTITUDE 15,000 FT

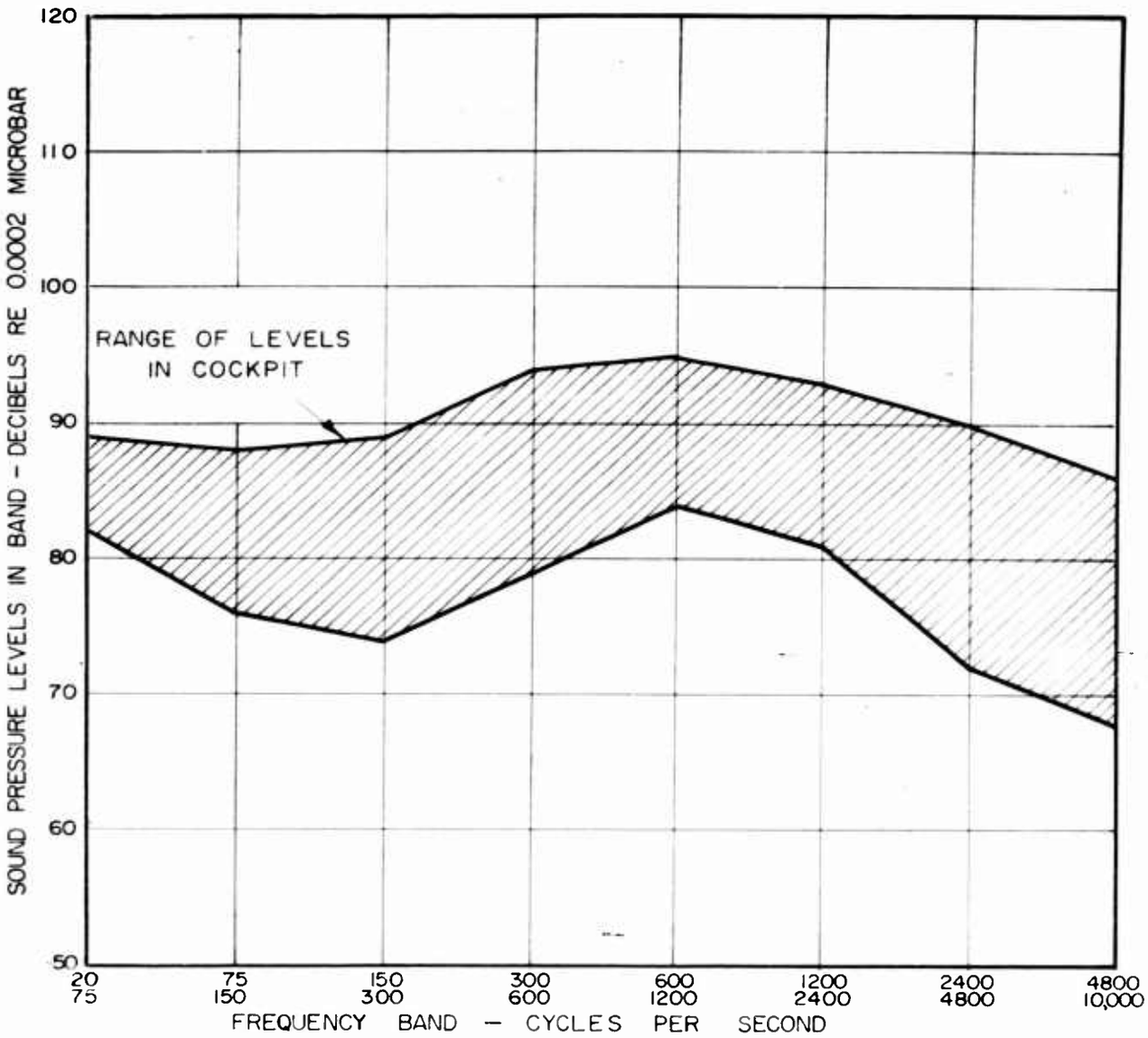

FIG. 43 TYPICAL SPL IN MILITARY AIRCRAFT.

SUBSONIC JET BOMBERS

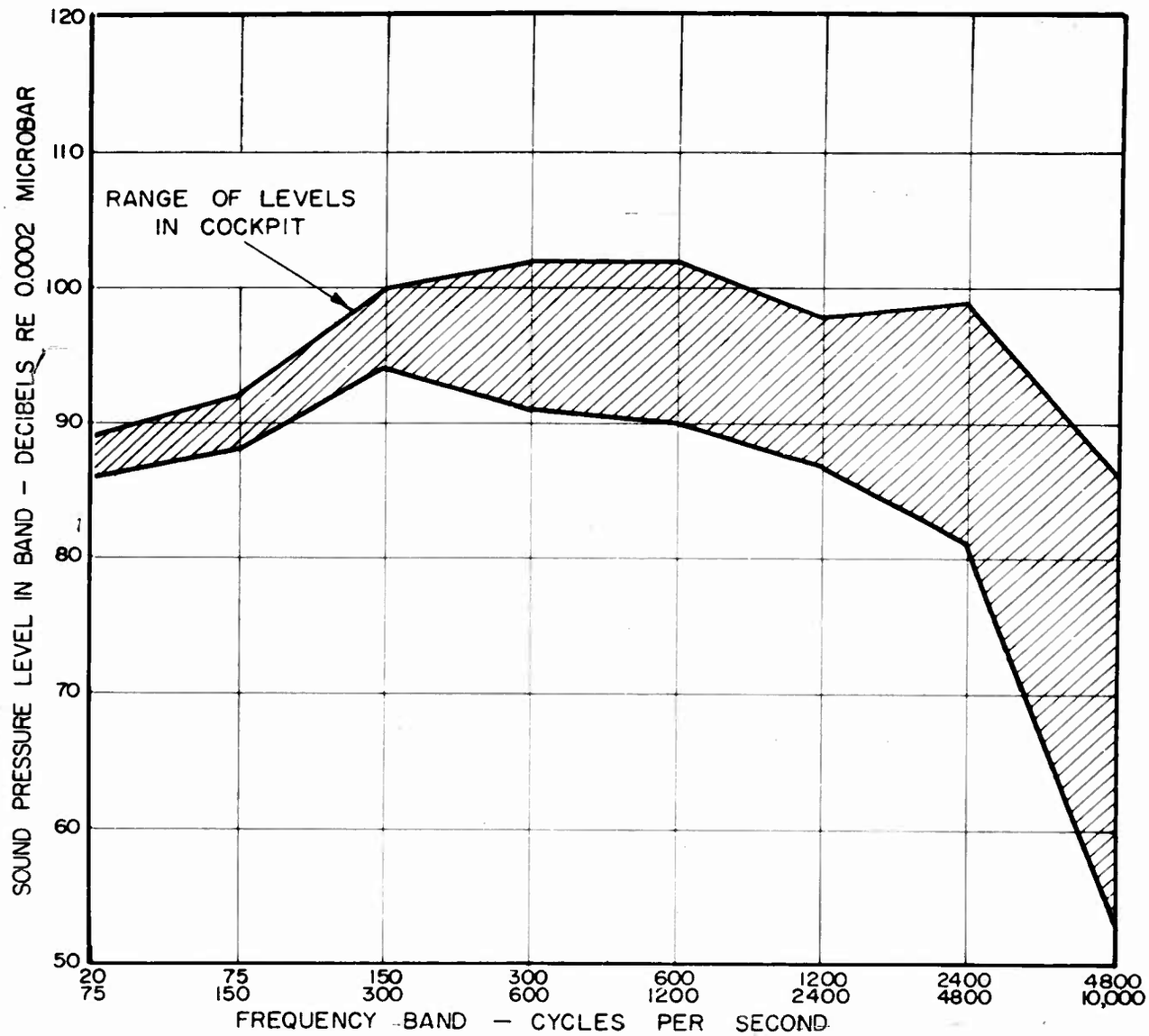

FIG. 44 TYPICAL SPL IN MILITARY AIRCRAFT.

SUBSONIC JET FIGHTERS

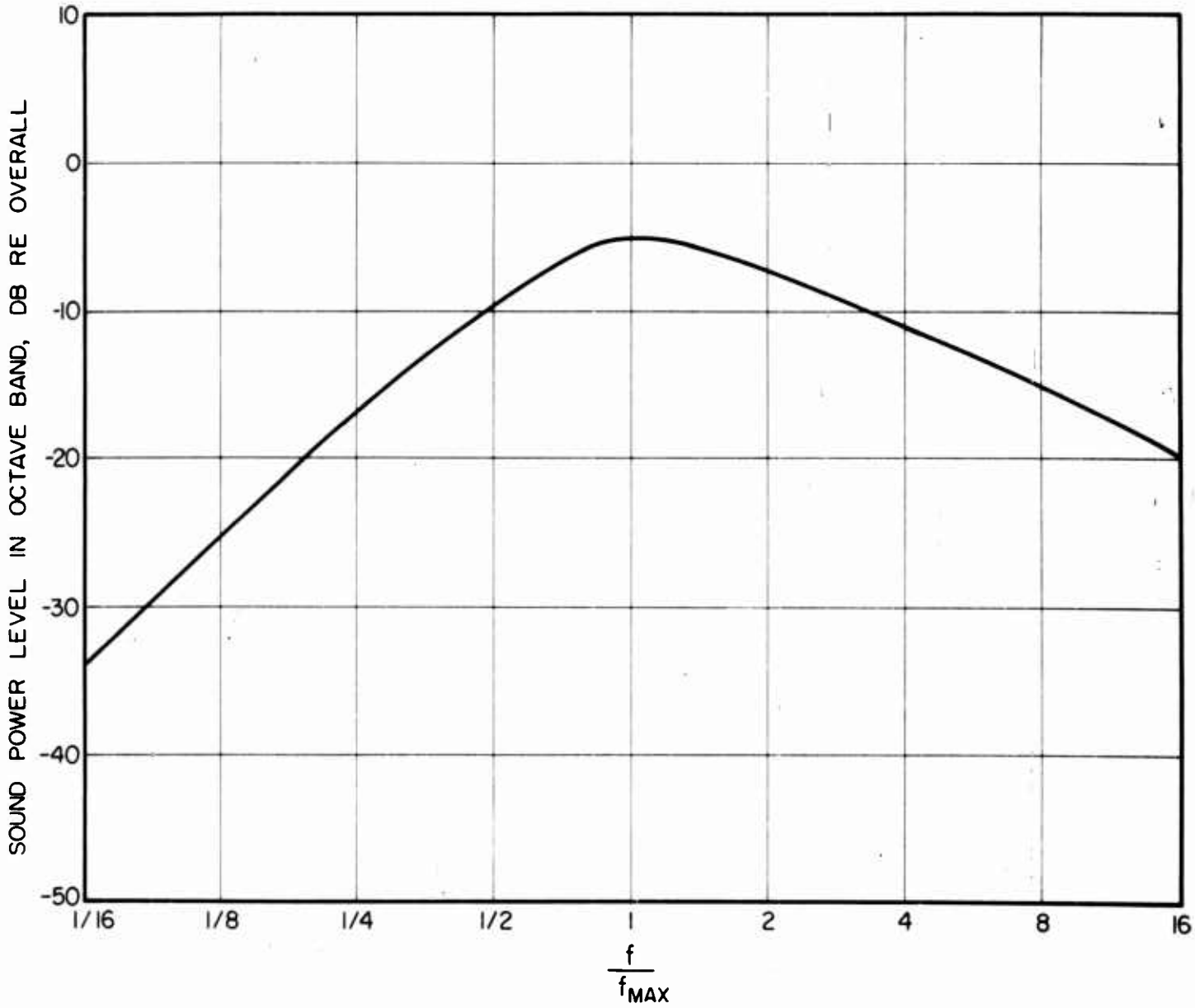

FIG. 45 PWL SPECTRUM OF AIR JET.

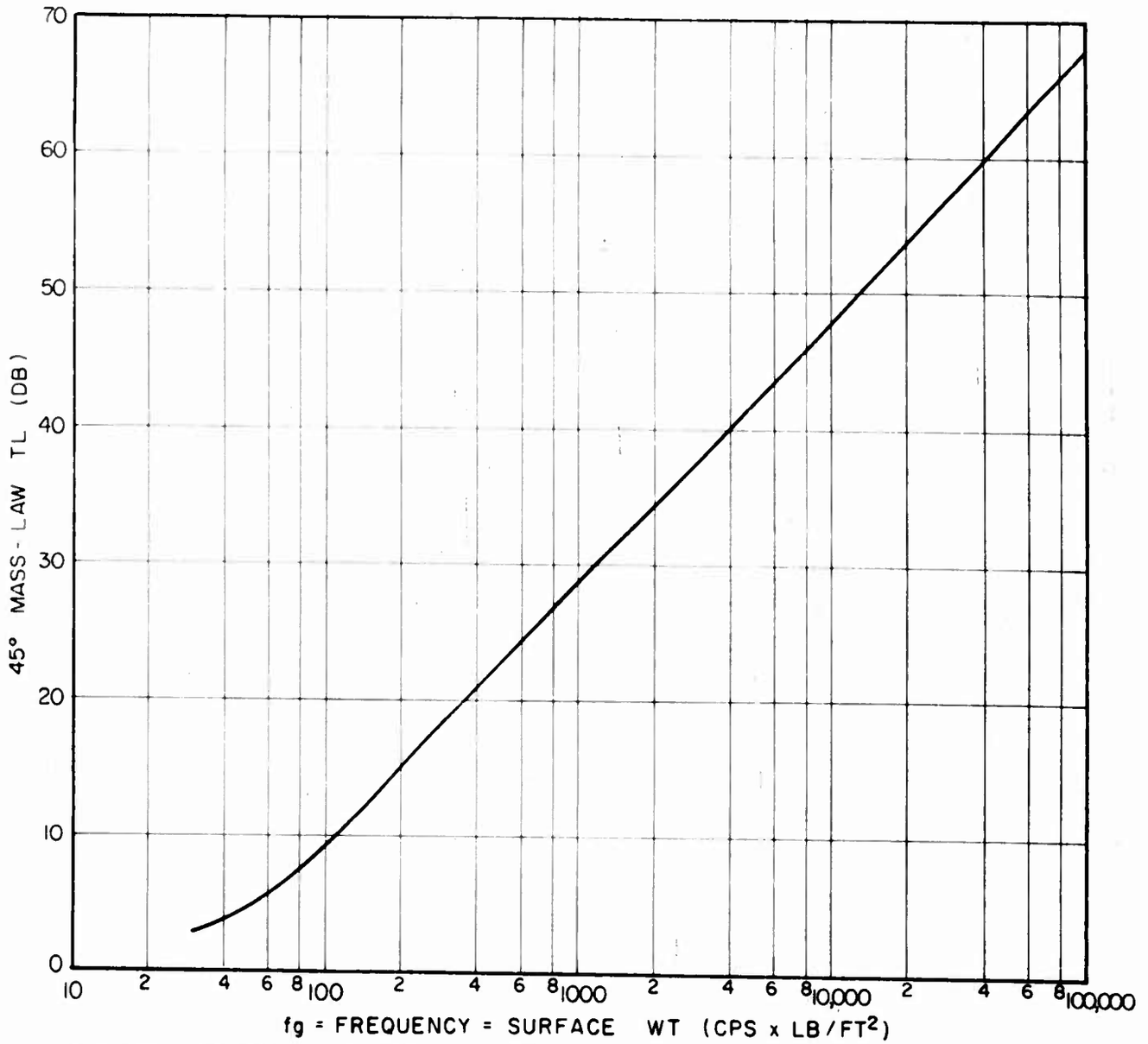

FIG. 46 REFERENCE MASS-LAW TRANSMISSION LOSS FOR FLAT PANELS.
ASSUMPTION: ROOM TEMPERATURE - SEA-LEVEL PRESSURE - 45° INCIDENCE

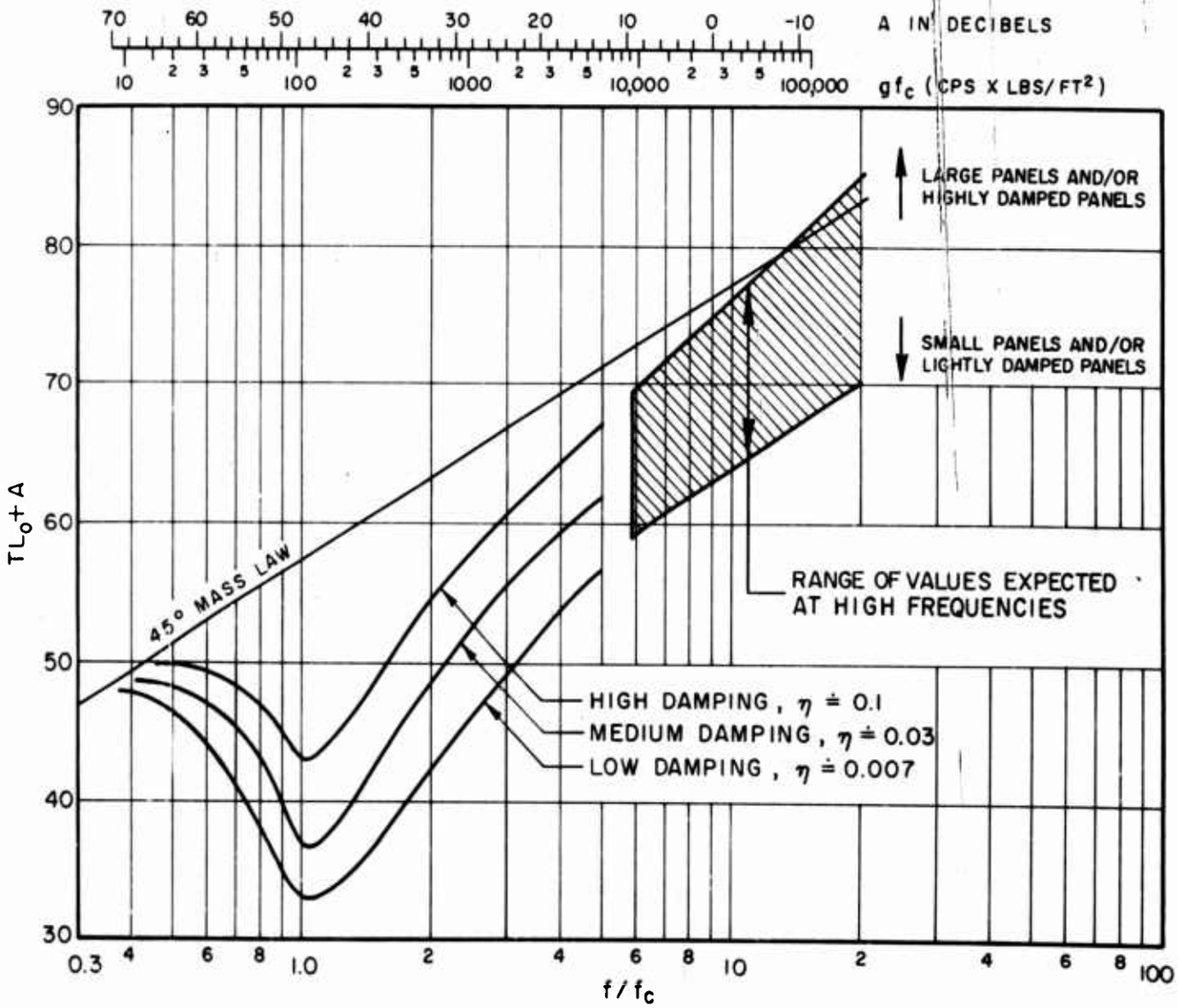

FIG. 47 TL_o FOR PANELS NEAR AND ABOVE THE COINCIDENCE FREQUENCY, f_c
g = PANEL SURFACE WEIGHT (LB/FT) ; η = DAMPING FACTOR.

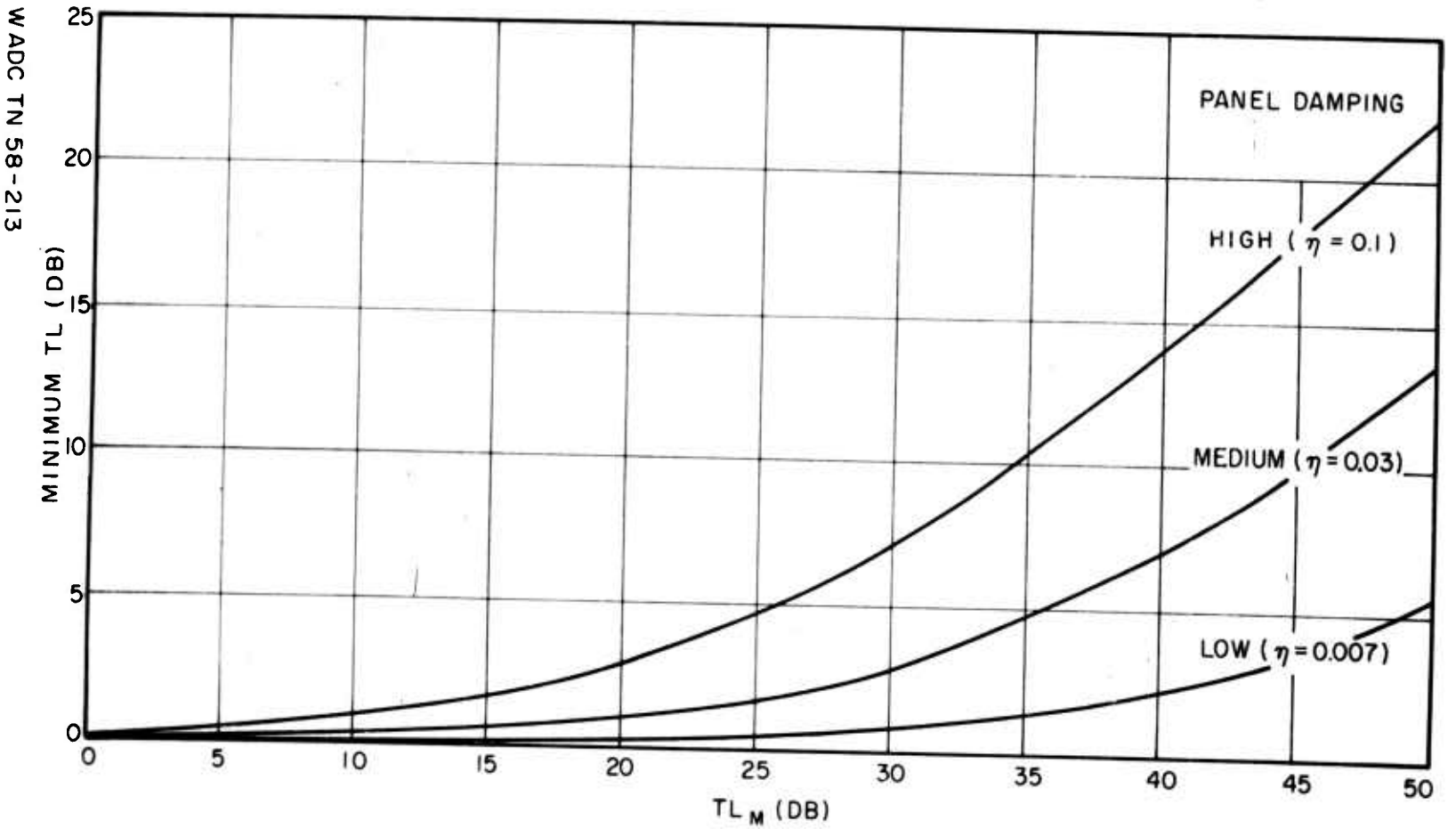

FIG. 48 MINIMUM TL AT PANEL RESONANCE, AS A FUNCTION OF MASS LAW TL COMPUTED AT RESONANCE FREQUENCY (TL_M)

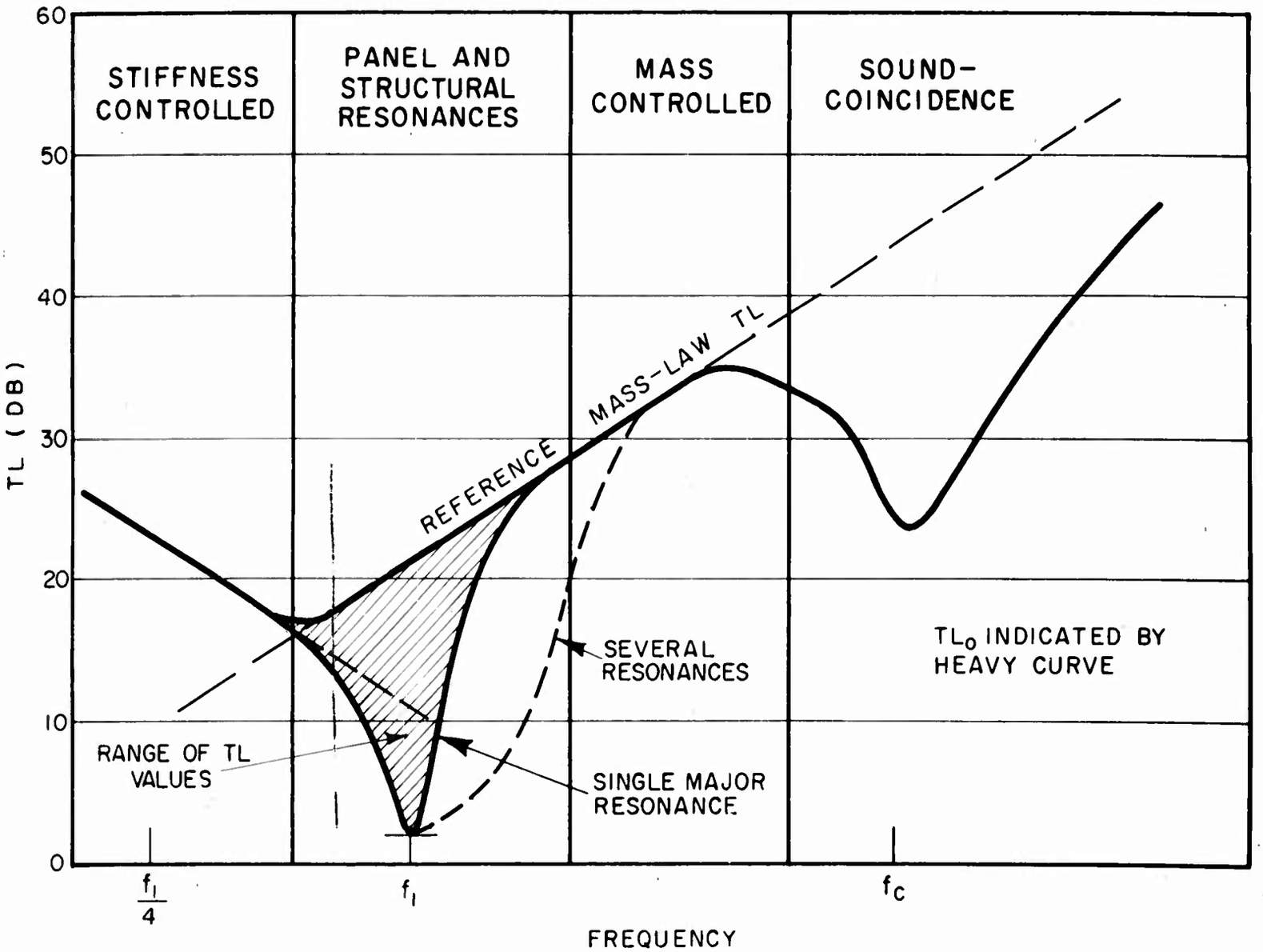

FIG. 49 CHART ILLUSTRATING PROCEDURES FOR ESTIMATING TRANSMISSION LOSS, TL_0

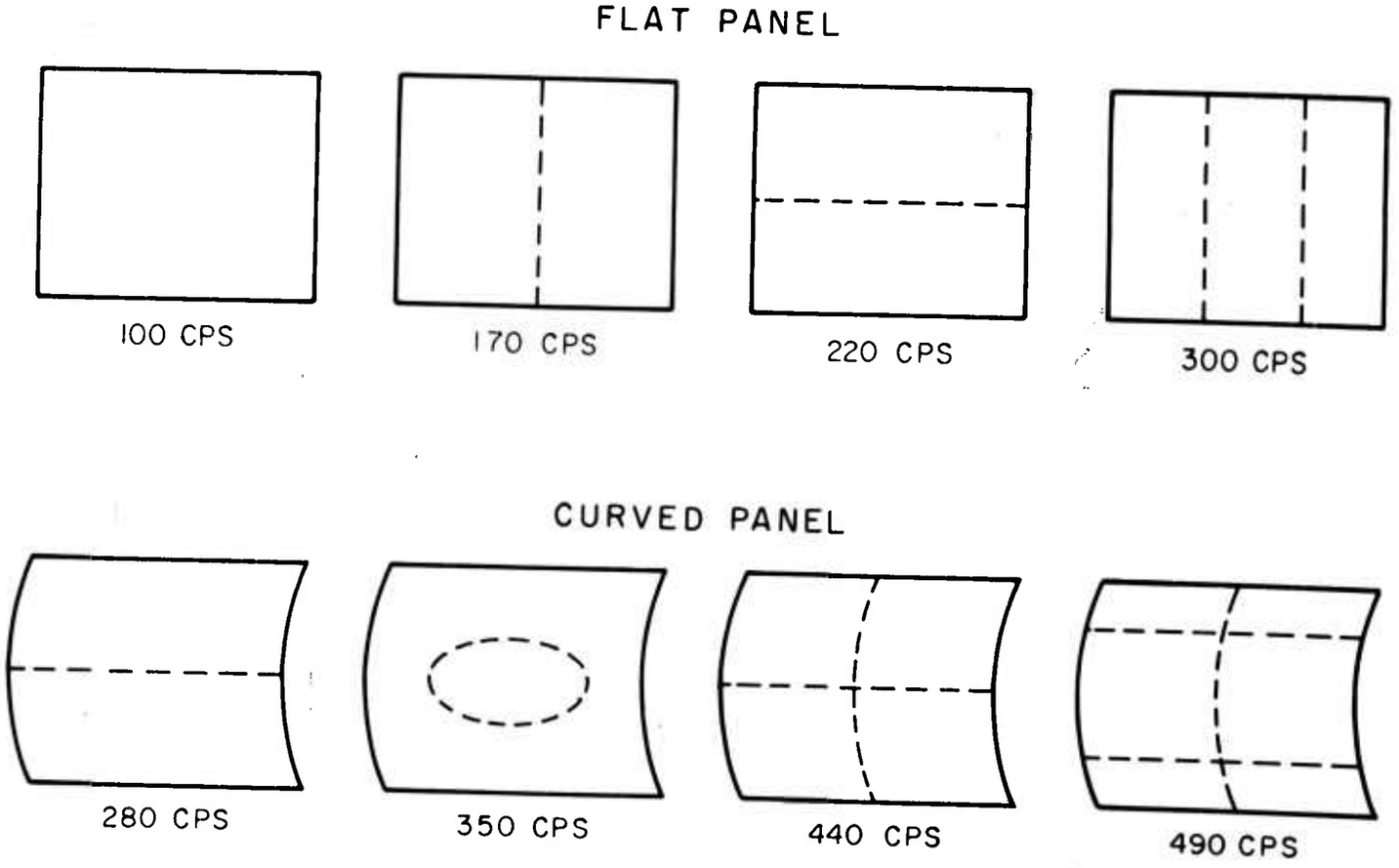

FIG. 50 EFFECT OF CURVATURE ON PANEL RESONANCE FREQUENCIES

(PANEL SIZE : 11 IN. x 13 IN. – 0.032 IN. DURAL , 4 FT RADIUS OF CURVATURE. AFTER REGIER.)

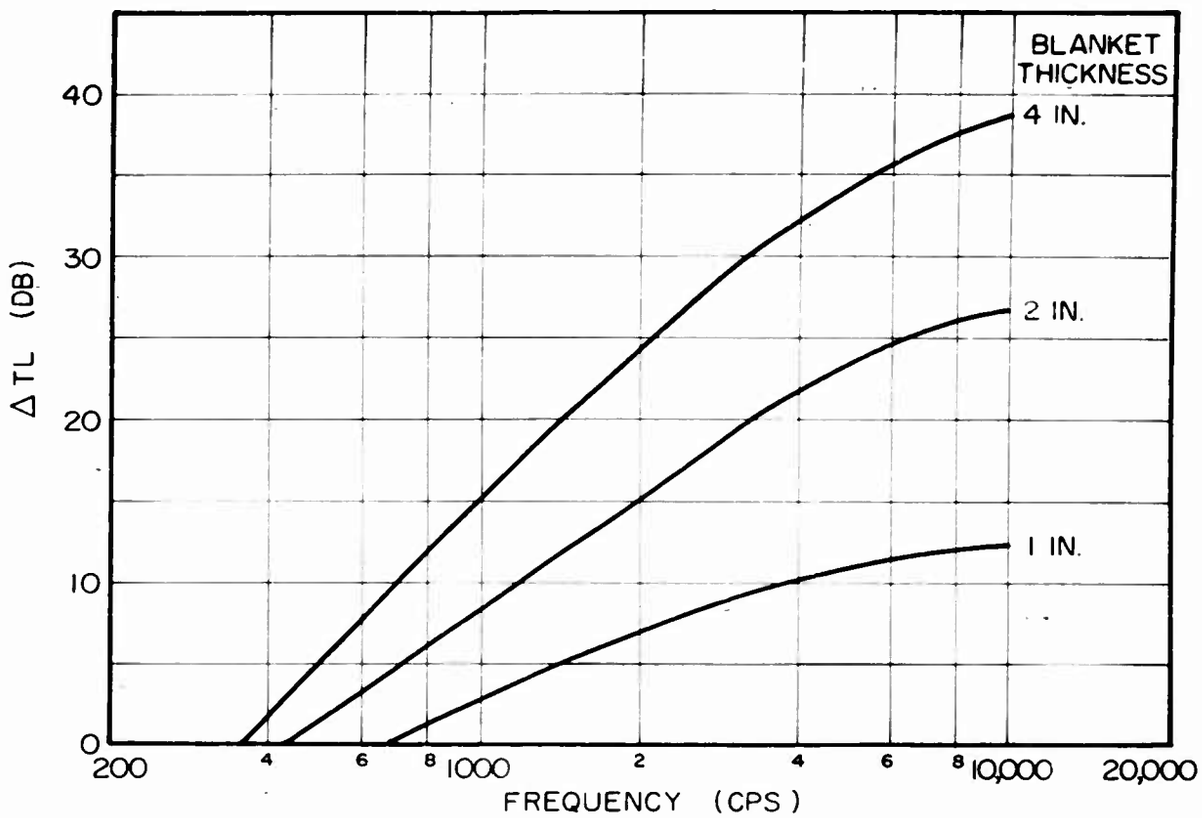

FIG. 51 APPROXIMATE TRANSMISSION-LOSS INCREASE (ΔTL) DUE TO ACOUSTICAL BLANKETS.

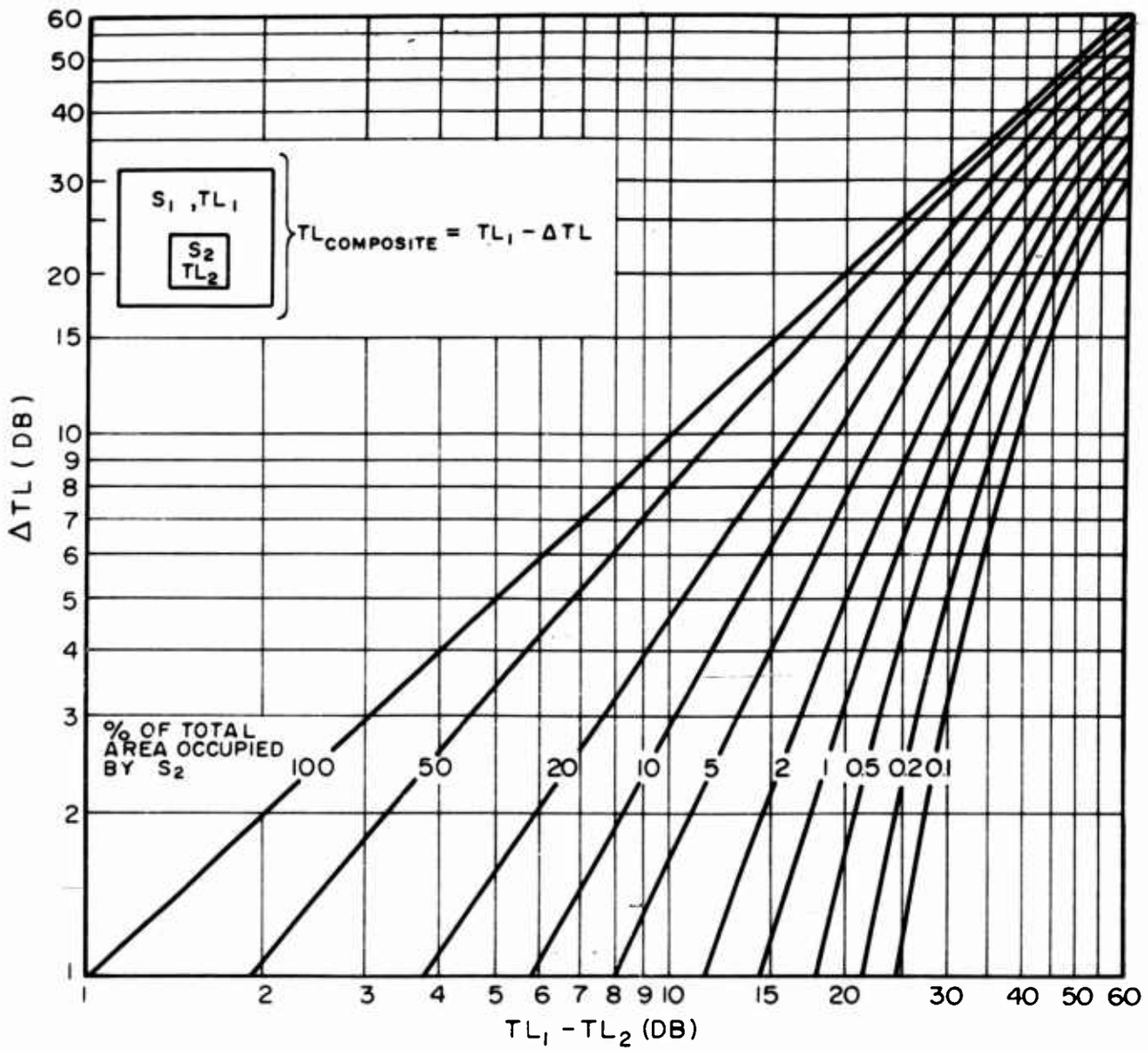

FIG. 52 CHART FOR DETERMINING EFFECTIVE TRANSMISSION LOSS, $TL_{COMPOSITE}$, OF A COMPOSITE PANEL.

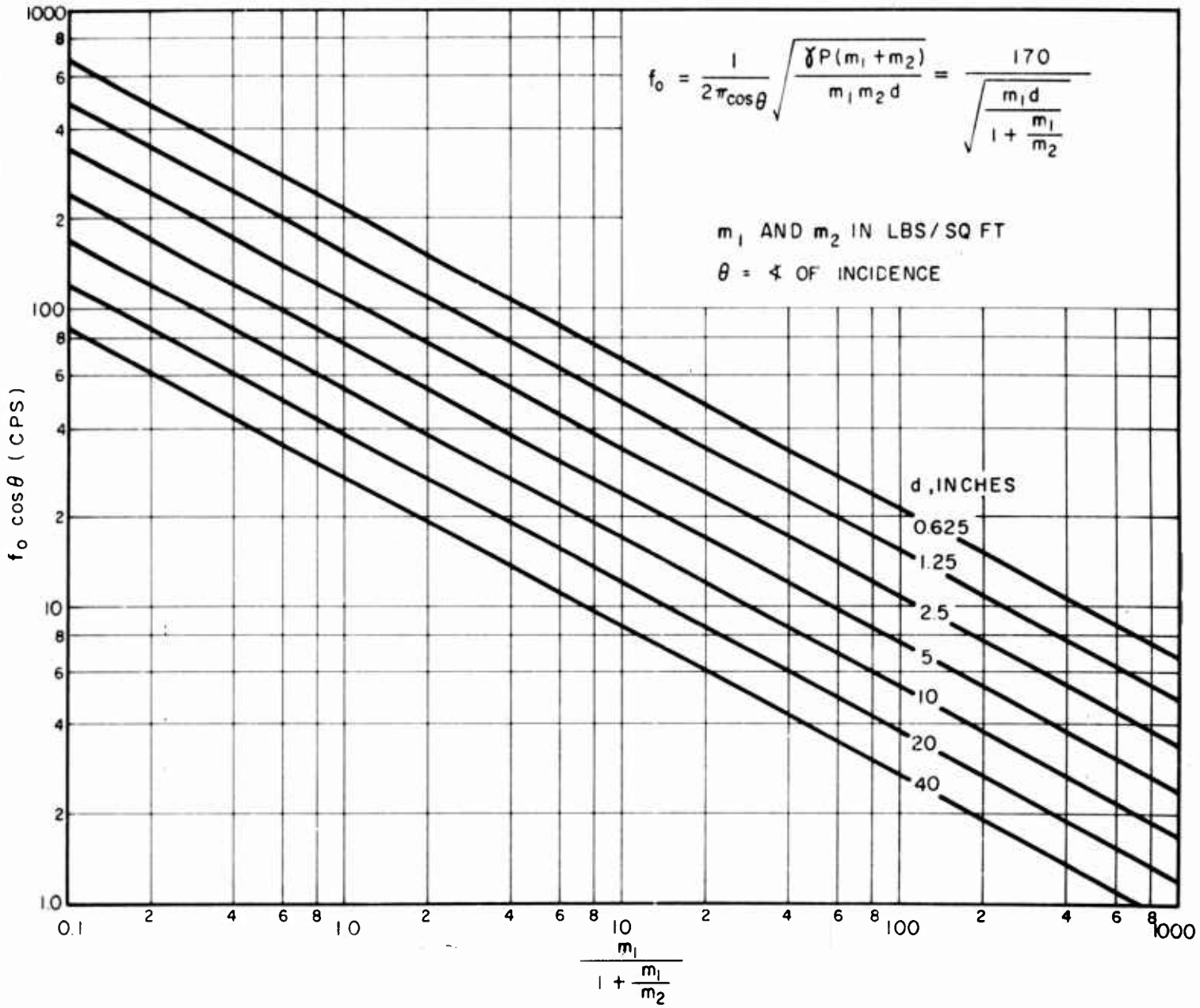

FIG. 53 DOUBLE WALL RESONANCE FREQUENCY

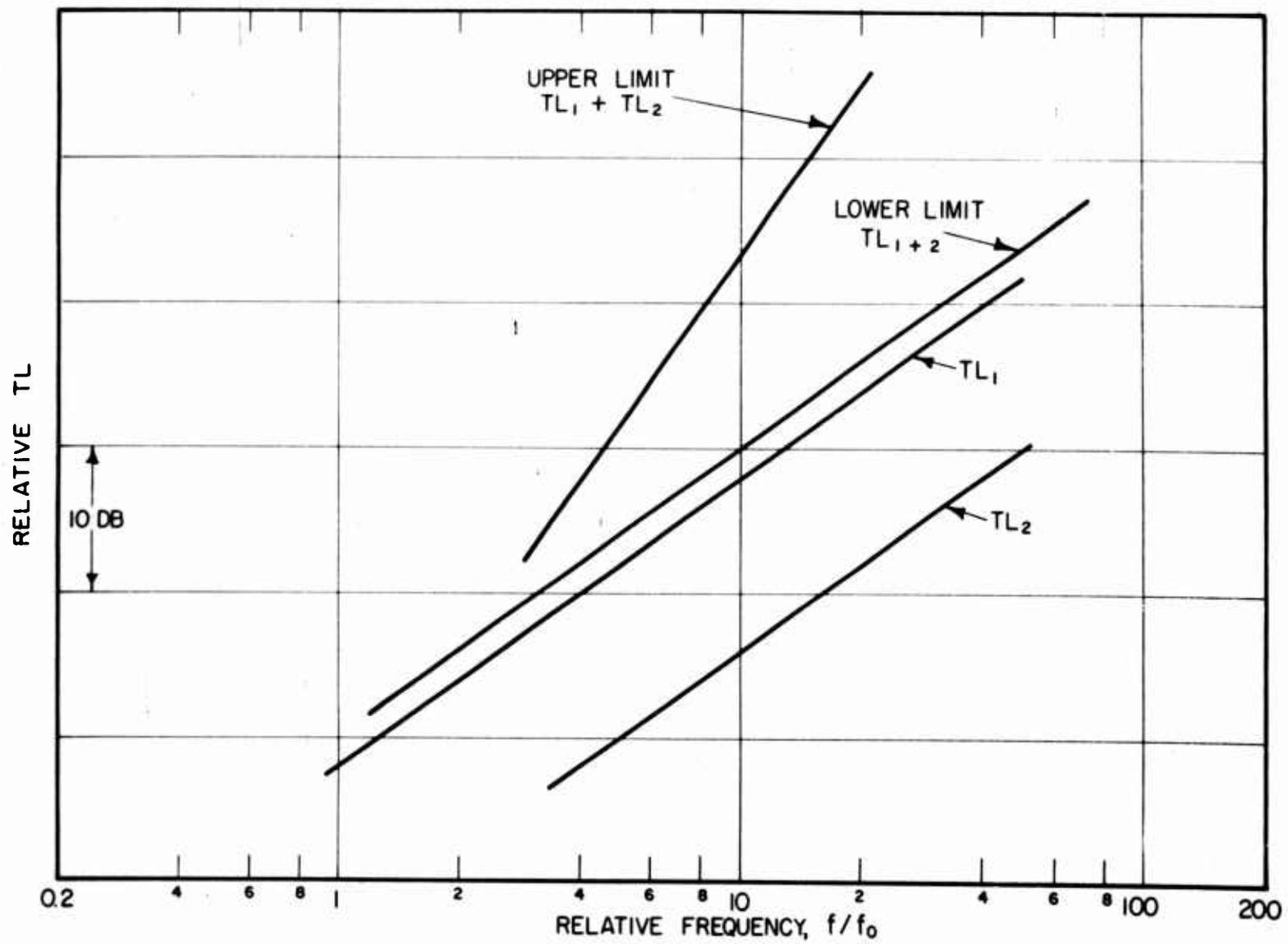

FIG. 54 APPROXIMATE THEORETICAL BEHAVIOR OF DOUBLE WALL APPRECIABLY ABOVE INTER-LEAF RESONANCE FREQUENCY, f_o

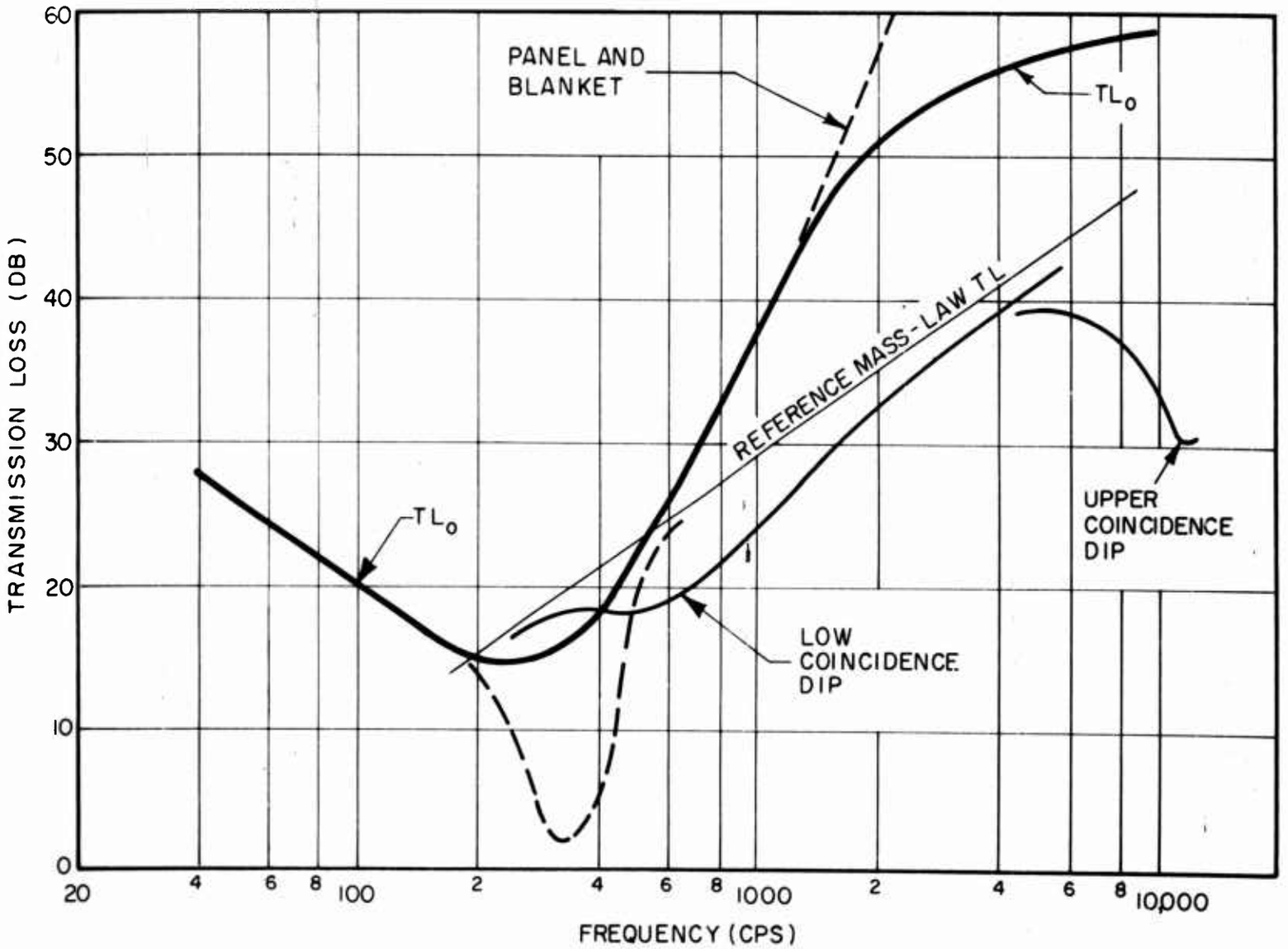

FIG. 55 ESTIMATION OF REFERENCE TRANSMISSION LOSS FOR A PASSENGER AIRCRAFT FUSELAGE

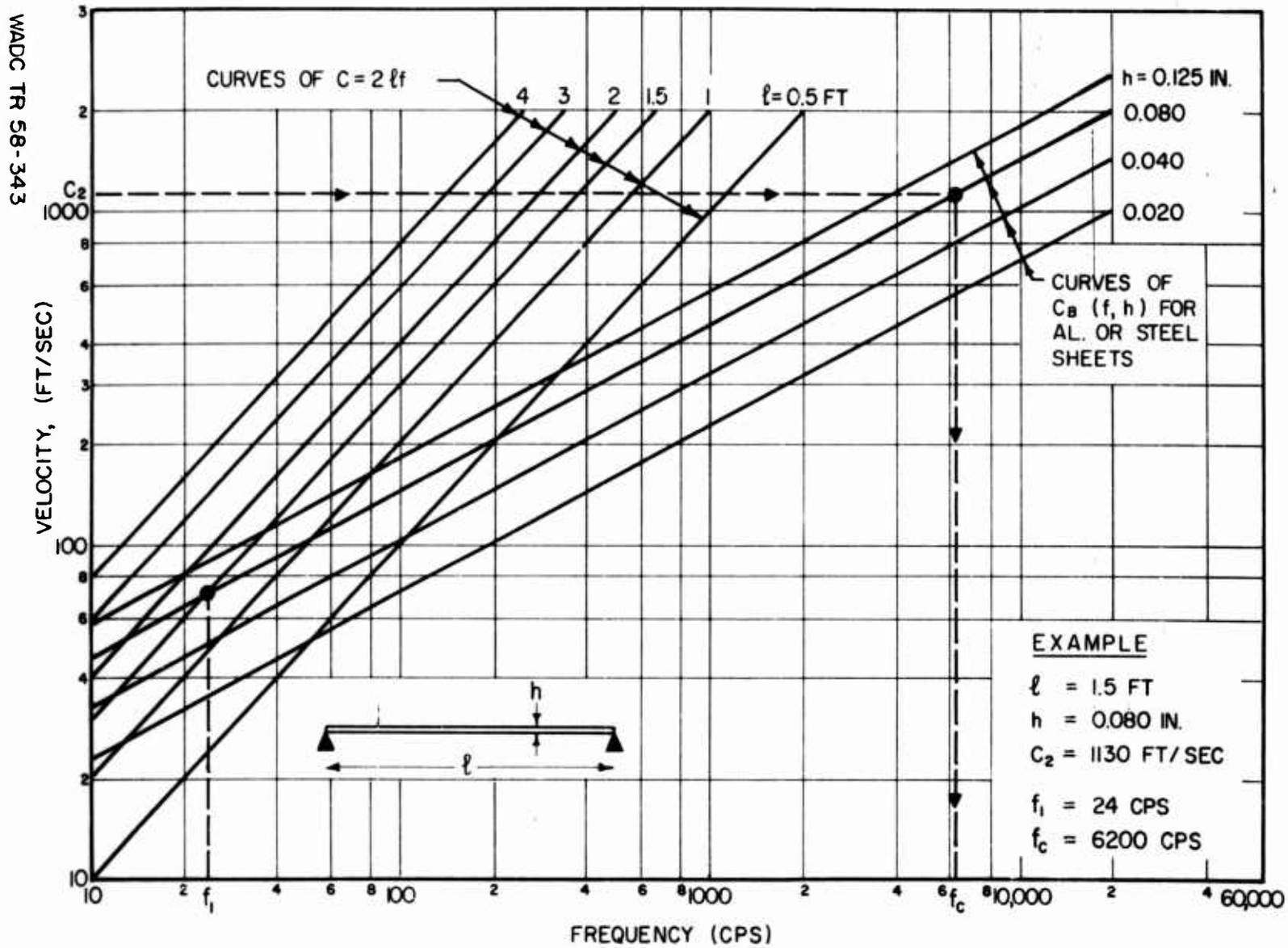

FIG. 56 CHART FOR DETERMINING THE FIRST RESONANCE FREQUENCY, f_1, AND THE SOUND COINCIDENCE FREQUENCY, f_c.
ALUMINIUM OR STEEL PANELS OF LENGTH l AND THICKNESS h;
END CONDITIONS: SIMPLE SUPPORTS.

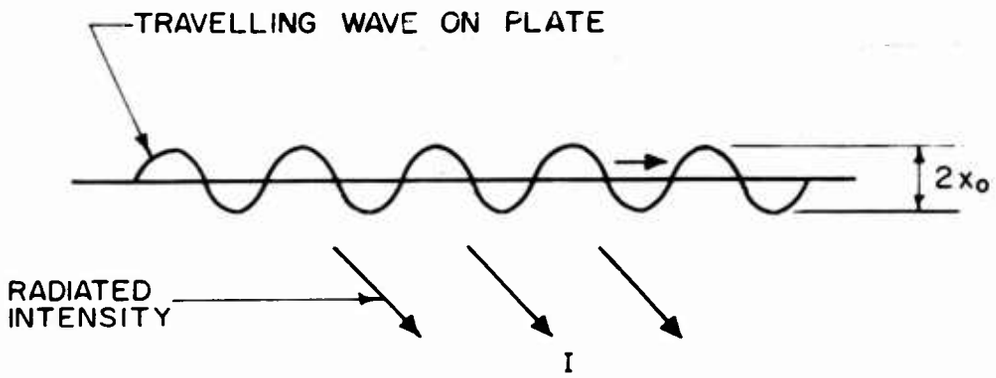

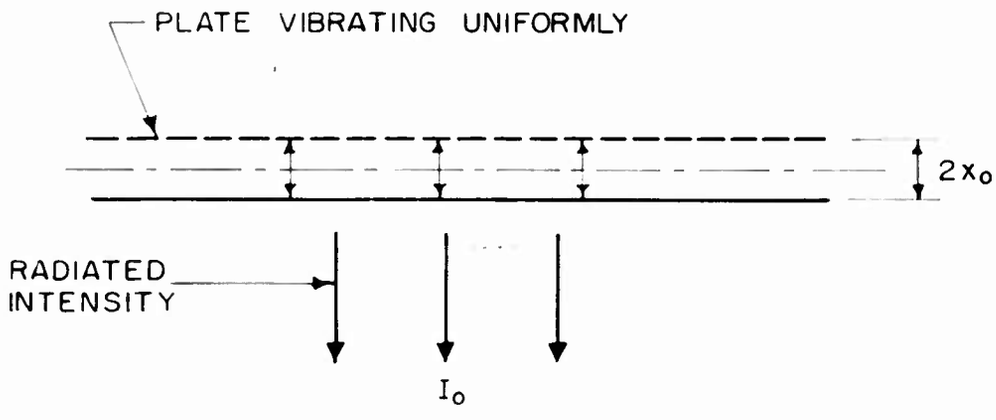

RADIATION FACTOR $S = \frac{I}{I_o}$

FIG. 57 DEFINITION OF RADIATION FACTOR, S.

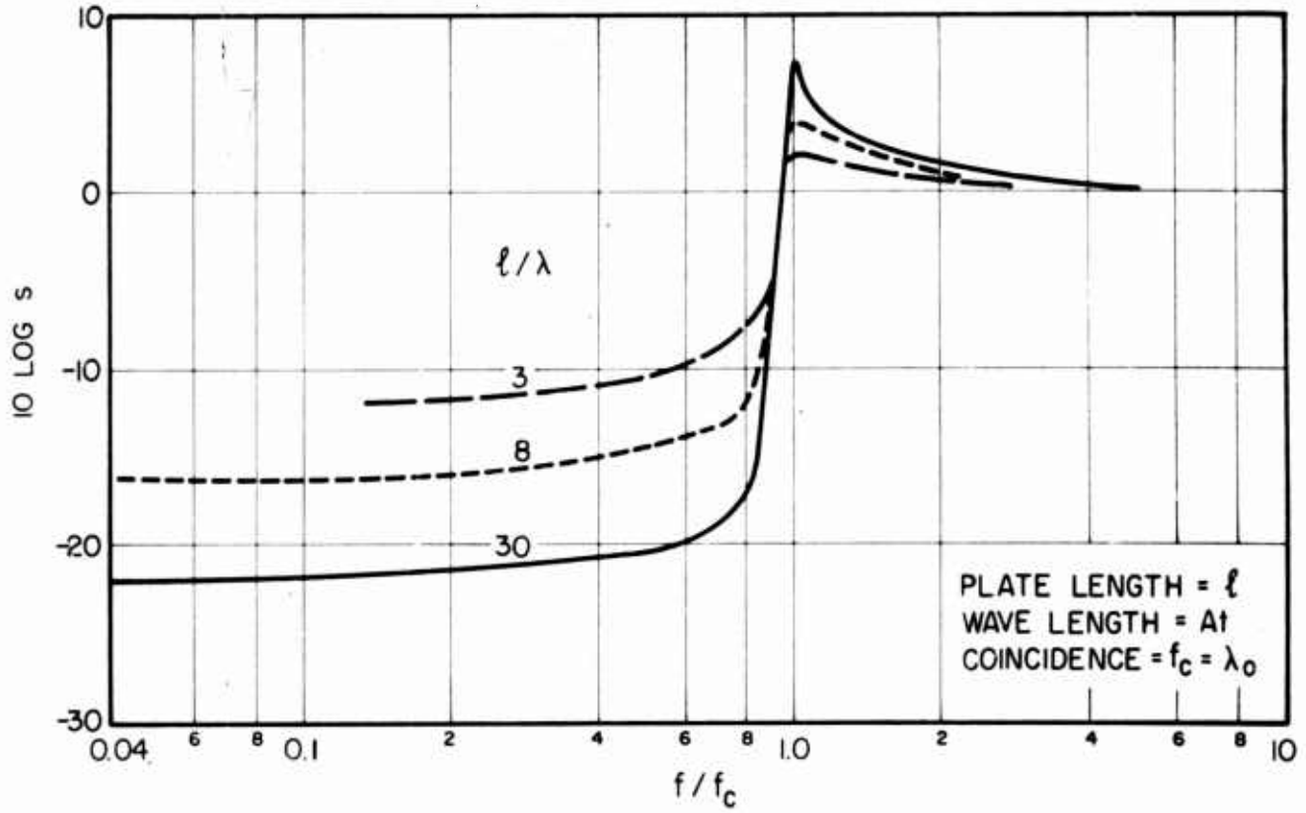

FIG. 58 RADIATION FACTOR, s, FOR TRAVELING BENDING WAVES ON A FINITE PORTION OF AN INFINITE PLATE.

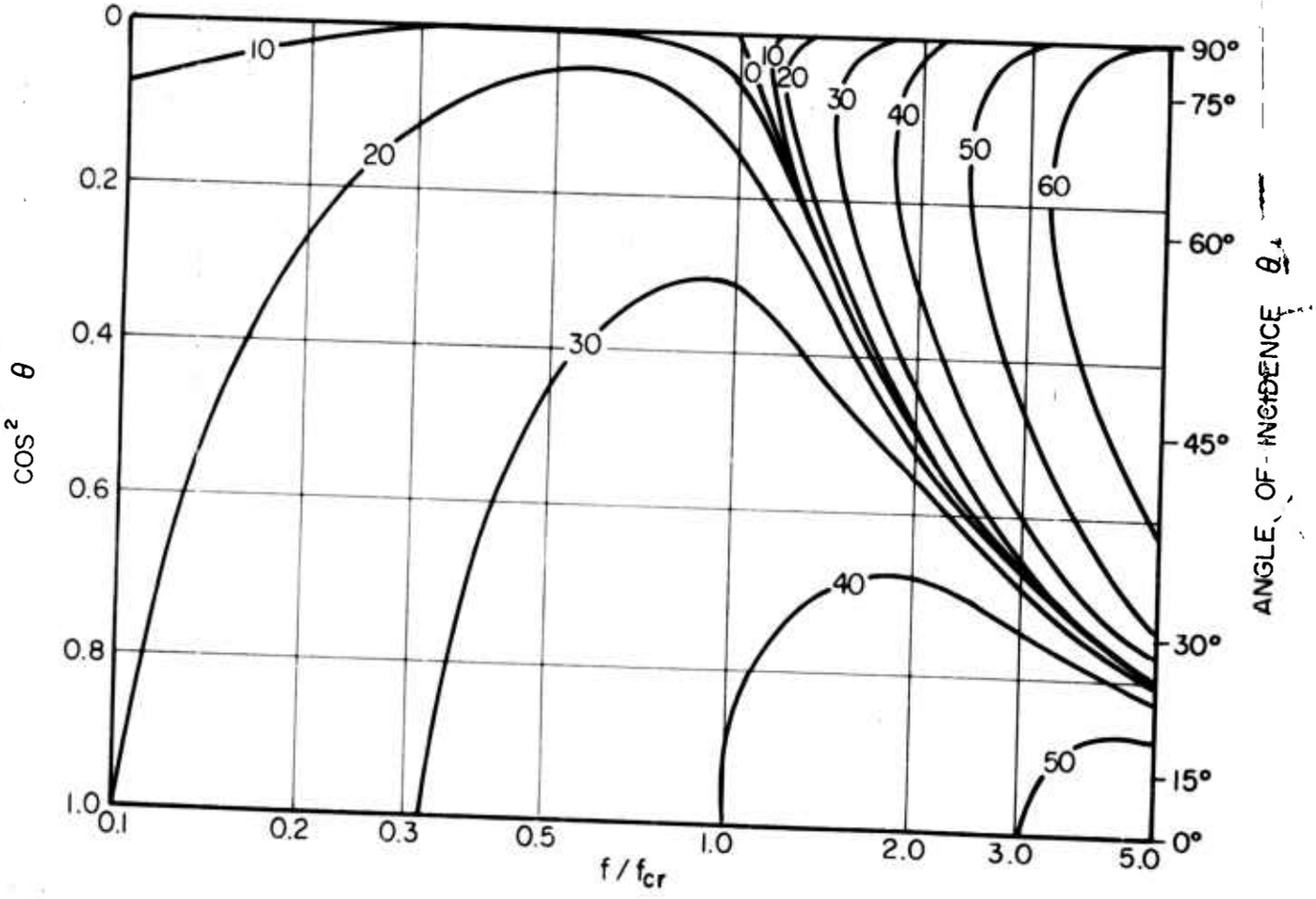

FIG. 59 CONTOURS OF EQUAL TRANSMISSION LOSS (DB) (CRITICAL FREQUENCY f_{cr} = LOWEST VALVE OF COINCIDENCE FREQUENCY f_c)

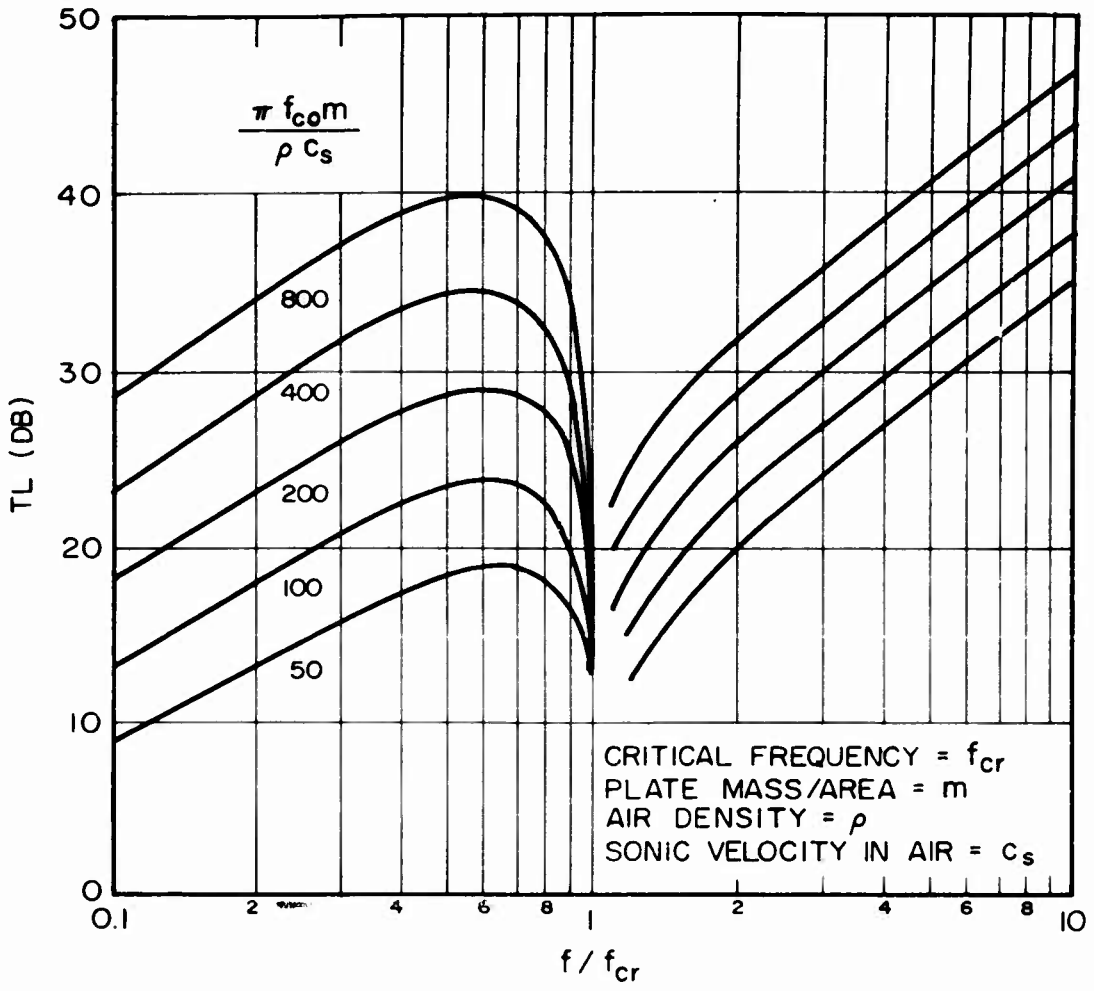

FIG. 60 TRANSMISSION LOSS AVERAGED OVER ANGLE OF INCIDENCE.

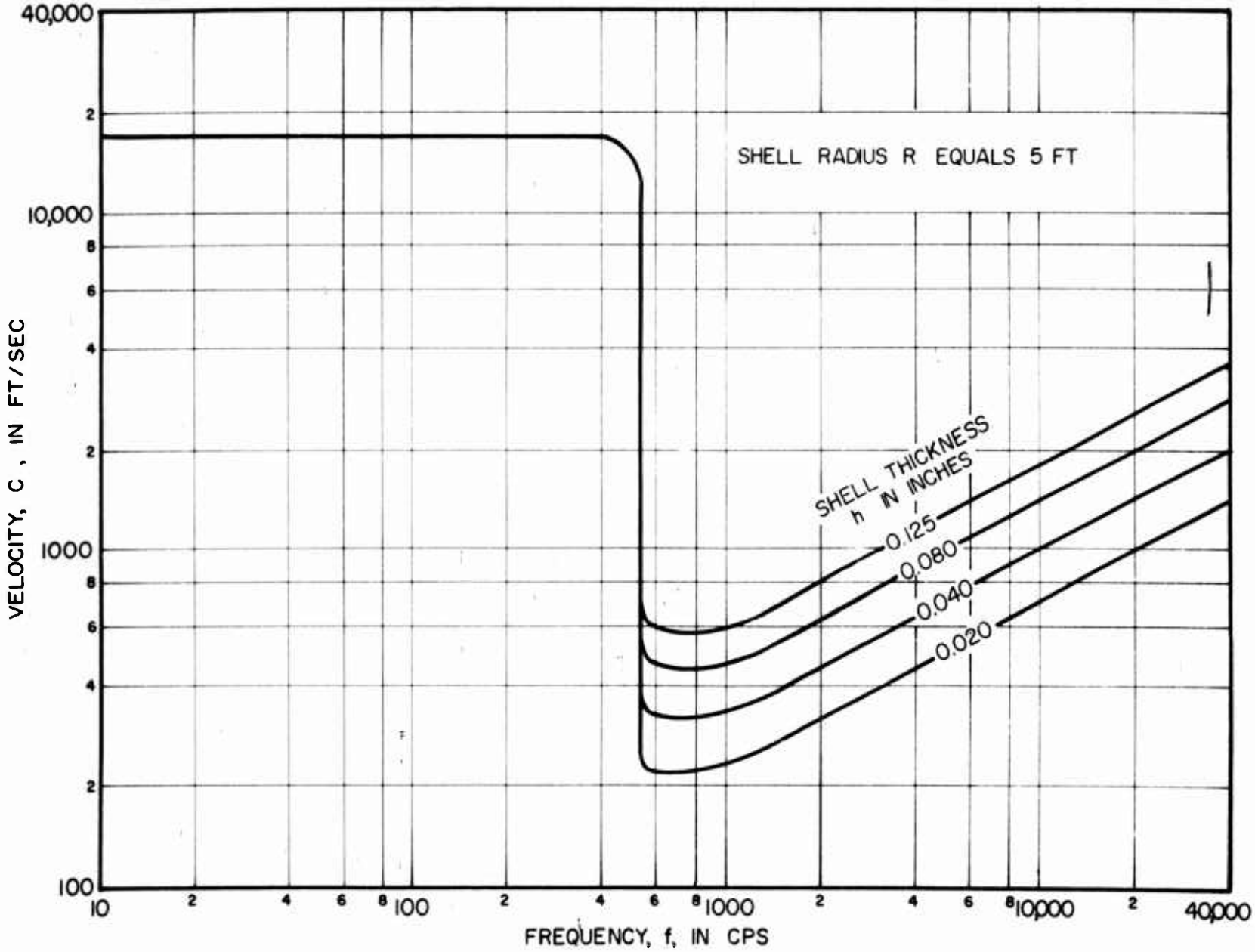

FIG. 61 FREE FLEXURAL WAVE VELOCITY, FOR ALUMINIUM OR STEEL CYLINDER NOT LOADED BY FLUIDS - n = 0.

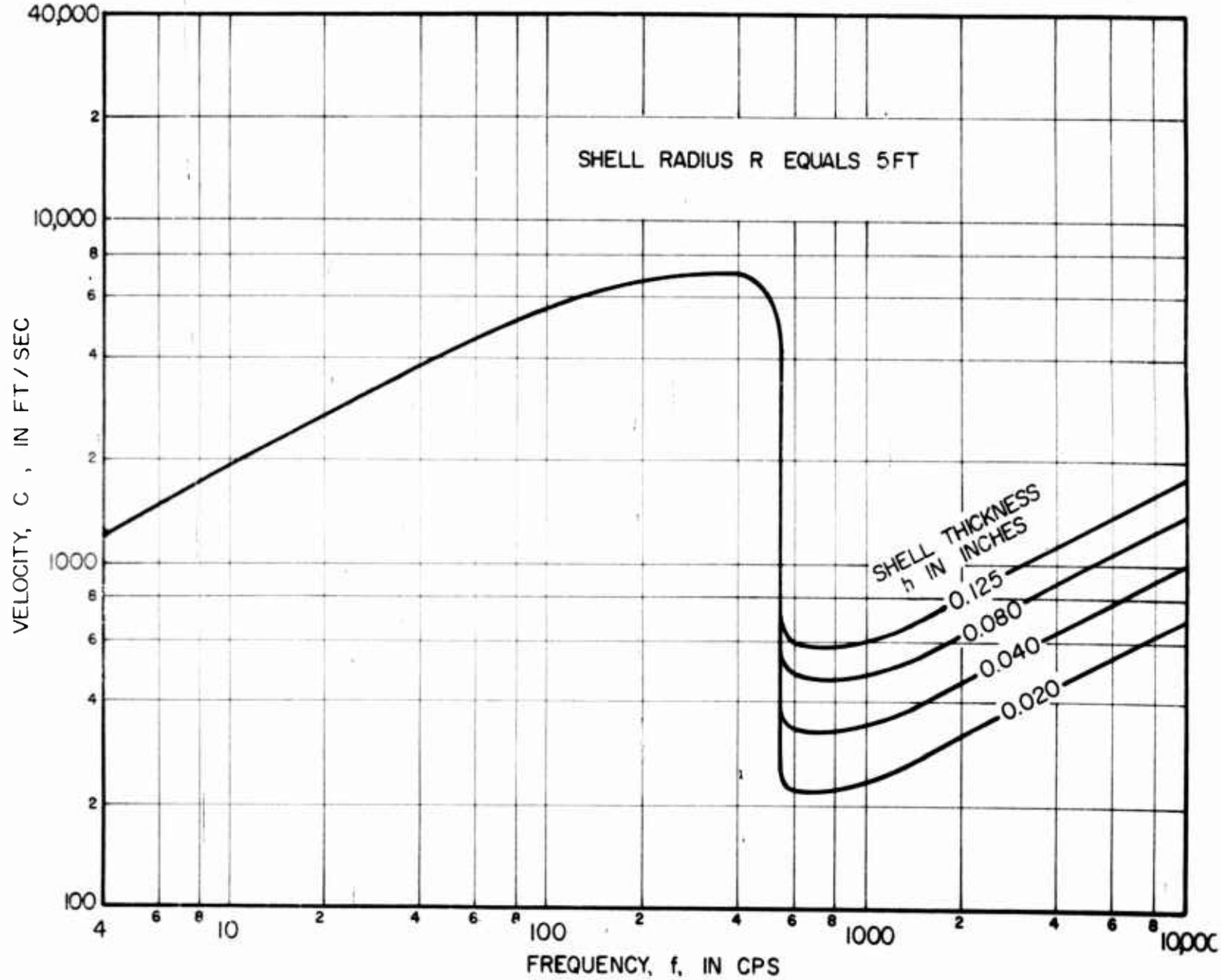

FIG. 62 FREE FLEXURAL WAVE VELOCITY, FOR ALUMINIUM OR STEEL CYLINDER NOT LOADED BY FLUIDS - n = 1.

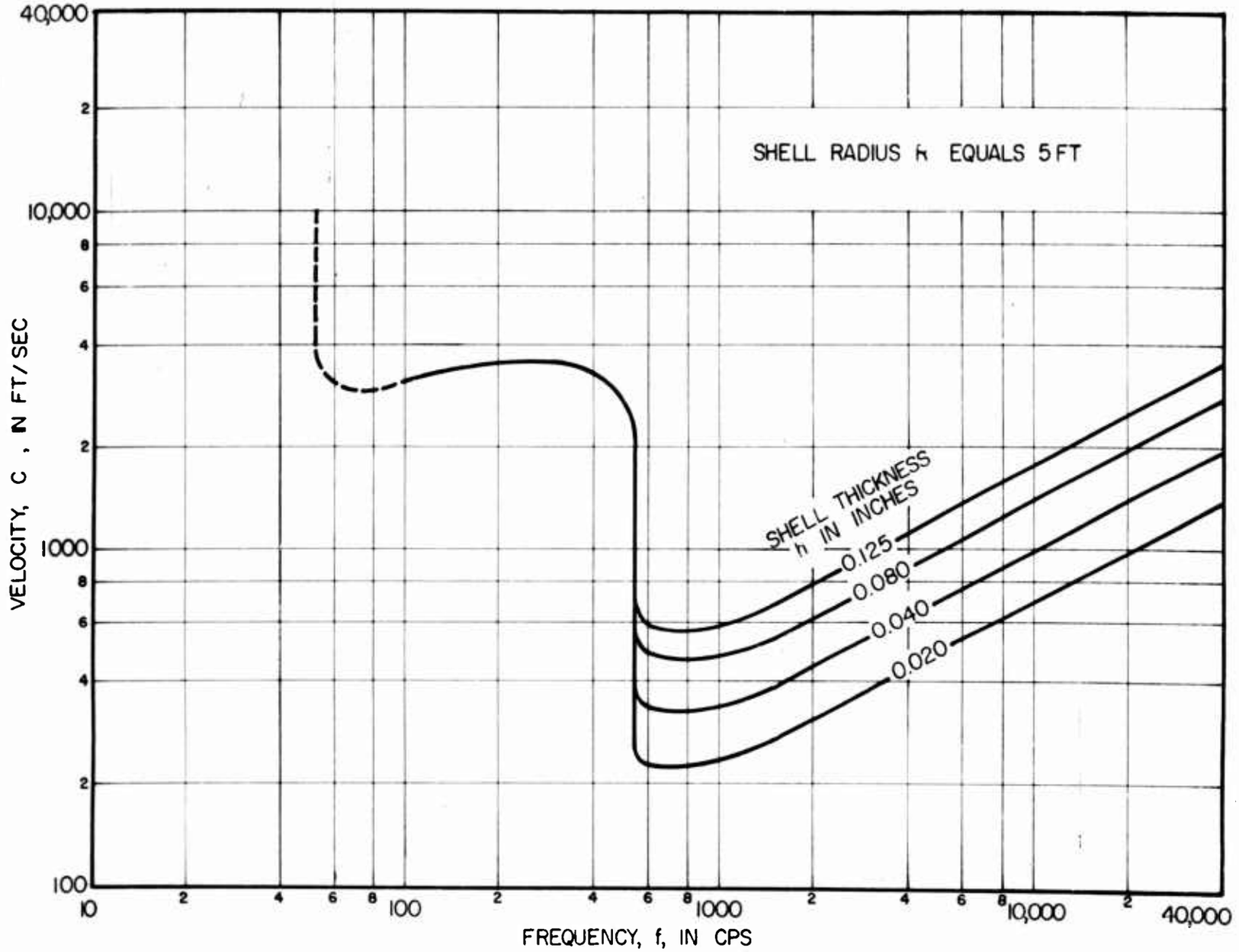

FIG. 63 FREE FLEXURAL WAVE VELOCITY, FOR ALUMINIUM OR STEEL CYLINDER NOT LOADED BY FLUIDS – n = 2.

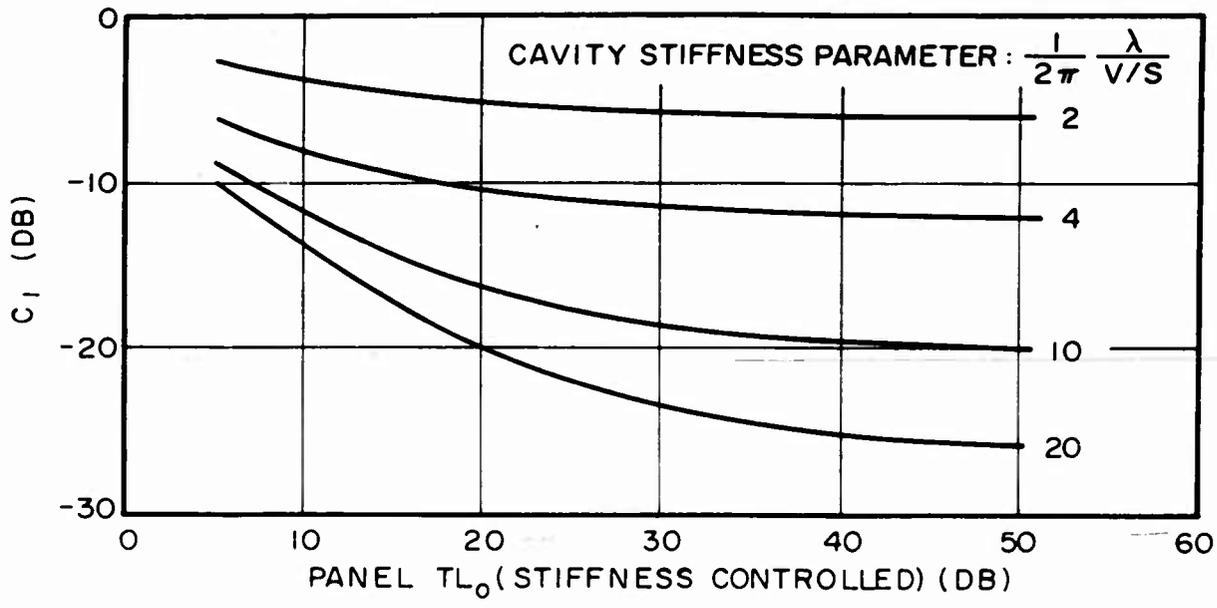

FIG. 64 C_1, CORRECTION TO TL_0 FOR STIFFNESS EFFECT OF SMALL RECEIVING SPACE

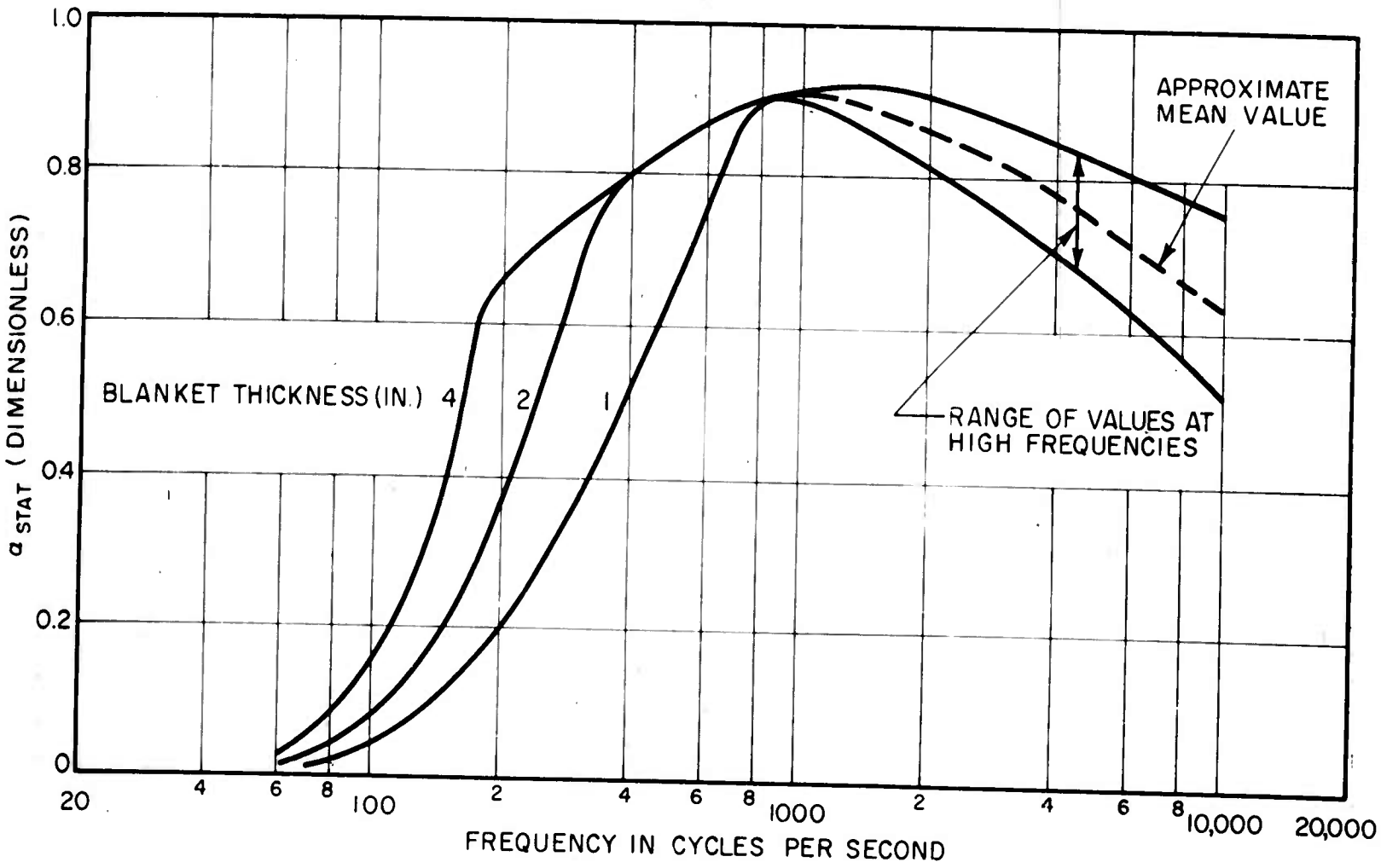

FIG. 65 APPROXIMATE STATISTICAL ABSORPTION COEFFICIENT, α_{STAT}, FOR SEVERAL THICKNESSES OF VERY FINE FIBER ACOUSTICAL BLANKETS (NO AIRSPACE BEHIND BLANKET)

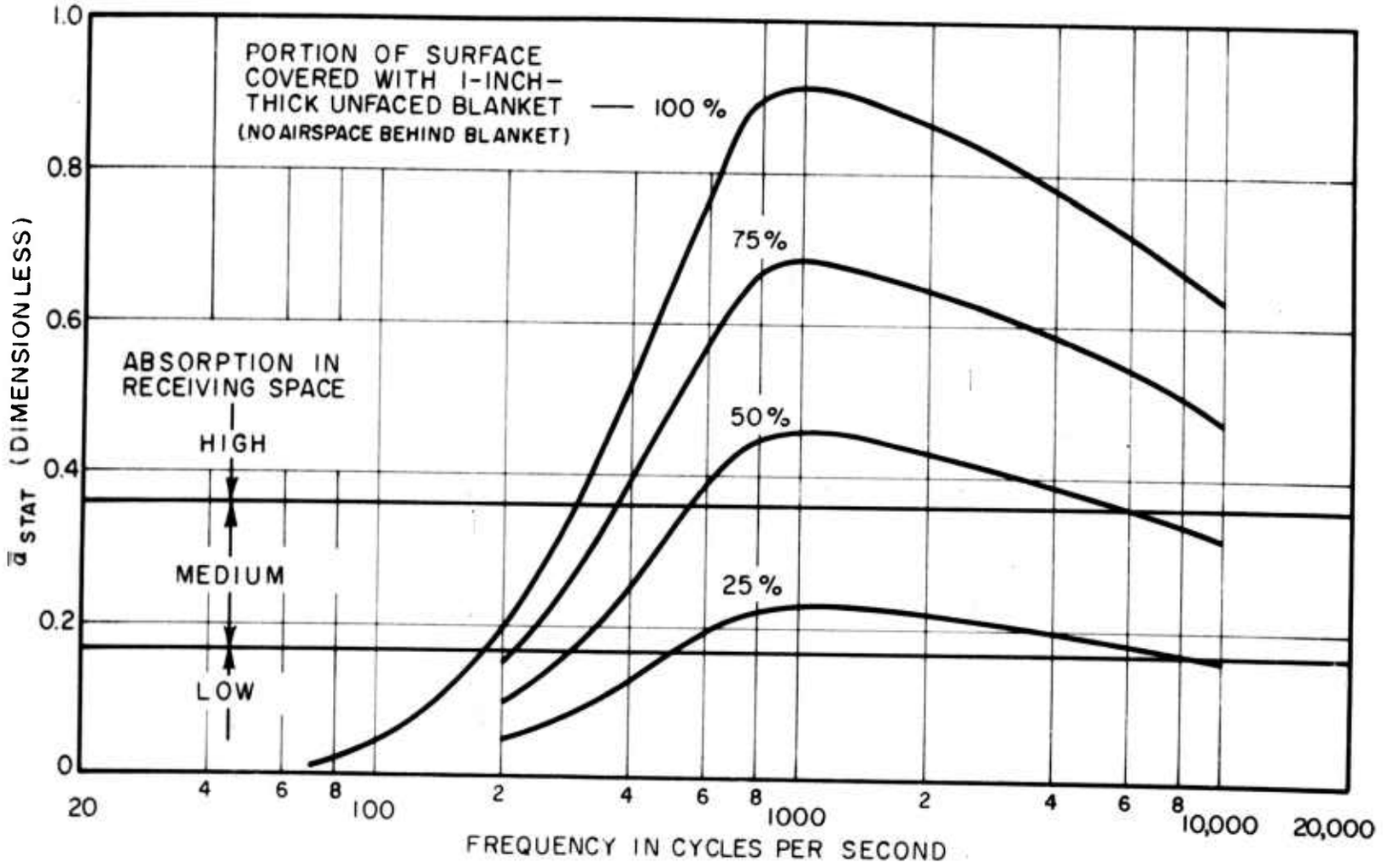

FIG. 66 APPROXIMATE AVERAGE STATISTICAL COEFFICIENT, $\bar{a}_{STAT}$, FOR RECEIVING SPACES TREATED WITH 1-INCH-THICK AIRCRAFT-TYPE ACOUSTICAL BLANKET

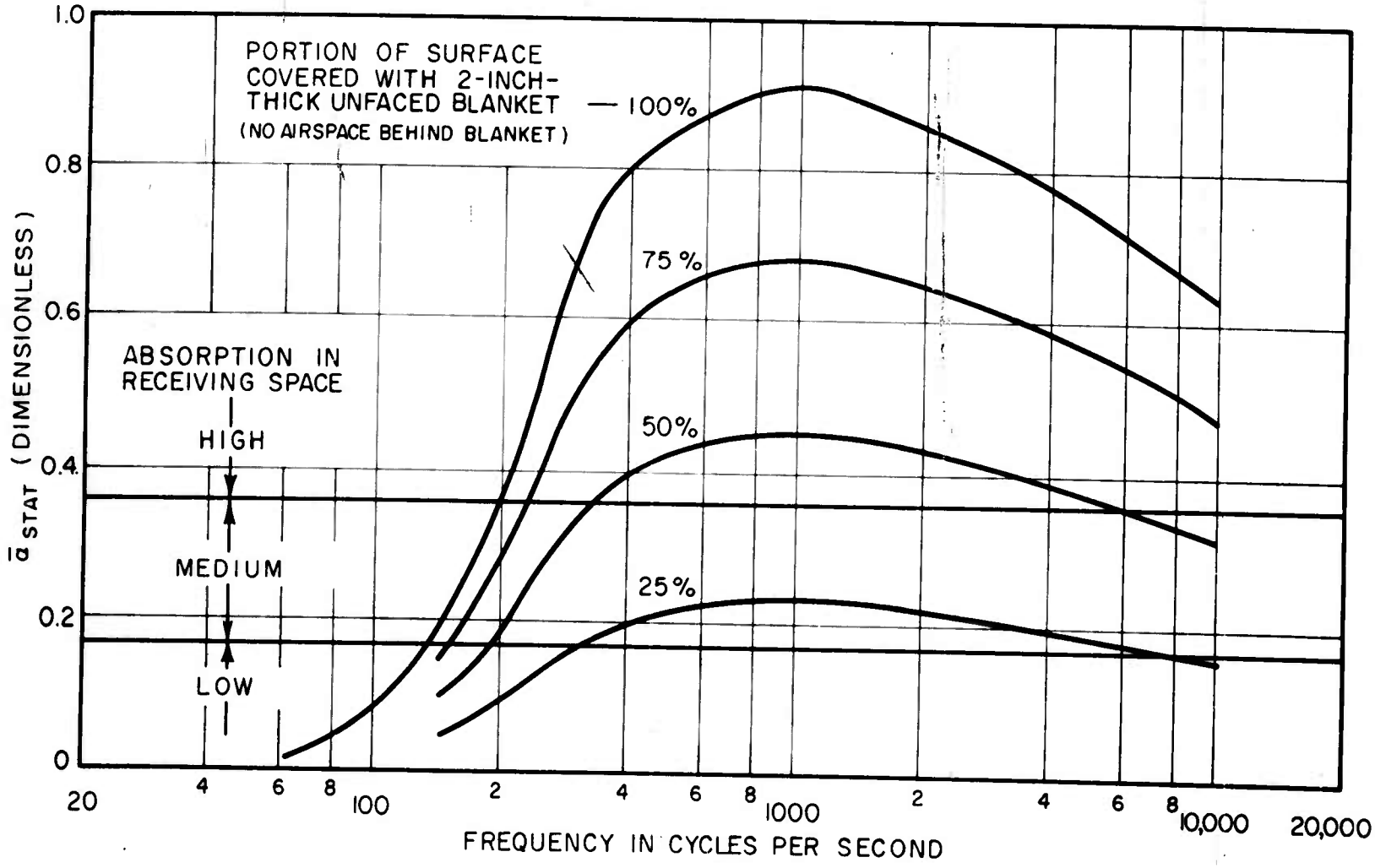

FIG. 67 APPROXIMATE AVERAGE STATISTICAL COEFFICIENT, $\bar{\alpha}_{STAT}$, FOR RECEIVING SPACES TREATED WITH 2-INCH-THICK AIRCRAFT-TYPE ACOUSTICAL BLANKET

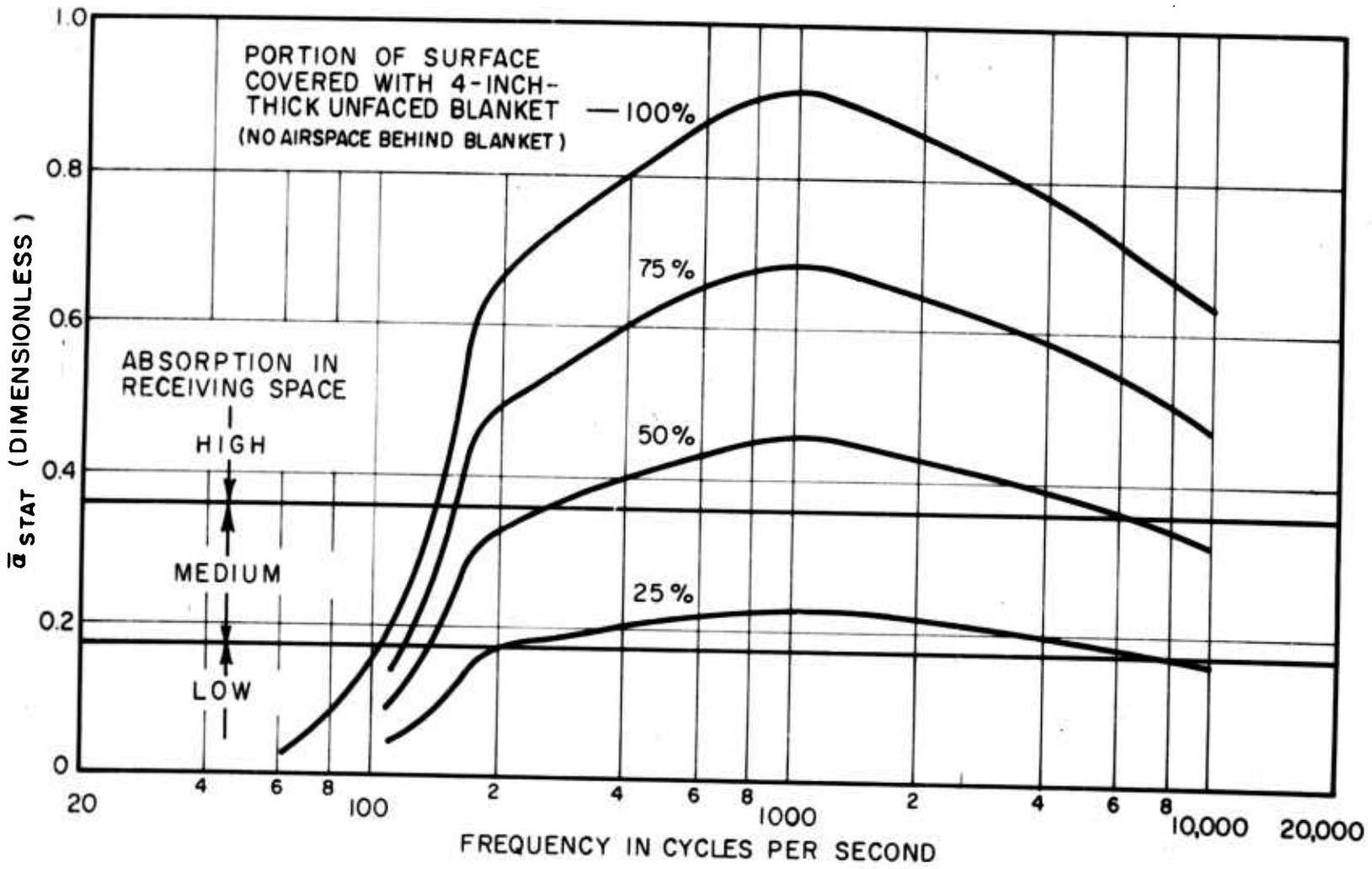

FIG. 68 APPROXIMATE AVERAGE STATISTICAL COEFFICIENT, $\bar{\alpha}_{STAT}$, FOR RECEIVING SPACES TREATED WITH 4-INCH-THICK AIRCRAFT-TYPE ACOUSTICAL BLANKET

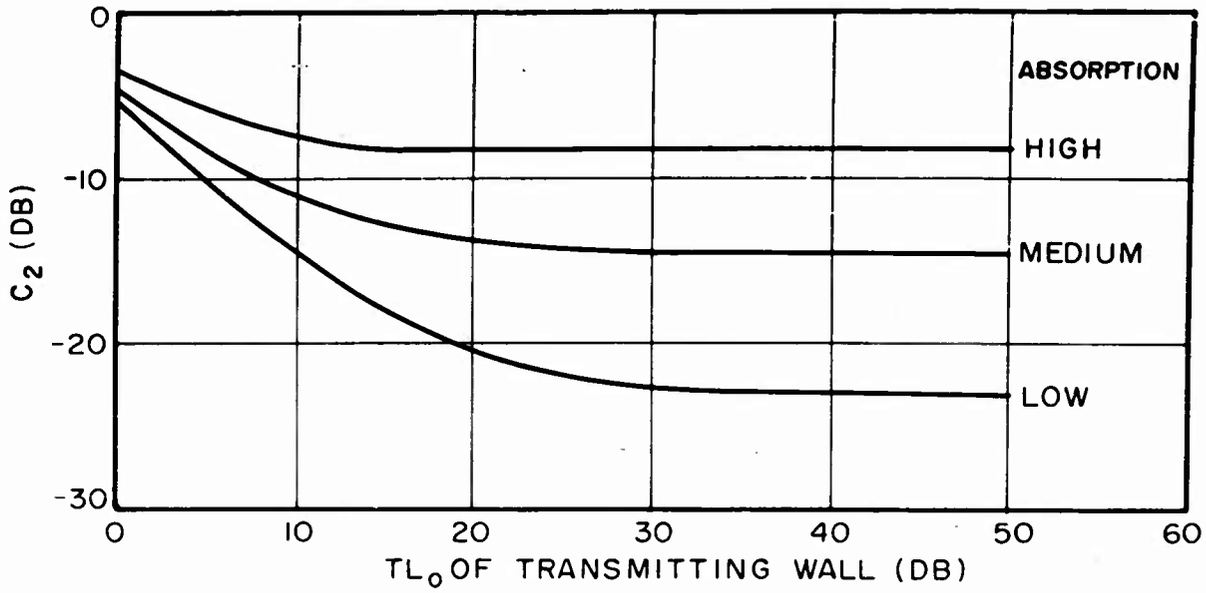

FIG. 69 C_2, CORRECTION TO TL_0 FOR MAXIMUM EFFECT OF STANDING WAVES IN MEDIUM-SIZED RECEIVING SPACE.

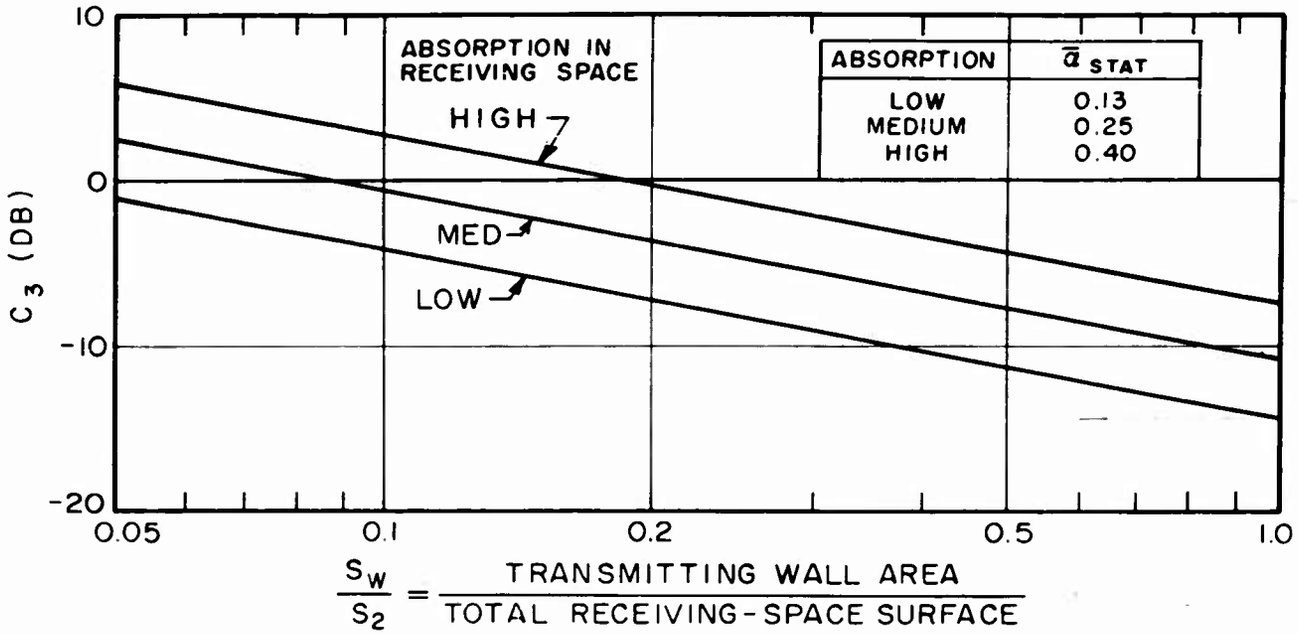

FIG. 70 C_3, CORRECTION TO TL_o FOR REVERBERATION IN LARGE RECEIVING SPACES.

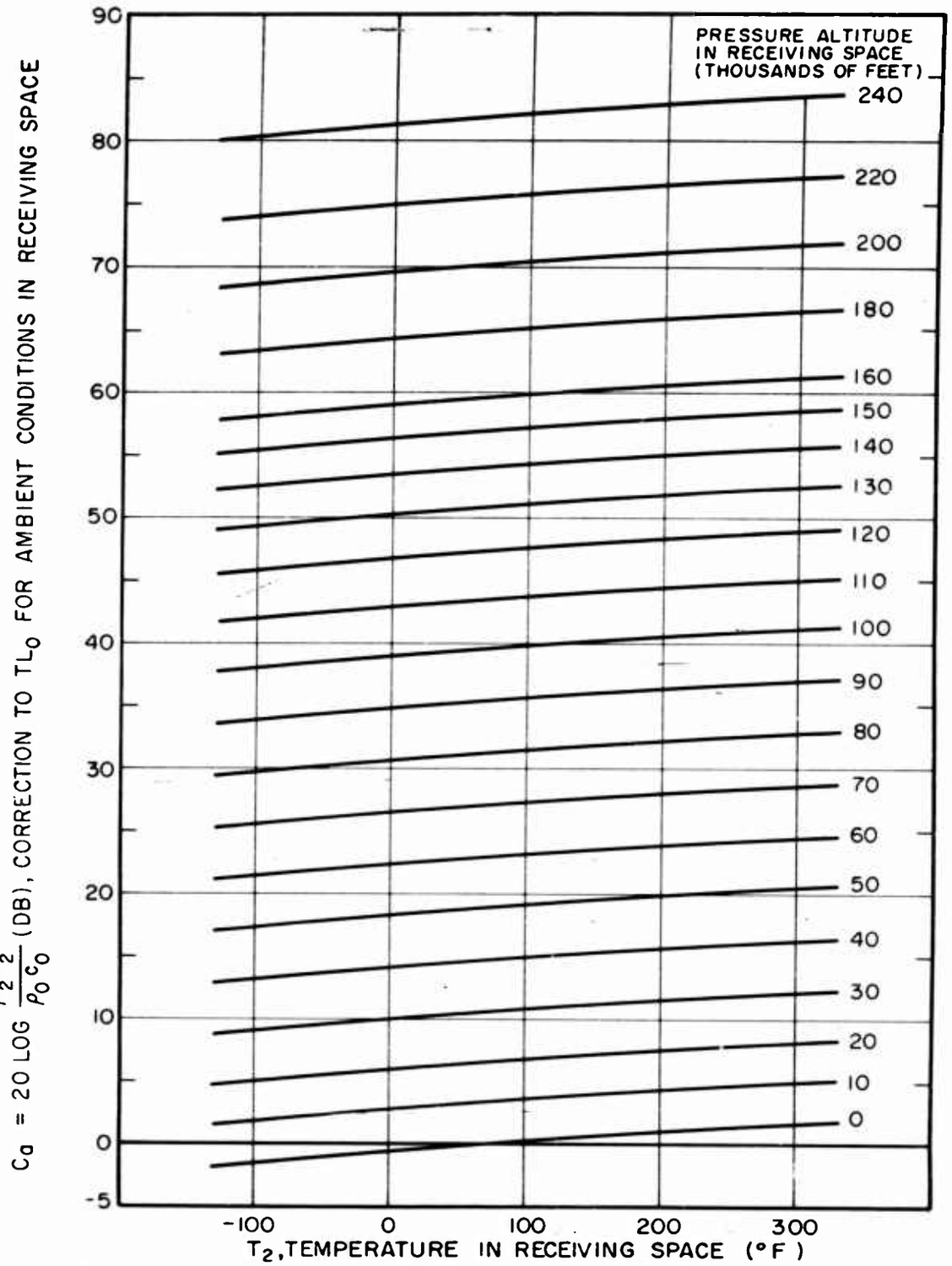

FIG. 71 CORRECTION TO TL_0 FOR AMBIENT CONDITIONS IN RECEIVING SPACE

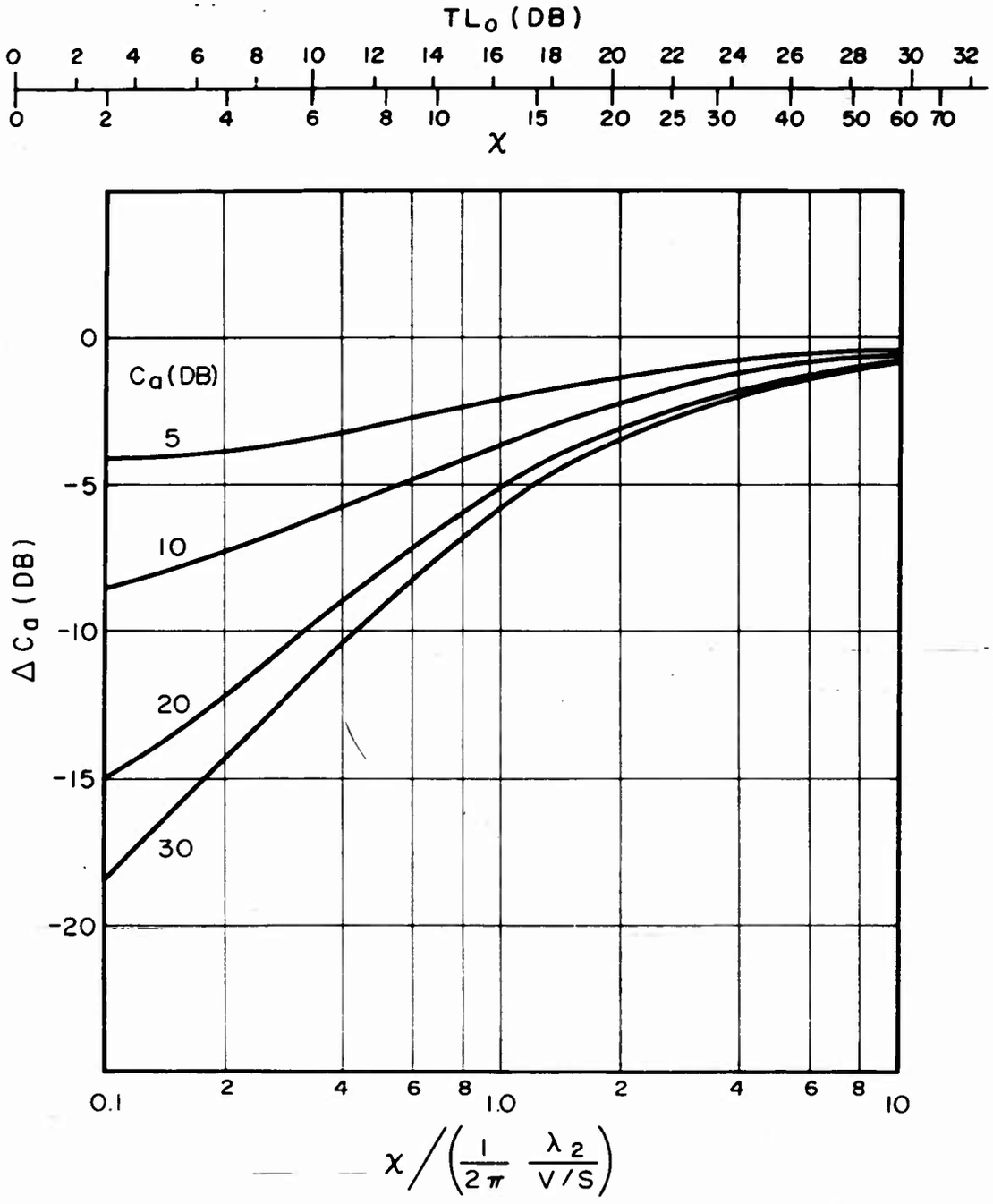

FIG. 72 CORRECTION TO C_a FOR SMALL RECEIVING SPACES

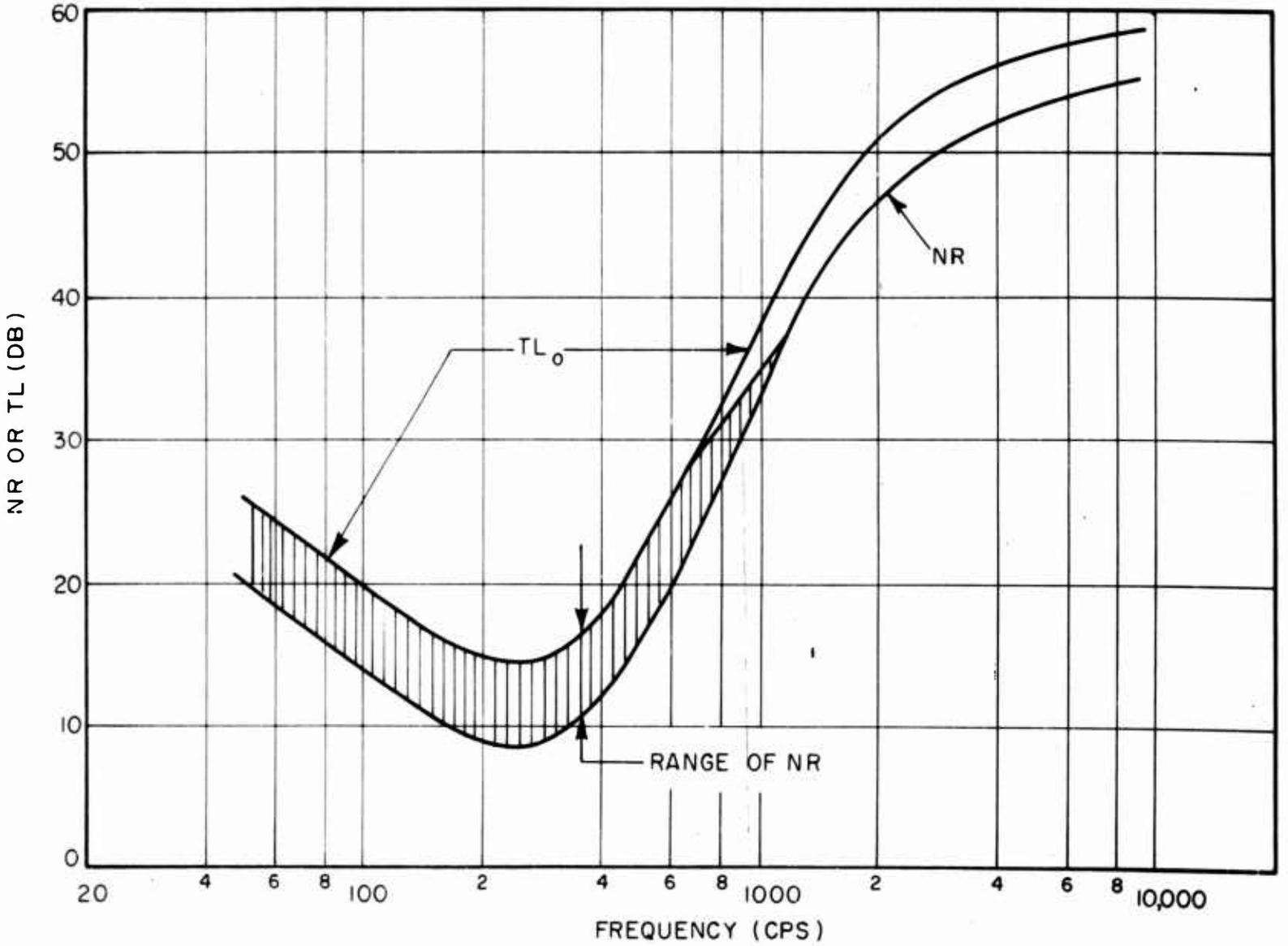

FIG. 73 ESTIMATION OF NR FOR A PASSENGER AIRCRAFT FUSELAGE

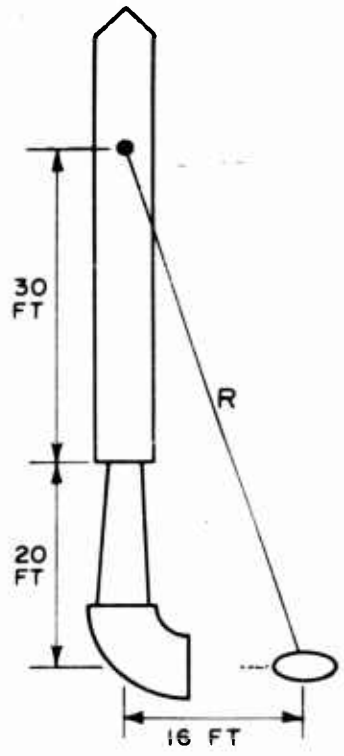

FIG. 74 GEOMETRY FOR EXAMPLE 3

APPENDIX A

"Vibration Frequency Charts"

by

J. N. MacDuff and R. P. Felgar

Reprinted with Permission from
Machine Design, 7 February 1957

Vibration Frequency Charts

1. Uniform beams
2. Variable-section beams
3. Continuous beams
4. Square plates
5. Rectangular plates
6. Cantilever plates
7. Circular plates
8. Rings
9. Circular membranes

By J. N. Macduff and R. P. Felgar

Professor
Mechanical Engineering Dept.
Duke University
Durham, N. C.

Engineer
General Engineering Laboratory
General Electric Co.
Schenectady, N. Y.

BEAMS and plates are common structural elements of mechanical design. It is often necessary to design these elements so that they have either a selected natural frequency or so that their natural frequencies are sufficiently far-removed from excitation frequencies to avoid resonance.

Tables and nomographs presented in this article provide a quick procedure for estimating natural frequencies of uniform and nonuniform beams, and uniform plates. These data enable the designer to assess the effect of changing the dimensions, type of support, and material of the structural element.

Data for the tables were obtained from readily available references. The theory underlying the data given for the natural frequencies of beams and plates assumes small deflections and neglects rotary inertia and shear effects. These restrictions must be kept in mind when determining frequencies from these data.

Method of Solution: The method is based on the use of a frequency constant defined as follows for the different types of structural elements:

Beams	$C = fL^2/k$
Square and rectangular plates	$C = fa^2/h$
Circular plates	$C = fr^2/h$

Symbols are defined for each case in Tables 1 to 10, appearing on the following pages, which give values of frequency constant C, or corresponding frequency function, for various mechanical structures and several modes of vibration. These tabulated values of C are based on the characteristic density and Young's modulus for steel.

The nomograph in Fig. 1 may be used with the proper frequency constant C and the characteristic dimensions to determine natural frequency directly. Nomographs in Figs. 2 and 3 present an alternate method for determining the natural frequency by first determining the value of L^2/k, a^2/h or r^2/h from the nomograph in Fig. 2 and then entering the nomograph in Fig. 3 with this item and the frequency constant. Figs. 1 to 3 are to be used with Tables 1 to 8 in which the values of the frequency constants are tabulated.

For materials other than steel, the material correction factor is obtained from the table in Fig. 4. With this factor, and the natural frequency, f_s, of a steel member of the same dimensions, the nomograph in Fig. 4 may then be used to determine the natural frequency.

Some of the less common mechanical structural members, such as membranes, have a frequency relation which is not defined by the foregoing nomographs. In such cases, numerical or slide rule calculation is necessary. The frequency constants for these members are given in Tables 9 and 10.

Example: Determine the fundamental natural frequency of a circular titanium plate, fixed at the center. Plate material is T1-75A titanium; plate radius, $r = 3$ in.; plate thickness, $h = 0.090$-in.; and estimated temperature of operation is 400 F.

From Table 7, $C/10^4 = 3.649$. From Fig. 1 then, the natural frequency of a steel plate of the same dimensions is $f_s = 370$ cps.

This result is also arrived at by the alternate procedure, Figs. 2 and 3. From Fig. 2, for $r = 3$ and $h = 0.09$, $r^2/h = 100$, and from Fig. 3, for a steel plate of the same dimensions, $f_s = 370$ cps.

Since plate material is titanium, final solution will be given by Fig. 4. From the table in Fig. 4, material correction factor for T1-75A titanium at 400 F is $K_m = 0.910$. From the nomograph then, for this value of K_m and $f_s = 370$ cps, frequency of the titanium plate is $f = 325$-350 cps.

This article is based on a paper entitled "Vibration Design Charts" presented at the ASME Annual Meeting in New York, November, 1956.

Table 1—Uniform Steel Beams

C = Frequency constant
f_n = Natural frequency, cps
$k = (I/A)^{1/2}$ = Radius of gyration, in.
L = Beam length, in.
M = Vibration mode number

Beam Structure	$C/10^4 = (f_n L^2/k)/10^4$				
	$M=1$	$M=2$	$M=3$	$M=4$	$M=5$
Clamped-Clamped / Free-Free	71.95	198.29	388.73	642.60	959.94
Clamped-Free	11.30	70.85	198.30	388.73	642.60
Clamped-Hinged / Free-Hinged	49.57	160.65	335.17	573.20	874.65
Clamped-Guided / Free-Guided	17.98	97.18	239.98	446.25	715.98
Hinged-Hinged / Guided Guided	31.73	126.93	285.60	507.73	793.33
Hinged-Guided	7.93	71.40	198.33	388.73	642.60

Table 2—Variable-Section Steel Beams

C = Frequency constant
f_n = Natural frequency, cps
$k = (I/A)^{1/2}$ = Radius of gyration, in.
L = Beam length, in.
M = Vibration mode number

Beam Structure	b/b_0	h/h_0	$C/10^4 = (f_n L^2/k)/10^4$		
			$M=1$	$M=2$	$M=3$
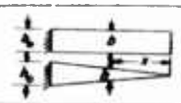	1	x/L	17.09	48.89	96.57
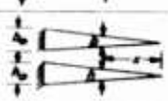	x/L	x/L	26.08	68.08	123.64
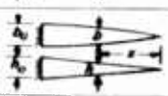	$(x/L)^{1/2}$	x/L	22.30	58.18	109.90
	$e^{x/L}$	1	15.23	77.78	206.07
	1	x/L	21.21* 35.05†	56.97	
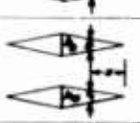	x/L	x/L	32.73* 49.50†	76.57	
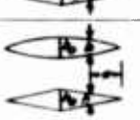	$(x/L)^{1/2}$	x/L	25.66* 42.02†	66.06	

*Symmetric. †Antisymmetric.

Table 3—Continuous Uniform Steel Beams

C = Frequency constant
f_n = Natural frequency, cps
$k = (I/A)^{1/2}$ = Radius of gyration, in.
L = Span length, in.
M = Vibration mode number
n = Number of spans

Beam Structure	n	$C/10^4 = (f_n L^2/k)/10^4$				
		$M=1$	$M=2$	$M=3$	$M=4$	$M=5$
Extreme Ends Simply Supported						
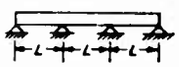	1	31.73	126.94	285.61	507.76	793.37
	2	31.73	49.59	126.94	160.66	285.61
	3	31.73	40.52	59.56	126.94	143.98
	4	31.73	37.02	49.59	63.99	126.94
	5	31.73	34.99	44.19	55.29	66.72
	6	31.73	34.32	40.52	49.59	59.56
	7	31.73	33.67	38.40	45.70	53.63
	8	31.73	33.02	37.02	42.70	49.59
	9	31.73	33.02	35.66	40.52	46.46
	10	31.73	33.02	34.99	39.10	44.19
	11	31.73	32.37	34.32	37.70	41.97
	12	31.73	32.37	34.32	37.02	40.52
Extreme Ends Clamped						
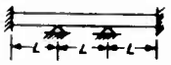	1	72.36	198.34	388.75	642.63	959.98
	2	49.59	72.36	160.66	198.34	335.20
	3	40.52	59.56	72.36	143.98	178.25
	4	37.02	49.59	63.99	72.36	137.30
	5	34.99	44.19	55.29	65.72	72.36
	6	34.32	40.52	49.59	59.56	67.65
	7	33.67	38.40	45.70	53.63	62.20
	8	33.02	37.02	42.70	49.59	56.98
	9	33.02	35.66	40.52	46.46	52.81
	10	33.02	34.99	39.10	44.19	49.59
	11	32.37	34.32	37.70	41.97	47.23
	12	32.37	34.32	37.02	40.52	44.94
Extreme Ends Clamped-Supported						
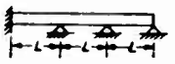	1	49.59	160.66	335.2	573.21	874.69
	2	37.02	63.99	137.30	185.85	301.05
	3	34.32	49.59	67.65	132.07	160.66
	4	33.02	42.70	56.98	69.51	129.49
	5	33.02	39.10	49.59	61.31	70.15
	6	32.37	37.02	44.94	54.46	63.99
	7	32.37	35.66	41.97	49.59	57.84
	8	32.37	34.99	39.81	45.70	53.63
	9	31.73	34.32	38.40	43.44	49.59
	10	31.73	33.67	37.02	41.24	46.46
	11	31.73	33.67	36.33	39.81	44.19
	12	31.73	33.02	35.66	39.10	42.70

Table 4—Square Steel Plates

a = Plate side, in.
C = Frequency constant
f_n = Natural frequency, cps
h = Plate thickness, in.
M = Vibration mode number

Plate Structure*	$C/10^4 = (f_n a^2/h)/10^4$					
	$M=1$	$M=2$	$M=3$	$M=4$	$M=5$	$M=6$
	3.40	8.32	20.66	26.71	30.32	
	6.77	23.43	26.07	46.75	61.44	
	13.72	19.99	23.26	34.98	59.93	63.47
	19.20	48.00	76.82	96.01	124.82	163.25

Table 4 (Cont.)

Plate Structure*	$C/10^4 = (f_s a^2/h)/10^4$					
	$M=1$	$M=2$	$M=3$	$M=4$	$M=5$	$M=6$
	23.01	50.28	57.06	83.79	97.58	110.13
	28.16	53.26	67.44	92.02	99.43	125.60
	35.01	71.42	105.36	128.03	128.71	160.72

*F = free, S = supported, C = clamped.

Table 5—Rectangular Steel Plates (First Vibration Mode)

$C/10^4 = (f_s a^2/h)/10^4$

a = Plate side, in.
C = Frequency constant
f_s = Natural frequency, cps
h = Plate thickness, in.

Plate Structure*	b/a	$C/10^4$	a/b	$C/10^4$
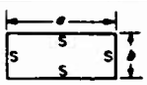	1.0	19.20		
	1.5	13.87		
	2.0	12.00		
	2.5	11.14		
	3.0	10.67		
	∞	9.60		
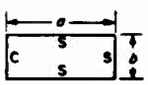	1.0	23.01	1.0	23.01
	1.5	18.39	1.5	15.15
	2.0	16.56	2.0	12.57
	2.5	16.18	2.5	11.43
	3.0	15.82	3.0	10.84
	∞	15.01	∞	9.60
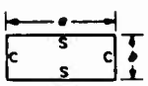	1.0	28.16	1.0	28.16
	1.5	24.37	1.5	16.90
	2.0	23.17	2.0	13.32
	2.5	22.64	2.5	11.80
	3.0	22.37	3.0	11.05
	∞	21.76	∞	9.60
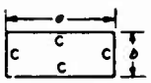	1.0	35.00		
	1.5	26.27		
	2.0	23.90		
	2.5	23.12		
	3.0	22.56		
	∞	21.76		

*F = free, S = supported, C = clamped.

Table 6—Cantilever Steel Plates

a = Plate side, in.
C = Frequency constant
f_s = Natural frequency, cps
h = Plate thickness, in.
M = Vibration mode number
θ = Skew angle, deg

Plate Structure*	$C/10^4 = (f_s a^2/h)/10^4$				
Rectangular Cantilever Plate					
a/b	$M=1$	$M=2$	$M=3$	$M=4$	$M=5$
 ½	3.41	5.23	21.36	9.96	24.18
1	3.40	8.32	20.86	26.71	30.32
2	3.38	14.52	21.02	91.92	47.39
5	3.36	33.79	20.94	548.60	103.03

Skewed Cantilever Plate		
θ	$M=1$	$M=2$
 15	3.50	8.63
30	3.85	9.91
45	4.69	13.38

*F = free, C = clamped.

Table 7—Circular Steel Plates

C = Frequency constant
f_s = Natural frequency, cps
h = Plate thickness, in.
r = Plate radius, in.
m = Number of nodal circles
n = Number of nodal diameters

Plate Structure*	$C/10^4 = (f_s r^2/h)/10^4$			
n	$m=0$	$m=1$	$m=2$	$m=3$
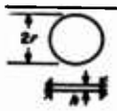 Circular Plate Clamped at Boundary				
0	9.936	39.713	89.516	
1	20.651			
2	33.906			
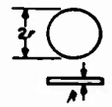 Circular Plate With Free Boundary				
0		8.832	39.487	
1		19.970	58.255	
2	5.110	34.295		
3	11.902	51.491		
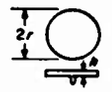 Circular Plate Clamped at Center				
	3.649	20.349	59.053	116.490

Table 8—Steel Ring Vibrating In Its Own Plane

C = Frequency constant
f_s = Natural frequency, cps
h = Ring thickness, in.
n = Number of full waves around periphery
r = Mean ring radius, in.

Ring Structure	$C/10^4 = (f_s r^2/h)/10^4$				
	$n=2$	$n=3$	$n=4$	$n=5$	$n=6$
	2.51	7.10	13.6	22.2	32.2

Table 9—Circular Steel Membranes

C_f = Frequency function
f_s = Natural frequency, cps
h = Membrane thickness, in.
m = Number of nodal circles
n = Number of nodal diameters
s = Tension of periphery, lb/in.

Membrance Structure	$C_f = f_s r/(s/h)^{1/2}$						
m	$n=0$	$n=1$	$n=2$	$n=3$	$n=4$	$n=5$
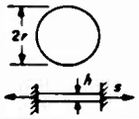 1	14.09	22.49	30.12	37.46	44.56	51.55
2	32.41	41.22	49.44	57.30	64.94	72.22
3	50.79	59.71	64.94	76.45	84.55	92.18
4	69.28	78.09	86.90	95.12	103.34	111.56
5	87.48	96.88	105.68	113.91	122.13	130.35
6	106.27	115.08	123.89	132.69	140.91	149.13
7	124.47	133.87	142.68	150.90	159.70	167.92
8	143.26	152.07	160.88	169.68	178.49	186.71

Table 10—Longitudinal Vibration of Steel Beams

C_f = Frequency function
f_s = Natural frequency, cps
L = Beam length, in.
n = Number of halfwaves along beam length

Beam Structure	$C_f/10^4 = f_s L/10^4$					
	$n=0$	$n=1$	$n=2$	$n=3$	$n=4$	$n=5$
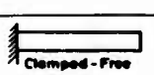 Clamped-Free	5.05	15.15	25.25	35.35	45.46	55.56
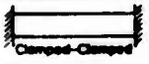 Clamped-Clamped		10.10	20.20	30.30	40.41	50.51

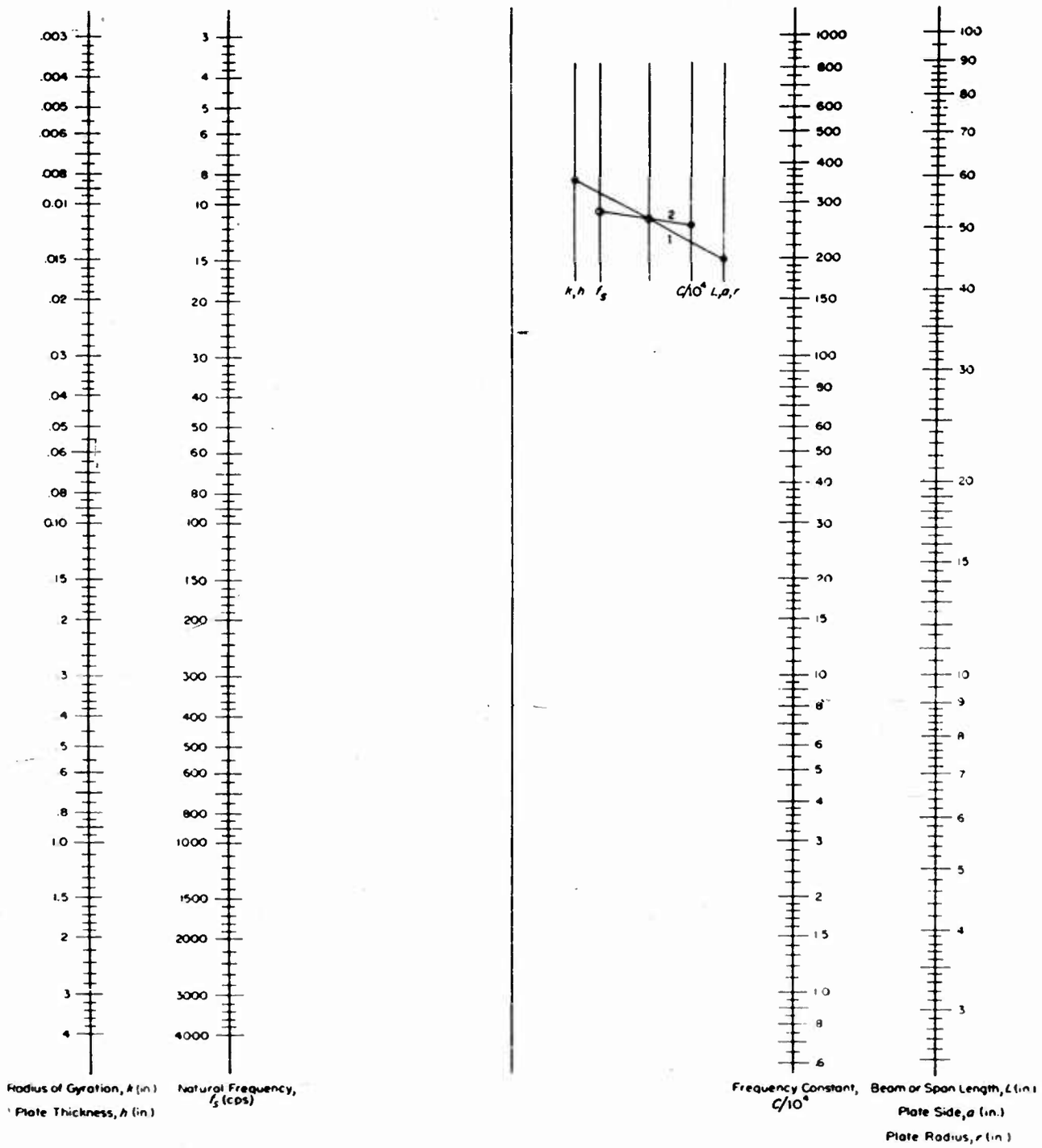

Fig. 1 — Nomograph for determination of natural frequency f_s from frequency constant C, in Tables 1 to 8.

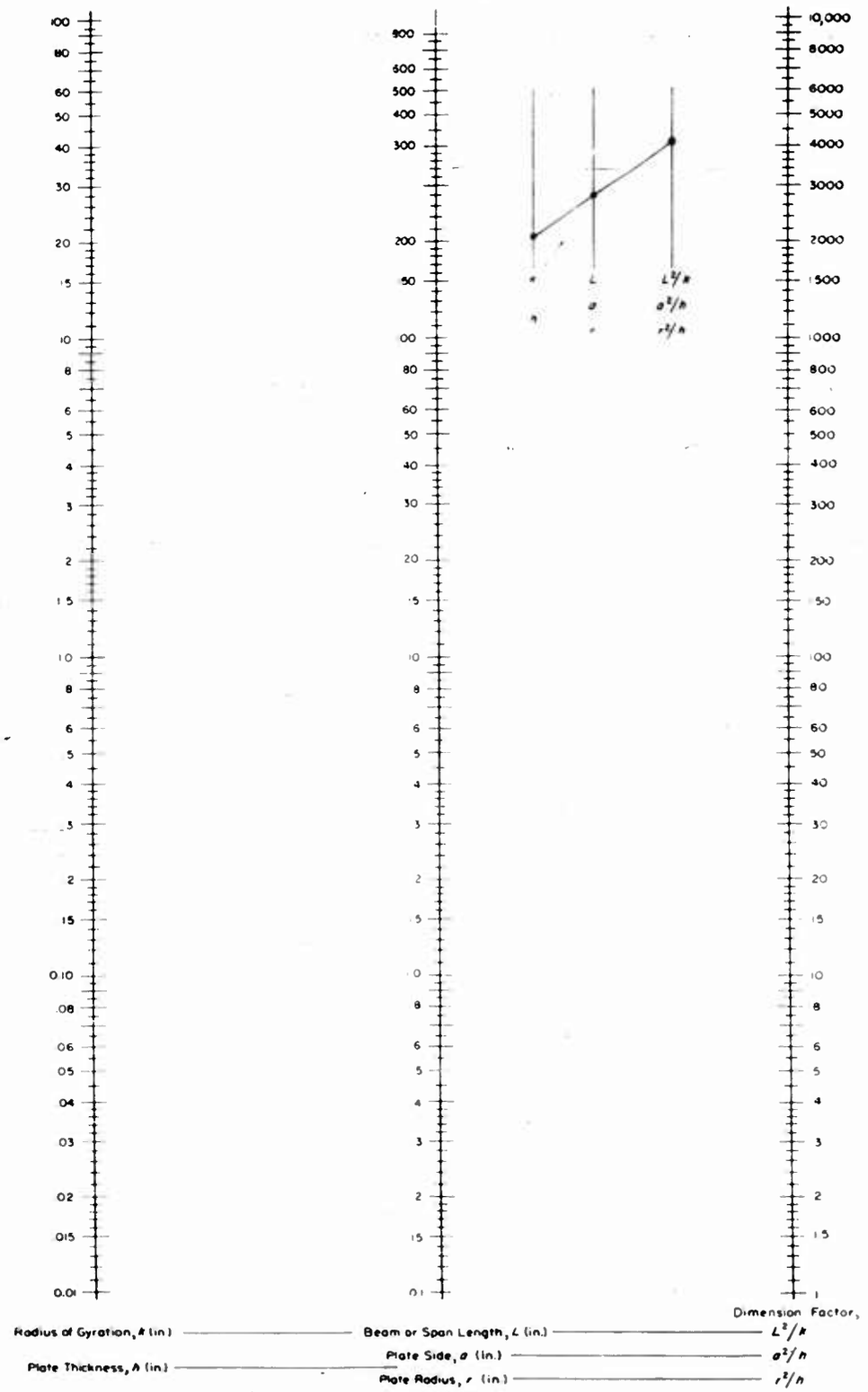

Fig. 2—Nomograph for determination of dimension factors, L^2/k, a^2/b and r^2/b in frequency constant equations of Tables 1 to 8.

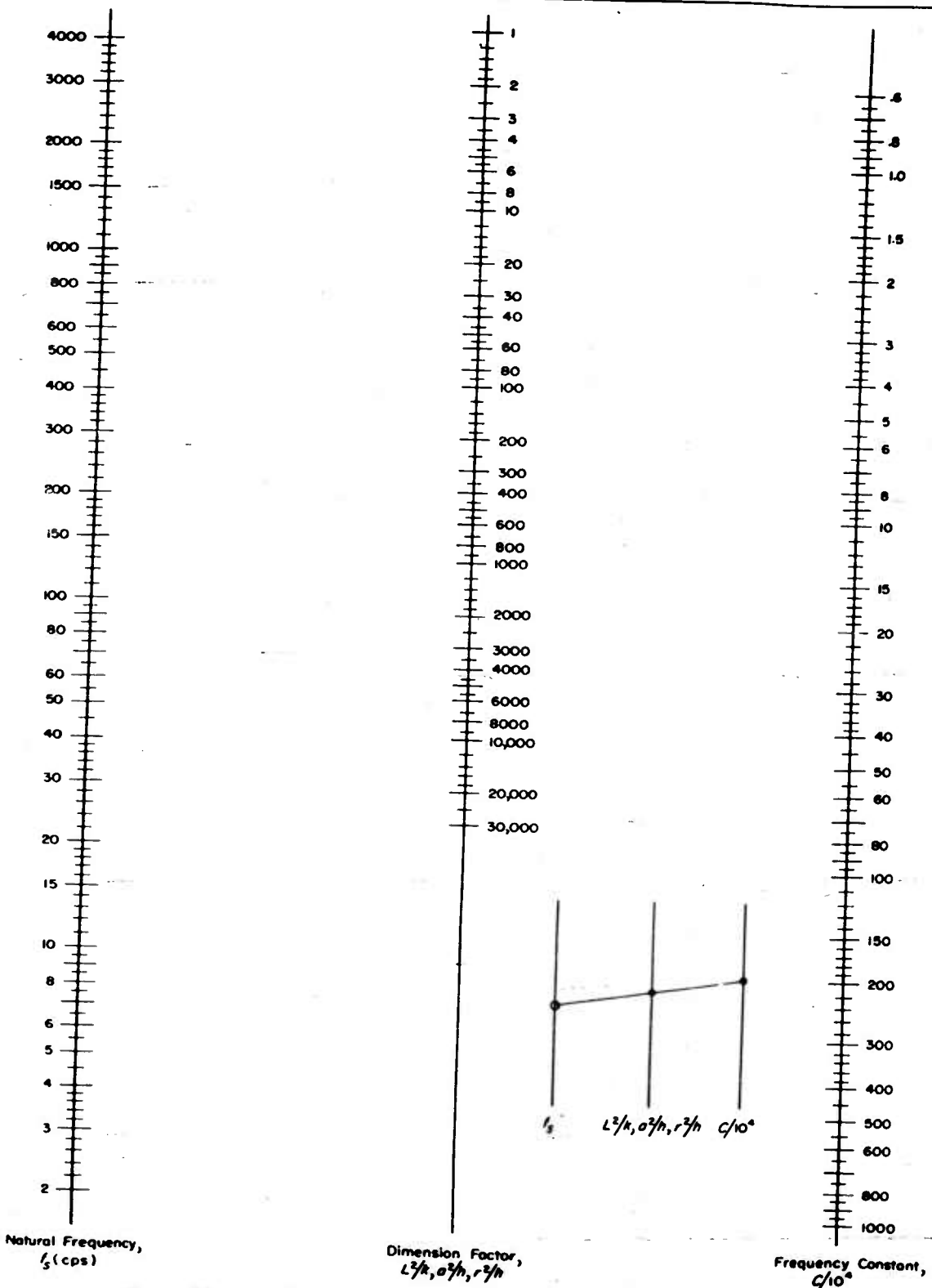

Fig. 3—Nomograph for alternate solution of natural frequency f_s from frequency constant C and dimension factor determined from Fig. 2.

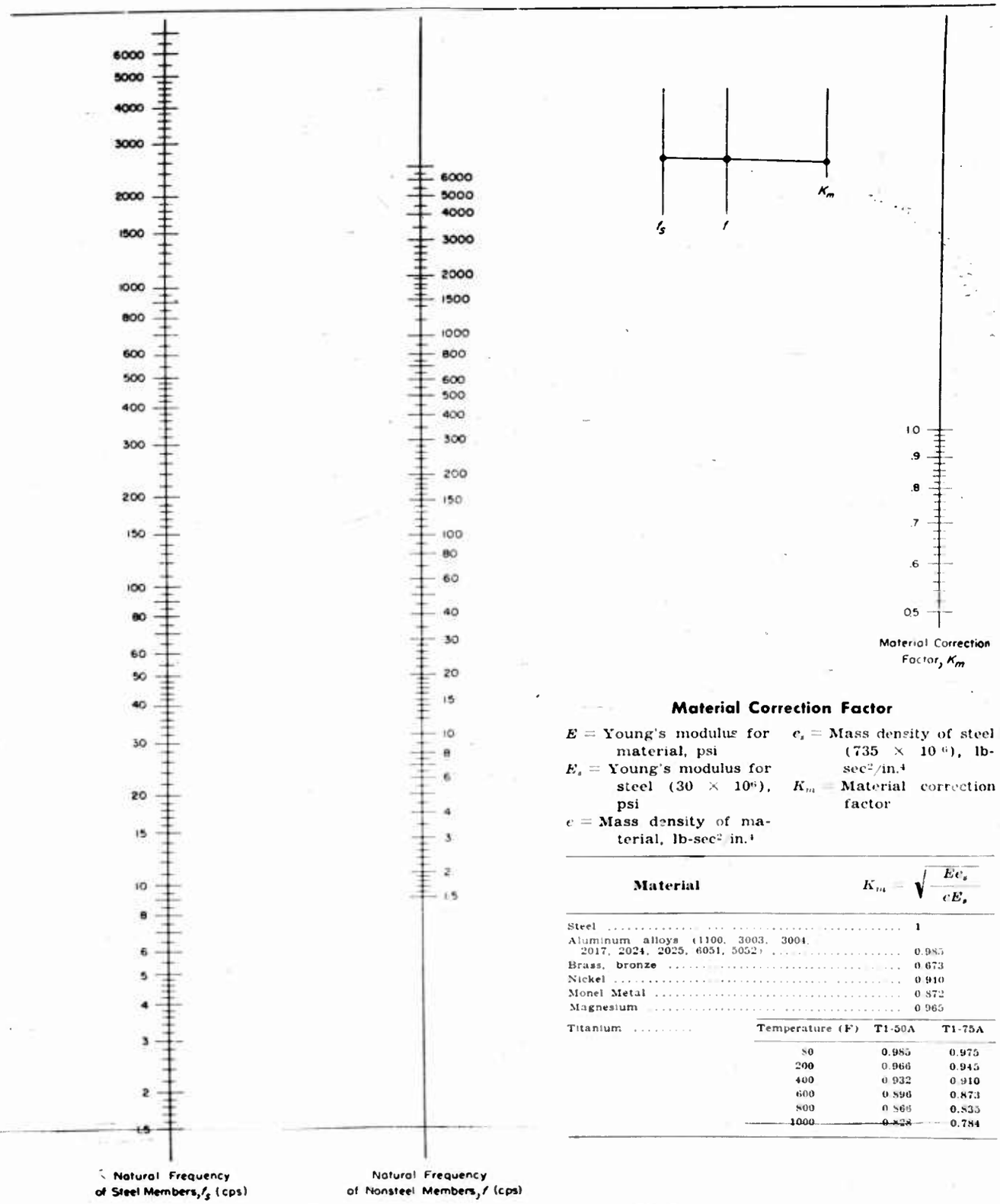

Material Correction Factor

E = Young's modulus for material, psi

E_s = Young's modulus for steel (30×10^6), psi

c = Mass density of material, lb-sec^2/in.^{4}

c_s = Mass density of steel (735×10^{-6}), lb-sec^2/in.^{4}

K_m = Material correction factor

Material	$K_m = \sqrt{\frac{Ec_s}{cE_s}}$
Steel	1
Aluminum alloys (1100, 3003, 3004, 2017, 2024, 2025, 6051, 5052)	0.985
Brass, bronze	0.673
Nickel	0.910
Monel Metal	0.872
Magnesium	0.965

Titanium	Temperature (F)	T1-50A	T1-75A
	80	0.985	0.975
	200	0.966	0.945
	400	0.932	0.910
	600	0.896	0.873
	800	0.868	0.835
	1000	0.828	0.784

Fig. 4—Correction table and nomograph for determination of correction factor K_m and natural frequency f for nonsteel structures.